INELASTIC ANALYSIS OF THE LOOP TACK TEST FOR PRESSURE SENSITIVE ADHESIVES

By

Youngjin Woo

A DISSERTATION SUBMITTED TO THE FACULTY OF
VIRGINIA POLYTECHNIC INSTITUTE AND STATE UNIVERSITY
IN PARTIAL FULFILLMENT OF THE REQUIREMENTS FOR THE DEGREE OF
DOCTOR OF PHILOSOPHY
IN
CIVIL ENGINEERING

Raymond H. Plaut, Chair

David A. Dillard

Siegfried M. Holzer

Kamal B. Rojiani

Mahendra P. Singh

September, 2002
Blacksburg, Virginia

Keywords: Loop tack test, Pressure sensitive adhesive, Tack, Finite element analysis

INELASTIC ANALYSIS OF THE LOOP TACK TEST FOR PRESSURE SENSITIVE ADHESIVES

by

Youngjin Woo

Committee Chair: Raymond H. Plaut

Civil and Environmental Engineering

(ABSTRACT)

A numerical analysis of the loop tack test is presented to study the behavior of the strip and the influence of several factors, and the results are compared with experimental ones. The numerical results can be applied to model the performance of a pressure sensitive adhesive (PSA). Since the simulation of the loop tack test includes geometrical and material nonlinearities, it is solved numerically by the finite element method. The finite element program ABAQUS is used throughout the research. As the teardrop shaped loop is pushed down onto the adhesive and then pulled up, the variation of the loop behavior is investigated using two-dimensional (2D) and three-dimensional (3D) models. A bilinear elastic-plastic constitutive law is used for the strip. The deformation of the pressure sensitive adhesive is approximated as uniaxial extension of independent adhesive strands. A Winkler-type nonlinear elastic foundation and a viscoelastic foundation are used to model the PSA. A nonlinear elastic spring function is used, which is composed of a compression region for the bonding phase and a tension region for the debonding phase. A debonding failure criterion is assumed, in which an adhesive strand will debond when it reaches a certain length. During the bonding phase, it is assumed that the loop is perfectly bonded, and the contact time is not included. Curves of the pulling force versus the top displacement (i.e., tack curves) are obtained throughout the simulation. A parametric study is made with respect to the nonlinear spring function parameters, experimental uncertainties, and strip thickness. Anticlastic bending behavior is shown in the 3D analysis, and the contact patterns are presented. The effects of the elasticity modulus of the PSA for the elastic foundation and the displacement rate for the viscoelastic model are investigated.

Acknowledgments

I would like to express my deepest appreciation to my advisor, Dr. Raymond H. Plaut, for continuing guidance, invaluable suggestions, and support throughout the last three years. I also would like to thank Dr. David A. Dillard for technical suggestions, useful comments, and advice. I want to extend my gratitude to all my other doctoral committee members, Dr. Siegfried M. Holzer, Dr. Kamal B. Rojiani, and Dr. Mahendra P. Singh, for serving on the dissertation committee.

I am indebted to Stacy Coulthard for her experimental work. I also wish to thank John Hennage and Lei Zang for providing their experimental results.

I wish to acknowledge Dr. Christopher Chul Ha, Dr. Raul H. Andruet, and Dr. Don Ohanehi for many useful discussions and help. It is a pleasure to acknowledge Meeok Kim, Changsun Jin, Hyun Shin, Hyunsoo Park, and all my Korean colleagues in the Department of Civil and Environmental Engineering for unlimited friendship.

The support provided for my research by National Science Foundation Grant No. CMS-9713949 is greatly appreciated. I am also grateful for the partial support provided by the Center for Adhesive and Sealant Science (CASS).

Finally, I wish to thank my wife, Eunok, for her devotional sacrifice and love for the last 8 years. Without her dedication I would not have done this work. I feel grateful to our two sons, Changhee and Taehee, my parents, and other family members for their love, support, and encouragement. Especially, to my mother and father, I would like to give thanks from the bottom of my heart, even though it is not enough, for their devotional support and unconditional love. I would like to dedicate this dissertation to them.

Table of Contents

List of Tables

List of Figures

Chapter 1. INTRODUCTION

Pressure sensitive adhesives (PSAs) are widely used materials in our modern life, such as in packaging, labels, medical applications, the automotive industry, and the shoe industry. Accurate and appropriate test methods for PSAs are needed to determine that a given adhesive will perform satisfactorily for its intended use. Fundamentally, characteristics of PSAs are categorized by peel adhesion, cohesive strength, and tack. Tack is the dominant property of PSAs, and is defined by ASTM as the ability of an adhesive to form a bond of measurable strength to another surface under conditions of low contact pressure and short contact time. To determine the tack property, various testing methods are suggested, for example, rolling ball tack test, probe tack test, and loop tack test. The loop tack test is one well-known method. The ends of an adhesive strip are folded to form a teardrop shape. The bottom of the loop is brought in contact with a rigid substrate at a constant rate until the contact length in the longitudinal direction reaches a certain amount (usually 25.4mm). After a short contact time (usually 1 sec), the top of the loop is brought upward at the same rate as in the bonding phase until detachment occurs. The pulling force is recorded as a tack curve. The objective of this research is to investigate the behavior of the strip and the influence of several factors in the loop tack test, considering inelastic and viscoelastic effects in terms of a finite element analysis, and to compare with experimental results.

The initial elastic analysis of the loop tack test for PSAs by Williams (2000) made some simplifying assumptions. Her results did not show a plateau in the pulling force region, a final sharp peak in the force-displacement curve, and the localized curvature at the peel front especially for a thin strip, as appears in experimental results. Unlike her work, the present study includes plasticity effects in the loop, anticlastic bending behavior, extensibility, and time-dependent viscoelastic behavior of the adhesive, as well as several separation rates. The adhesive is approximated by uniaxial extension of strands representing fibrils which are progressively extended during pulling. It is assumed that a strand will fail if it reaches a certain elongation.

The numerical analysis of the loop tack test is carried out using the commercial FEM software ABAQUS. The mesh of the strip is generated using hybrid beam elements (B21H) and four-node shell elements (S4R). PSAs are modeled as Winkler-type nonlinear elastic or viscoelastic foundations. The parameters in the nonlinear spring model used in the Winkler-type foundation are cho-

sen based on experimental results. Nonlinear finite element analysis theories are applied to the numerical simulations to evaluate the different nonlinear effects (material and geometric nonlinearities). A parametric study is presented to understand the effects of the nonlinear spring function parameters (β_1, β_2, β_3), contact area, length of loop, and strip thickness on the tack curve. Results of several experiments (loop tack test, DMA test, uniaxial tensile test, and Arcan tensile test) carried out mostly by others are used to compare with the numerical results and determine properties of the adhesive and the strip.

1.1 Williams (2000)

Williams (2000) carried out an initial analysis of this research for her Master's thesis, with the restrictive assumptions of elastic adhesive, elastic backing, and inextensible material. She presents a formulation of the basic loop tack test mathematically, and develops a simple numerical solution procedure to compute the essential characteristics of the behavior of the loop. Using the shooting method, numerical solutions are obtained. The mechanics of the loop tack test are studied to determine the effects of various factors on adhesive performance. These factors include the stiffness of the backing, the stiffness and thickness of the adhesive, the elongation of the adhesive before debonding, and the contact time.

As mentioned, throughout her work, various assumptions are made. The strip is unstrained when it is flat. It is thin, uniform, inextensible, and nonlinearly elastic. Anticlastic curvature is neglected, as well as the weight of the strip. As the loop is pulled upward, it continuously debonds from the substrate at the ends of the contact zone when the adhesive reaches a certain critical elongation, which depends on the pressure that has been applied at that location and, in one part of her study, on the time of contact (but indirectly, since time dependence is not included in the analysis). The adhesive is assumed to be located on the substrate rather than on the loop, which is equivalent if the influence of the adhesive on the bending stiffness is neglected, and if the resisting forces only depend on the vertical elongation of the adhesive. The adhesive is modeled as an elastic Winkler-type foundation, i.e., a continuous distribution of independent vertical linear elastic springs (Plaut et al., 2001).

She developed four cases to model the loop tack test, based on characteristics of the test. Due to symmetry, only half of the loop is analyzed and the loop is treated as an elastica. The first case is point contact, the second case is flat contact, the third case is pushing and pulling, and the last case adds contact time dependence. The point contact case depicts the loop right before debonding from the substrate, and the profile of the loop has only a single point of contact. The force is applied to the top of the loop and the opposite reaction occurs at the contact point. Flat contact expresses the forced triangulation in the experiment, that is, it is made to model the localized curvature at the peel front. For this analysis, the adhesive tape is assumed to be nonlinearly elastic and the relationship of the curvature and bending moment is defined by Ramberg-Osgood nonlinear theory as follows:

$$\frac{d\theta}{dS} = \frac{M}{EI_0} + \hat{\beta}\left(\frac{M}{EI_0}\right)^n \tag{1.1}$$

in which β and n are positive constants, and EI_0 is the initial bending stiffness of the loop. Values of β and n are determined by trying to use values for a good fit of an acceptable curve shape. Up to these cases, only the pulling procedure was considered. In the pushing and pulling case, the adhesive is analyzed as being on the substrate, with the backing pushing into the adhesive. Such a case includes the whole cycle of the loop tack test. The fourth formulation is basically the same as the previous one but considers the adhesive's contact time with the substrate and makes the analysis more realistic. The contact time is computed from the change of height during pushing and pulling, assuming that the pushing and pulling speeds are constant and that the dwell time is negligible.

The computer program Mathematica is used to implement the algorithms and to obtain numerical solutions in an approximate step-by-step procedure. The maximum force required for separation of the loop from the substrate is the tack or pull-off force. The shooting method usually works well, but convergence to the desired solution may be sensitive to the initial guesses. Sometimes the method converges to a mathematical solution which does not represent the actual physical loop, such as the triangular shape in the pulling procedure. The pulling force curve results do not show a plateau and a final sharp peak in the force-displacement curve, as often appears in experimental results. The results show that the pulling force increases as the stiffness of the backing or

the thickness of the backing or adhesive decrease, or as the stiffness of the adhesive or the length of the loop increases.

1.2 Pressure Sensitive Adhesive

Pressure sensitive adhesives (PSAs) are materials that develop measurable adhesion upon contact with a substrate by the application of a light pressure without requiring a chemical reaction, with no curing of the adhesive, and with no loss of solvent during the adhesion process. Such properties imply that intimate contact between the substrate and the adhesive must be established rapidly and under slight pressure, but also that the energy necessary to separate the adhesive from the substrate must be sufficient for the specific application (Creton 1997). In modern human life, PSAs are widely used materials in modern industry (packing, release coatings, labels, hospital products , etc.) and are expected to be relied upon much more in the near future. Their uses extend from the mending of wounds and surgical incisions to securing the chafing strips in Airbus flaps, which are bonded with acrylic PSAs. In civil engineering, roofs of buildings may be bonded with PSAs for holding the roof and sealing it. According to the Pressure Sensitive Tape Council (PSTC) (1994), PSAs are defined as materials with the following properties:

- Aggressive and permanent tack
- Adhere with no more than finger pressure
- Require no activation by any energy source
- Have sufficient ability to hold onto the adherend
- Have enough cohesive strength to be able to be removed cleanly from the adherend

The beginning of the pressure-sensitive adhesive industry was in the medical application of adhesive tapes and plasters. It is not entirely clear at which point these medical adhesive tapes closely resembled pressure-sensitive adhesives of today. During the mid-19th century, natural rubber was added to the adhesives formula that previously contained resins and beeswax. The invention of rubber pressure sensitive adhesives is attributed to Dr. Henry Day. Such adhesives consisted of India rubber, spirits of turpentine, turpentine extract of cayenne pepper, litharge, pine gum, and other ingredients. A U.S. patent to Shecut and Day was issued in 1845. A German patent was issued in 1882 to druggist P. Beiersdorf for a plaster based on gutta-percha. In 1899, natural

rubber based, zinc oxide containing adhesive was developed. The adhesive plasters were produced industrially in larger quantities by the turn of the past century. For quite some time, PSA applications were limited to first aid uses. The first electrical insulating tapes were produced during the period 1920-1930. This was not strictly a pressure sensitive tape, but a friction tape. We can find utilization of pressure sensitive tape other than medical applications historically, such as paint masking applications and transparent synthetic film tape in industry for a tremendous variety of purposes (Satas, 1982).

A large variety of elastomers have been used as PSAs. The first material to gain widespread use was a natural rubber-based adhesive. Natural rubber-based PSAs are still used in a number of PSA tape applications, including masking tape, where they exhibit removability after painting and baking. One of the primary attributes of natural rubber-based PSAs is their low cost, but they also are used extensively because of their high peel strength when properly formulated. However, these adhesives had one important defect. Because of unsaturation in the backbone of the base polymer, the adhesive had a noticeable tendency to yellow and to crosslink, thus becoming brittle. In general, natural rubber-based PSAs were unstable to long term exposure to the environment. This problem led to the advent of a number of new base resins which did not suffer from these deficiencies. A group of such base elastomers were the acrylates. The two primary acrylates used in PSAs are 2-ethyhexyl acrylate and iso-octyl acrylate. Acryic-based PSAs are used in a wide variety of applications from transparent tape to medical tapes. In comparison to natural rubber-based PSAs, acrylates are more expensive, but they have excellent weathering characteristics. Both PSAs need to be crosslinked to obtain the cohesive strength necessary to meet all of the requirements of a PSA. Another group of base resins for PSAs, the block copolymer-based elastomers, meets these requirements through phase separation, but these elastomers suffer from oxidative instability in much the same way as natural rubber-based adhesives. Block copolymer-based PSAs are used in a wide variety of applications but most commonly in packing tapes. There are several other types of PSAs, but the above three types of base elastomers form the majority of PSAs (Pocius, 1997).

Creton (1997) divides PSAs into three classes according to performance, which are removable, semi-permanent, and permanent PSAs. For the removable PSAs, a high compliance is required in order to establish contact very easily, but, conversely, low adhesion is necessary. The most well-known application is the Post-It note, but masking tape or mounting spray adhesives are also good

examples. For the semi-permanent PSAs, which are the most common type of adhesive, medium compliance and a relatively good adhesion are necessary, but no long-term resistance to the environment is needed as the lifetime is typically of a few months at the most. The standard office tape, label, or the ubiquitous finger bandage fall into this category. In the last one, permanent PSAs, the critical property is very high adhesion and very high creep resistance, as well as good resistance to the environment.

The advantages and disadvantages of using PSAs are described by Aubrey (1992). The advantages are that there is no storage problem, no mixing or activation is necessary in bond formation, no waiting is involved in this bond formation, and often the bond created by the PSA is readily reversible. Disadvantages are that the adhesive strength, especially for peeling and shearing, is low, bonds cannot be easily formed on unsuitable or rough surfaces, and PSAs are expensive in terms of cost per unit bond area.

To understand the behavior of PSAs and determine that a given PSA will perform satisfactorily for its intended use, three properties of PSAs are determined with three basic characteristics (Satas, 1989; Skeist, 1990; Aubrey, 1992; Johnston, 1994; Zosel, 1994; Pocius, 1997):

- Tack

Tack is an indication of how quickly an adhesive can wet out, and so come into intimate contact with a particular surface, and eventually reach its optimum adhesion. Dahlquist (1959) pointed out that tack is not a well-defined property such as viscosity or elasticity, but depends upon the mode of the test procedure. A rigorous definition requires standardization of contact pressure, dwell time, rate of separation, and surface of the adherend. Many empirical tests have been devised, some intended to measure tack under light pressure, others at very short contact times. Some tests attempt to combine both features. The tack property is the main topic of the present study, so that a more detailed description is given in the following section.

- Peel strength

Peel adhesion is the force required to remove a pressure sensitive tape which has been applied to a standard test panel, using definite pressure to make contact, from the panel at a specified angle and speed (PSTC). The resistance to peel is determined by measuring the force required to peel away a strip of tape from a rigid surface at a specified peel front angle at constant rate as shown

Figure 1.1a. It is tested most commonly by the 180° peel angle but somtimes 90° or lower angles are used. Peeling at 90° is subject to less error and is probably more related to practical situations, but requires more complicated test equipment than 180° peeling. The peeling rate and the temperature have been the most widely investigated experimental parameters. One of the most difficult problems in designing a standard peel test is the standardization of the method of applying the tape to the test surface.

- Shear strength

This property indicates the resistance of an adhesive to shearing forces. The standard method of determining shear strength is the “static” shear test which measures the time required to pull a defined area of a tape from a test panel under a constant load. The test is commonly carried out at room temperature or at 40°C. Although it may be adequate for routine assessment of tape performance under simulated service conditions, it gives little information about intrinsic properties of the adhesive itself. This is partly because there are at least three modes of failure possible in the test. First, the adhesive may undergo a true shear failure in which viscous flow is involved. Second, the tape may appear to slide intact from the plate. Third, peeling may occur from the unloaded end of the tape. The latter two effects involve peeling phenomena and are best corrected by increasing the level of peel strength. A schematic of the shear test is shown in Figure 1.1b.

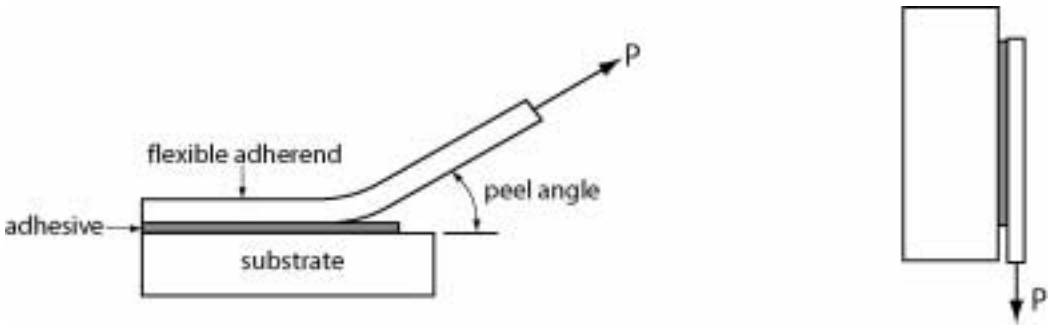

(a) Peel test (b) Shear test

Figure 1.1 Diagram of tests for PSAs

These three basic characteristics provide an understanding of how quickly and how firmly the adhesive will stick and how strongly it will resist any applied force. There are many standard test specifications laid down by different authorities to assess these properties and many differences in detail between them. Reviews of properties of PSAs and test methods include Aubrey (1977, 1992), Satas (1989), Skeist (1990), Johnston (1994), Chuang et al. (1997), Creton (1997), and Pocius (1997).

1.3 Tack

As described in the previous section, pressure sensitive adhesives (PSA) are usually described by three parameters: tack, peel adhesion, and shear resistance. Unlike peel adhesion and shear resistance, the concept of tack is difficult to define. According to Johnston (1983), it has been called diverse names which are tack, wet grab, quick stick, initial adhesion, finger tack, thumb-tack, quick grab, quick adhesion, and wettability in the PSA industry. Tack is one of the most important properties of PSAs which is defined by Zosel (2000) as the ability of an adhesive to form a bond of measurable strength to another material under conditions of low contact pressure and short contact time. The PSTC defines it as “that which allows a pressure sensitive adhesive to adhere to a surface under very slight pressure.” The American Society for Testing and Materials (ASTM) defines tack as “the force required to separate an adherend and an adhesive at the interface shortly after they have been brought rapidly into contact under light load of short duration.” However, it is not clear how long short duration is and how much load slight or light is. The definition of a test method for quick stick, PSTC test method 5, describes these unclear points as “that property which causes the tape to adhere instantly using no external pressure,” indicating a time frame of zero, and the applied pressure being the weight of the tape only.

Tack is not merely a material property of the adhesive, but also depends on the adherend properties and the process conditions. That is, tack is sensitive to a wide range of factors, such as the adhesive used, contact load, dwell time, adherend, temperature, humidity, and the adhesive’s flow characteristics. Due to the interaction of these variables, it is hard to describe tack by a unified theory (Hu et al., 1998). Some of the factors that can influence tack are summarized in Duncan et al. (1999). They described factors influencing tack, which are adhesive application (uniformity,

weight, and thickness of the adhesive layer), contact pressure, dwell time, test speed, test temperature, humidity, adherend surfaces, adherend compliance, specimen conditioning, and adhesive activation. Creton and Leibler (1996) attempted to better understand the dependence of tack on the pressure and contact time, and to quantitatively relate the results to the molecular structure of the adhesive and the roughness of the substrate. Zosel (1989b) demonstrated that good tack performance is characterized by the formation of fibrils. Zosel (1997) presents experimental studies of the influence of the contact formation on the adhesive or interfacial fracture energy and tack of polymers.

The easiest test method of measuring tack is touching the finger lightly for a short time to a pressure sensitive adhesive and then quickly withdrawing it. Numerous standard tack test methods have been developed for PSAs by different organizations and presented by Johnton (1983), Pizzi and Mittal (1994), Roberts (1997), Pocius (1997), and Duncan et al. (1999). They can be divided into three broad categories: those using a rolling ball, those using a modification of the peel test, and those using some form of probe. However, the results produced by different techniques are not always comparable. It is thought that some of these differences may be due to the viscoelastic response of the adhesive, since dwell times and separation rates vary between test methods. The standard tack test methods fall into the following categories as mentioned above (Mizumachi, 1985; Satas, 1982; Pocius, 1997; Duncan et al., 1999):

- Rolling Ball Test

The rolling ball test has been the oldest and most widely used for at least 50 years. In the common form of the rolling ball tack test, a stainless steel ball with 1.1cm (7/16 in.) diameter is released at an elevation on an inclined tack so as to roll down and at the bottom come into contact with the horizontal, upward-facing adhesive. The distance the ball travels out along the tape is measured as tack. It is primarily intended for quality control of adhesive tapes, but may also be used to investigate adhesive coatings. Since the motion of the ball is closely related to bonding and debonding processes which occur simultaneously at the surface of contact, it is believed that the rolling motion of the ball on a pressure sensitive adhesive reflects tackiness of the adhesive. However, this test does not provide the level of control needed to understand tack, since the rate of application of the force varies somewhat as the ball travels the length of the tape.

- Loop Tack Test

There are two different modifications of the peel test for tack which are the loop tack test and the quick-stick test. In the loop tack test, a loop is attached to the jaws of a tensile testing machine. The loop is brought into contact with the pre-cleaned substrate by lowering the loop at a specified rate till it contacts a certain area of the panel. The tensile testing machine is then reversed and the force to remove the tape is recorded. More detail is given in a later section.

- Quick Stick Test

In the Pressure Sensitive Tape Council's "Quick-Stick" test, the tape is placed on the flat stainless-steel plate test surface with no contact pressure beyond that of its own weight. The tape is then peeled from the surface at $90°$ at 300mm/min (12 in./min) and the maximum peel force is taken as the tack value. This test, although functionally measuring the level of tack, does not provide the information necessary to understand tack, since the pressure and the rate of application of the tape are not controlled. The backing stiffness also has a marked effect, since stiffer backings do not allow easy intimate contact of the adhesive to a surface.

- Probe Tack Test

The probe tack tests are mechanical simulations of thumb or finger tack tests. In them, the tip of a probe is brought into contact with a supported adhesive under low contact pressures for a short time and then pulled away at a fixed rate, during which the peak force of separation is measured. In this test method, the effect of the tape backing is eliminated because the tape is either rigidly affixed to a steel plate or mounted on an annular ring of known weight. The test can be used for quality control or research purposes.

The methods of measuring tack include the contact of two surfaces (adhesive and test substrate) under light pressure for a short time, followed by a separation step, the force (or energy) of separation being taken as a measure of tack (Aubrey, 1992). Thus, the procedure for measuring tack is a two-stage process of bond formation and bond separation. During bond formation, contact in molecular dimensions between the adhesive and the adherend is established in isolated spots of the geometric contact area, the number and size of which increase with contact time by deformation and flow as well as by wetting. The bonding process is not well understood in a quantitative sense. According to Dahlqist (1969), quanlitatively it is assumed that good bonding is achieved if the adhesive has the following properties:

- Ability to wet the adherend, which implies that the surface energy of the adhesive must be less than that of the adherend;
- Low viscosity in terms of small shear displacements of polymer chain segments, but not necessarily at large displacements;
- Relaxation times of elastic deformation which are substantially less than the time of contact;
- Low elastic modulus and high deformability to permit conformation to the contour of the surface.

The second step, bond separation under the influence of external forces at a certain rate, is connected with deformation of the adhesive joint and the creation of two new surfaces under destruction of the interface (Zosel, 1989b). Control of tack is important so that the right level of initial bond strength is achieved. If the tack is too low, then the bond may rupture during manufacture, or if the tack is too high, then repositioning of substrates may be difficult. Tack is normally determined from the force required to separate two components joined by a soft viscoelastic bonding material. Tack gives an indication of how quickly an adhesive can wet and make intimate contact with a surface. That is, high tack forces on separation are associated with effective wetting of the surface (Duncan and Lay, 1999).

1.4 Loop Tack Test

The loop tack test is widely used in the adhesive tape and PSA industries, primarily as a quality control tool. The test methods can be divided into two different types depending on which substrate the adhesive coats. In one, the adhesive is on the forming loop. This test is used to test adhesive tapes. In the other, the adhesive is on the rigid base plate. This test method tends to be used for double-sided tapes, pressure sensitive adhesives, and coatings. The most popular method is the FINAT Test Method No. 9. The steps involved in the test, which are shown in Figure 1.2, are described below.

Step a: Initial flat strip (Figure 1.2a).

Step b: Form the loop from the tape (Figure 1.2b).
The specified length of tape should be bent back until around 10mm or so of the ends are in contact. If the adhesive is on the backing, the adhesive surface should be on the outer surface.

Step c: Clamp the loop in the movable test machine grips (Figure 1.2c).

The formed loop should be connected to a load measuring device with sufficient range and sensitivity (normally specified in the test method). The loop should be aligned such that the edges of the tape will be at a right angle to the edge of the base plate.

Step d: Lower the loop (Figure 1.2d).

The loop should be lowered, pushing down onto the base surface, until the tape makes contact over the required area. Although the standard test methods do not require it, measurement of the 'push down force' can help check for consistency among different tapes.

Step e: Pull the loop off the surface (Figure 1.2e).

Once the loop has contacted the required area of the base plate, the direction of the test machine should be reversed. The area in contact should be inspected visually for any imperfections in the contact (e.g., wrinkles or bubbles). The test should run until the tape is detached from the plate. The pulling force versus top displacement of the loop is recorded.

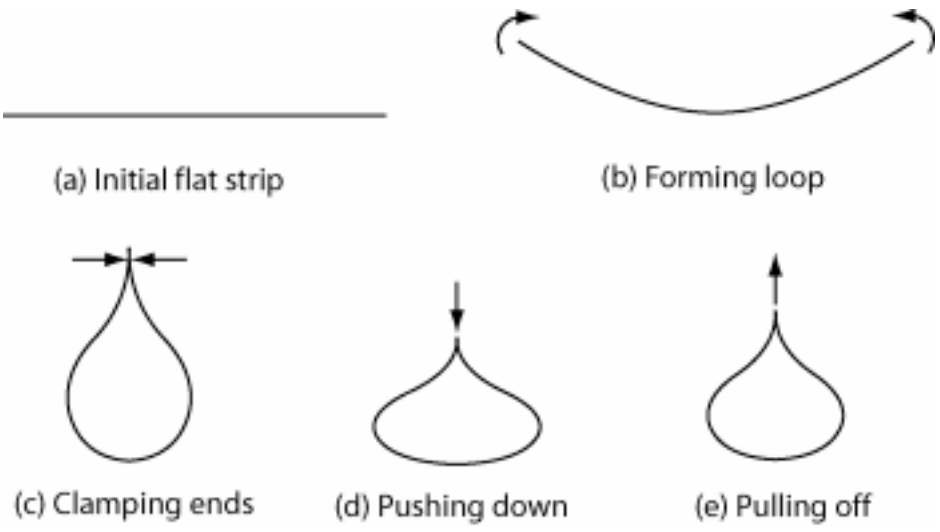

Figure 1.2 Steps in the loop tack test

Some previous reviews and work on the loop tack test have been carried out by Johnston (1983), Satas (1989), Pizzi and Mittal (1994), Roberts (1997), Chung et al. (1997), Le et al. (1999), and Tobing and Klein (2000). Loop tack tests have the advantage of requiring only simple fixtures mounted on standard tensile testers, being quite easy to carry out, and being acceptably reproducible. Even in a single test, however, they are subject to variable peel angles and contact times. They also suffer from the large influence the stiffness or flexibility of the tape backing plays in the magnitude of the force measured. The cause of this influence is the compression zone that presses the adhesive into contact with the adherend just ahead of the zone where adhesive and tape are being peeled off, and the manner in which the compression magnitude depends on the backing properties. Loop tack tests can very effectively assess the tack of adhesives on film or sheet (paper) backings for applications that are closely approximated by test conditions (Satas, 1989). Duncan and Lay (1999) pointed out drawbacks of the loop tack test in their report. If the backing material has little stiffness, then there may be difficulties in forming the loop into a repeatable shape. This can be compounded by static electricity effects. Alignment of the loop with respect to the substrate plate is another potential problem, particularly with low stiffness tapes which may be prone to twisting. There is a degree of subjectivity in the decision as to when the tape is in full contact with the plate, and when to reverse the direction of the machine. Thus the contact area and/or dwell time may vary. The downwards contact pressure exerted through the loop will depend on the stiffness of the tape. Thus different tapes will give different contact pressures that will lead to different measured tack strengths even if the adhesive is the same.

Duncan et al. (1999), Hu et al. (1998), and Roberts (1997) presented standard loop tack test methods as follows:

- BS EN 1719 Adhesive-tack measurement for pressure sensitive adhesive - determination of loop tack, British Standards Institution
- BS 7116: 1990 Double sided pressure sensitive adhesive tapes, British Standards Institution
- FINAT Test Method No. 9 (FTM9) “Quick stick” tack measurement (loop tack)
- TLMI LIB1, Tag and Label Manufacturers Institute
- TLMI LIB2, Tag and Label Manufacturers Institute

As mentioned above, the FINAT FTM9 method is widely used in the adhesive tape industry. In the FINAT method for measuring loop tack, a strip of material 25mm wide and at least 175mm long is

formed into a loop and brought into contact with a glass plate at a rate of 300mm min^{-1}. After a contact area of 25mm^2 is attained, the loop is then separated at the same speed. The standard methods tend to specify different ways of expressing the tack. The BS methods specify that tack is taken from the peak force (from the median of three replicates). The FINAT method is more ambiguous - the maximum force is recorded, but the method then specifies that 'Quick Stick tack is expressed as the average value (ignoring the initial peak) and range for the five strips tested'. The statement 'ignoring the initial peak' is open to different interpretations and does not follow from the rest of the procedure. The statement can be ignored and the tack expressed as the mean of the maximum forces measured, provided that is agreed and recorded as the method for determining the tack.

As an alternative to physical experiments, a virtual experiment approach was undertaken by Hu et al. (1998), Duncan and Lay (1999), and Duncan et al. (1999). In their work, a finite element model was created of the tape loop using 2 node linear, in-plane beam element and surface using ABAQUS and run through the four steps of the tack test. The shapes of the loop throughout the virtual test agreed very well with digitized video images of an actual test. However, their model does not have an element set of the adhesive. The interaction between the adhesive and the plate was represented using the *SURFACE BEHAVIOR subroutines in ABAQUS. Since it does not consider higher contact pressure produced by the stiffer tapes, the computed tack from ABAQUS in their work does not physically make sense with respect to different thicknesses of the strip.

1.5 Viscoelastic Property of Pressure Sensitive Adhesive

When a pressure sensitive tape is appied to a substrate, the adhesive is expected to spontaneously spread on the surface with little or no applied pressure. That is, the PSA is expected to act as a liquid. This "liquid" nature of a PSA indicates that its behavior is a rate process affected by time, temperature, and the applied stress. However, when the adhesive is peeled or a weight is hung from it, we expect the adhesive to resist the force. That is, it should act as a solid. This contradictory behavior is available from viscoelastic material (Pocius 1997). The viscoelastic material properties are determined by dynamic mechanical measurements (DMA). From this test, the two components of the complex dynamic shear or tensile modulus, the storage modulus G' (or E')

and the loss modulus G'' (or E''), are determined as a function of temperature and angular frequency. The viscoelastic properties of the materials can govern tack properties in two ways; one is that during bond formation the achievement of good contact is related to the dynamic storage modulus E', and the other is that during debonding the energy dissipated upon deformation is related to the loss modulus E'' (David et al., 2000).

As mentioned, adhesives often begin as liquids. A significant portion of a material's ability to perform as an adhesive depends upon its ability to "wet" a surface. Wetting of a surface does not depend just on interfacial characteristics, but also depends on the ability of the material to flow on the surface with or without applied force. Thus, the characteristics of the adhesive as a liquid are important in the generation of adhesive bonds. Some adhesives are never fully solids but retain much of the character of liquids through their use. These materials are termed viscoelastic. Most polymeric materials have some degree of viscoelastic character. Certain adhesives, known as pressure sensitive adhesives, make great use of this characteristic.

Dahlquist (1966) proposed the correlation of viscoelastic properties and adhesive performance of PSA's. He states that in order for a PSA to wet a substrate properly during the short time of contact chraracteristic of a tack test, the one second compressive creep compliance at the use temperature must be greater than 10^{-7}cm^2/dyne and preferably as high as 10^{-6}cm^2/dyne. However, the Dahlquist criterion is rarely quoted in its original form, but is reformulated in term of DMA test data. In this form the criterion states that the absolute value of the complex shear modulus, $|G^*| = (G'^2 + G''^2)^{1/2}$, measured at 1 rad/s should not exceed 3.3×10^4 Pa (Christensen and Flint, 2000). Chang (1991) suggested a viscoelastic window (VW) of different types of PSA based on dynamic storage (G') and loss (G'') moduli at bonding and debonding frequencies. It was found by Chang and in recent studies that the glass transition temperature and dynamic storage modulus (G') at the application temperature are the most important parameters for pressure sensitive adhesive performance.

Viscoelastic properties of PSAs have been presented by Chu (1989), Chang (1997), Creton (1997), and Pocius (1997). Correlation of tack and viscoelasticity was reported by Duncan (1999). The performance of PSAs (e.g., peel, tack, and shear) depends on the viscoelastic response of the bulk viscoelastic properties of the adhesive, as well as the surface energies of the adhesive and adherend. Bonding is a low rate process at low deformation that occurs when the PSA is brought

into contact with a surface, while debonding in a tack or peel test is a high rate process, depending on the thickness of the adhesive. The shear strength test is a creep test carried to high deformation. The viscoelastic behavior of an adhesive controls its response in adhesive testing and is an important factor in controlling its performance (Chu, 1989).

Viscoelastic models for PSAs have been discussed by Hata (1972), Mizumachi (1985), Mizumachi and Hatano (1989), and Yarusso (1999), among others. They used two or more parallel Maxwell elements. These act like a fluid, and as time increases, the deformation under constant force keeps increasing. These papers mention several possible failure criteria, such as a critical value being reached by the stress, by the strain, by the strain in a spring, by the strain in a dashpot, by the total stored energy in the springs, or by the strain energy density in the springs. In Duncan (1999), modeling of creep of viscoelastic materials is conducted in ABAQUS using a sum of exponential relaxations characterized by a relaxation magnitude constant and time constant (the *VISCOELASTIC option). These constants are determined by fitting Prony series to time-dependent input data supplied to the finite element analysis (FEA) package. A Winkler-type viscoelastic foundation is presented in Kuczma and Switka (1990), Kuczma (1992), Kuczma and Demkowicz (1992), and Drozdov and Gertsbakh (1993).

1.6 Deformation Modes and Debonding Failure Criterion of Pressure Sensitive Adhesives

If a tape is pulled off of a surface, some of the adhesive may stay on the surface, or all of it may remain on the tape. The first case is called cohesive failure, and the second is interfacial failure. An important usage property of a commercial pressure sensitive adhesive is the ability to debond from the substrate without leaving much residue (Lakrout et al. 2000), that is, it should exhibit interfacial failure. Recently, Lakrout et al. (1999, 2000) have shown in their probe tests that the debonding process of PSAs generally proceeds in the following manner:

1. Homogeneous deformation of the film in tension.
2. Nucleation of the cavities at the interface between the film and probe (the number and location of these cavities are related to the presence of air pockets trapped at the interface between the film and probe).

3. Simultaneous expansion of these cavities as interfacial cracks.
4. Growth of the cavities in the direction normal to the plane of the film and formation of a fibrillar structure.
5. Fracture of the fibrils by creep or debonding of the foot of the fibril from the probe.

Based on this observation, a schematic deformation mechanism during debonding procedure in the loop tack test can be anticipated as illustrated in Figure 1.3.

Creton (1997) reviewed three main mechanisms of fracture occurring in the peel of PSAs with respect to varying rates of peel, as follows:

- At low rates of peel or high temperatures, the bond typically fails cohesively in the adhesive layer by fibril formation with eventual breakdown.
- When the rate of peel is increased or the temperature is decreased, the debonding mechanism may experience a transition to a situation where fibril formation is followed by debonding of the fibrils from the substrate. This transition is not always observed.
- Finally, if the rates are increased further, all adhesives undergo a transition to fracture without fibrillation and with a very small amount of deformation.

Lin et al. (2000) also presented three distinct mechanisms of failure during the pull-out phase of a Flat Punch (Tack) Test. According to them, failure of the adhesive can occur on the interface between the punch and the adhesive layer by crack propagation from the edge of the contact, by internal crack propagation, or by cavitation and fibrillation. In axisymmetric probe tests with a flat punch, fibrillation is quick to develop upon pull-off for many adhesives. Fibrillation is a common quality of the PSA debonding process that significantly contributes to the overall adhesion energy, but this behavior greatly complicates a quantitative analysis of adhesive failure. In Crosby et al. (2000), a simple analysis is used to develop a deformation map that can be applied to predict the failure mechanism. They categorized various deformation and failure modes of adhesively bonded elastic layers. It was stated that three main deformation modes can be used to categorize the early stages of the debonding processes of a compliant layer from a rigid substrate:

- Edge crack propagation
- Internal crack propagation
- Cavitation

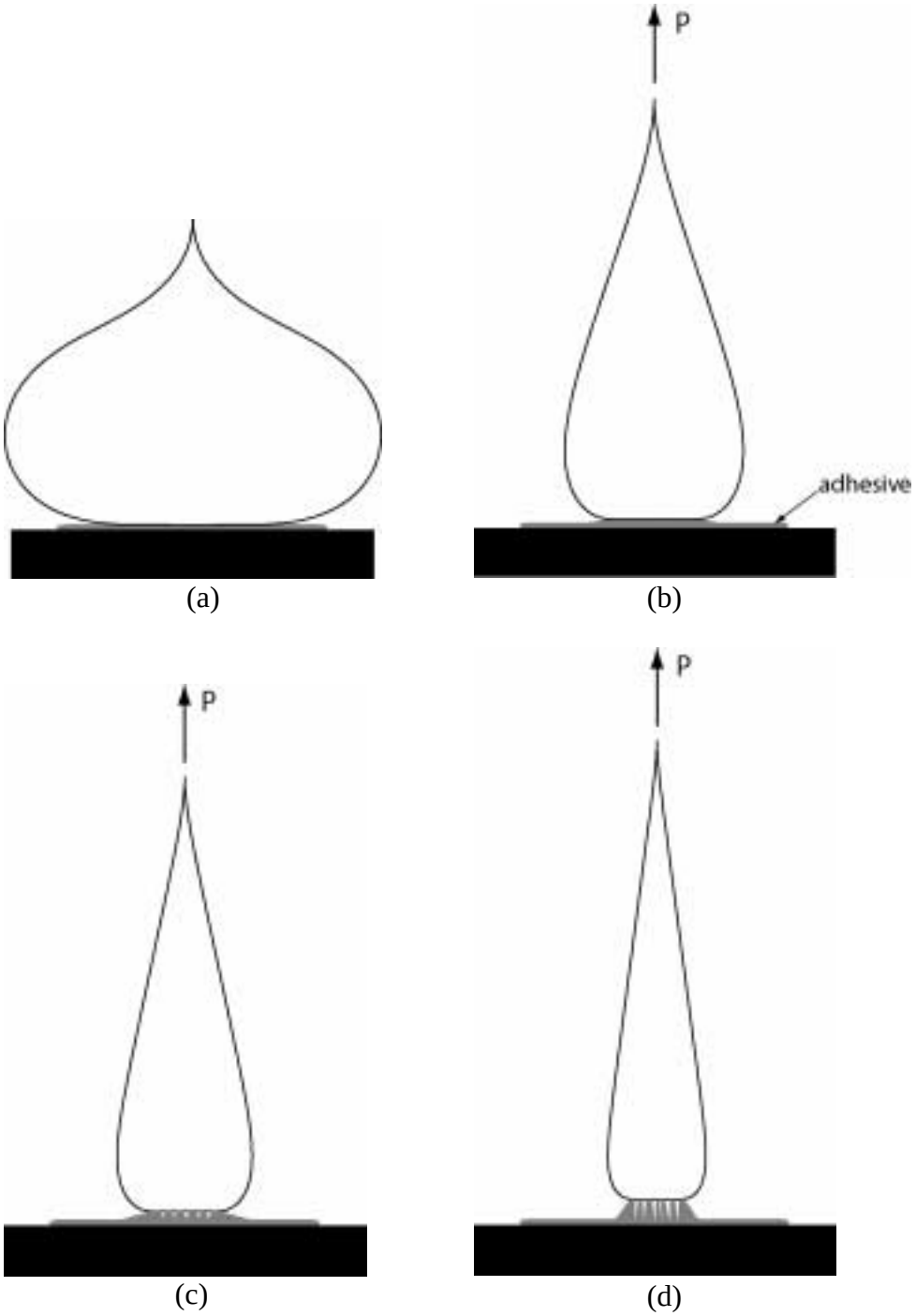

Figure 1.3 Schematics of the deformation mechanisms during the debonding phase in the loop tack test

In addition to these three main classes of deformation, the following two subclasses, related to the shape of the edge of the compliant layer, can also be defined:

- Edge crack fingering
- Bulk fingering

They considered two classes, which are the interfacial deformation modes (edge crack propagation, edge crack fingering, and internal crack propagation) and the bulk deformation modes (cavitation and bulk fingering). The former are governed by the energy release rate describing the driving force for crack propagation, whereas the latter are governed by the stress within the layer.

In the determination of a debonding failure criterion, if one treats the adhesive deformation as approximated by uniaxial extension of strands, one can qualitatively evaluate various possible strand detachment criteria for agreement with existing data. One possible failure criterion for debonding would be to assume that the adhesive deforms until a certain critical stress is reached. Such a criterion can predict the transition from cohesive to interfacial failure, but in the interfacial regime it predicts a peel force which decreases continuously with increasing rate. Such behavior is never observed in PSAs. Another possible criterion for strand debonding would be a critical strain level. However, the result of such a criterion is a peel force which increases with rate without bound. This is also physically unrealistic (Yarrusso, 1999). Sometimes, as the adhesive is pulled away, it forms fibrils. If these fibrils break, with part being left on the substrate (i.e., cohesive failure), Yarusso (1999) mentioned that the debonding criterion should be that a critical length of the fibril is reached. When none of the adhesive stays on the substrate, he suggests using the stored elastic energy density. But there is no universal agreement as to the best criterion to be used in each of these cases. In Plaut et al. (2000) and Williams (2000), it is assumed that the debonding criterion depends on the maximum pressure applied to the adhesive, and also in one case on the time of contact (assuming no dwell time exists between the pushing and pulling phases of the loop onto the substrate).

Several researchers (Crosby and Shull, 1999, 2000, Creton and Lakrout, 2000, Lin et al., 2000) adopted a fracture mechanics approach to analyze probe tests. The fundamental idea for any fracture mechanics approach is that the edge of contact between the spherical probe and the adhesive can be modeled as a propagating crack. As in conventional fracture mechanics, the energy

required to move the crack by an incremental distance can be calculated from the stress state, geometry, and material properties (Crosby and Shull, 1999). Sun and Chang (1995) used the fracture energy, defined by the Griffith criterion, to characterize the adhesive strength along the interface.

Basically, in the present study the adhesive failure mode is an interfacial deformation mode and the failure criterion for debonding assumes that the PSA will debond when it reaches a certain elongation, as Yarrusso (1999) described (more details will be given in a later chapter).

1.7 Plastic Behavior of Strip

Some loop tack tests with a stainless steel strip and VHB tape on a rigid surface were carried out at Virginia Tech recently by Stacy Coulthard, who was an undergraduate student in the Department of Engineering Science and Mechanics (ESM). After being tested, the strips were not straight any more, indicating that plastic behavior had occurred. In particular, some of the tapes had a crease at the center, where the last part of the loop debonded from the substrate. An analysis of the loop tack test including these effects has not been reported previously, and will be accomplished in this dissertation. However, the initial debonding of the loop from the substrate is similar to debonding in the peel test, and some studies have considered plasticity effects in the peel test.

Duke (1974) reviewed plasticity theories in peeling for a limited number of cases. A finite element analysis of elastic peeling has been presented by Crocombe and Adams (1981). Crocombe and Adams (1982) extended their finite element analysis to calculate the stress distribution ahead of the interfacial crack for an elastoplastic peel problem. Approximate methods to estimate adherend plastic dissipation based on elementary beam theory were presented by Gent and Hamed (1977). Atkins and Mai (1986) pointed out the importance of the residual strain energy during elastoplastic peeling. Kim and Kim (1988) and Kim and Aravas (1988) published a generalized elastic-plastic slender beam theory for the analysis of the detached part of the adherend in a peel test. They gave a closed-form solution for the maximum curvature, and hence the plastic dissipation, attained by an elastic-perfectly plastic adherend. Their expressions are in terms of the peel force, peel angle, adherend properties, and rotation at the root of the adherend, and it was shown that the plastic dissipation strongly depends on the root rotation. Williams (1993) analyzed the

role of root rotation due to the adherend compliance in the peel test. It was assumed that the adherend behaved elastically at the root, although elastic-plastic behavior was taken into account for the detached part of the adherend. Kinloch et al. (1994) derived a quantitative expression for the energy dissipated by plastic deformation due to bending of the beam and thereby corrected the measured peel force for such energy losses in peeling of laminated materials. Moidu et al. (1995) developed a model for the attached part of the flexible adherend adjacent to the root, by considering the deformation of an elastic-plastic beam on an elastic foundation, but they neglected the effect of foundation shear stresses on the plastic dissipation. Moidu et al. (1998) extended their previous work by including the effects of foundation shear stresses and a linear strain-hardening flexible adherend on the plastic work.

Stacy Coulthard and I conducted uniaxial tensile tests (see Appendices B.1 and B.2) on some Mylar strips and stainless steel strips, using an Instron 4204 testing machine in the ESM department, to determine their yield stresses and strain-hardening characteristics. The results showed elastic-plastic behavior, and the stress-strain curve in loading was almost bilinear, as shown in Figure 1.4, although the transition from elastic to plastic behavior is more gradual than in the ideal case. Therefore a bilinear elastic-plastic relationship will be used in the numerical analysis. In the bilinear model, the continuous curve is approximated by two straight lines, thus replacing the smooth transition curve by a sharp breaking point, the ordinate of which is taken to be the elastic limit stress or the yield strength σ_y. The first straight-line branch of the diagram has a slope of Young's modulus, *E*. The second straight-line branch, representing in an idealized fashion the stress-strain hardening range, has a slope of $E_t < E$. The stress-strain relation for monotonic loading in tension has the form

$$\varepsilon = \frac{\sigma}{E} \qquad \text{for } \sigma \le \sigma_y \tag{1.2}$$

$$\varepsilon = \frac{\sigma_y}{E} + \frac{1}{E_t}(\sigma - \sigma_y) \quad \text{for } \sigma > \sigma_y \tag{1.3}$$

The conventional incremental elastic-plastic models are formulated in terms of a yield criterion, a hardening rule, and a flow rule. The von Mises failure criterion is used to estimate the state of stress at the onset of yielding. An isotropic hardening rule is adapted to define how the yield criterion is modified by straining beyond initial yield. Therefore, the yield surface changes size uni-

formly in all directions such that the yield stress increases (or decreases) in all stress directions as plastic straining occurs. An associated flow rule is used to determine the state of stress at the corresponding plastic strain when an increment of plastic flow occurs. It states that as the material yields, the inelastic deformation rate is in the direction of the normal to the yield surface (the plastic deformation is volume invariant).

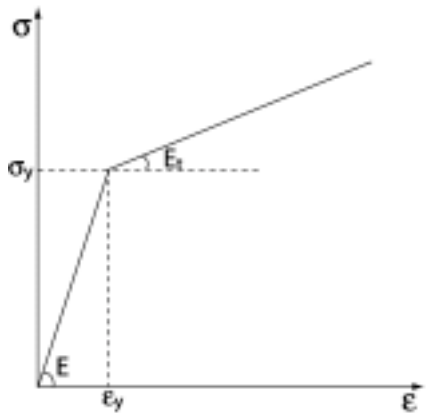

Figure 1.4 Stress-strain curve for elastic-linear work-hardening model

1.8 Anticlastic Bending Behavior of Loop

For applied pure bending along opposite edges as shown in Figure 1.5a, two different curvatures occur through the longitudinal and transverse directions (Figure 1.5b). This is called anticlastic bending behavior. Anticlastic bending behavior is already a well-known phenomenon in the analysis of the behavior of thin rectangular beams and plates. In the loop tack test, thin elastic rectangular strips (stainless steel or Mylar) are used so that we need to consider this effect to predict the contact pattern in the pushing procedure. Anticlastic bending behavior may be more important for small deflection theory. For large deflections this phenomenon may disappear, depending on the thickness-to-width ratio and the Poisson's ratio of the strip. Due to geometrically nonlinear effects, the plate tends to flatten in the transverse direction. In place of the plate

being saddle shaped, it is more cylindrical in nature as shown in Figure1.5c. William (2000) did not take anticlastic curvature into account in her work. Qi (2000) considered this effect in her contact simulation using finite element analysis with ABAQUS.

Lamb (1891) presented the first analytical investigation of this problem for beams and plates. Further research was conducted by Searle (1908), who showed that the shape of the distorted section depends upon the value of the parameter b^2/Rt. Ashwell (1950) gave a complete solution of a governing differential equation similar to Lamb's. Ashwell (1952) developed a theory to deal with initially curved rectangular plates subjected to pure bending about one axis, using von Karman plate theory. Fung and Wittrick (1954, 1955) applied Ashwell's ideas to plates of variable thickness in the lateral direction and plates with trapezoidal and rhombic planforms. Experimental studies of the stresses induced by anticlastic bending were made by Conway and Nickola (1964) and Bellow et al. (1965). Bellow et al.(1965) found that initial imperfections in the plate did not influence their results. Pomeroy (1970) presented expressions for the effect of the lateral flattening on the longitudinal moment-curvature relation. Pao (1970) began to address the anticlastic curvature issue for composite plates. Hyer and Bhavani (1984) investigated experimentally the suppression of anticlastic effects in composite plates and extended Pao's theory, including initial lateral and longitudinal curvature.

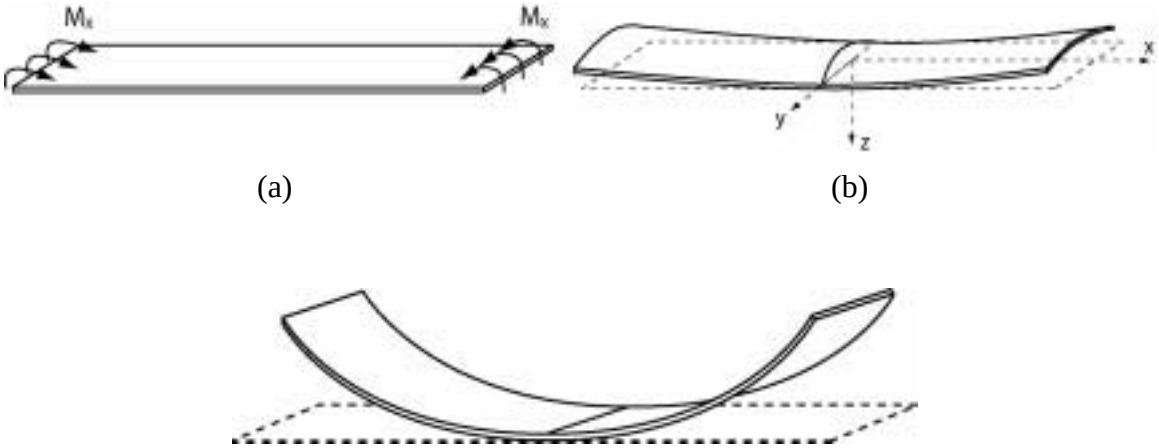

(a) (b)

(c)

Figure 1.5 Anticlastic bending behavior

Based on classic plate theory, consider a plate bent by a uniform bending moment M_x, as shown in Figure 1.5a. The displacement of the middle surface in the z direction measured from the x axis being denoted by *w*, the approximate formulas for curvatures of the plate, analogous to the well-known formula for curvature of a beam, are

$$\frac{1}{R_x} = -\frac{\partial^2 w}{\partial x^2} \qquad \frac{1}{R_y} = -\frac{\partial^2 w}{\partial y^2} \tag{1.4}$$

$$M_x = -\frac{Et^3}{12(1-\nu^2)}\left[\frac{\partial^2 w}{\partial x^2} + \nu\frac{\partial^2 w}{\partial y^2}\right] \tag{1.5}$$

$$M_y = -\frac{Et^3}{12(1-\nu^2)}\left[\frac{\partial^2 w}{\partial y^2} + \nu\frac{\partial^2 w}{\partial x^2}\right] \tag{1.6}$$

where R_x and R_y are the radii of curvature of the middle surface in the longitudinal direction and transverse direction, respectively, t is the thickness of the plate, and ν is Poisson's ratio. These equations define the deflection surface of the plate provided the moments M_x and M_y are given. In the particular case where M_y=0, the rectangular plate (Figure 1.4) is bent as a beam. From equation 1.6 we have for this case

$$\frac{\partial^2 w}{\partial y^2} = -\nu\frac{\partial^2 w}{\partial x^2} \tag{1.7}$$

The plate has two curvatures of opposite sign, so that it is bent into an anticlastic surface as shown in Figure 1.5 (Timoshenko and Gere, 1963).

Initially, when 1/R is very small, the above classical plate theory is valid. However, as 1/R is increased, the effect of the longitudinal membrane forces becomes appreciable and must be considered. According to Lamb's theory, to investigate the transverse distortion, consider a transverse strip of *dx* cut from the plate. The longitudinal membrane forces on either side of this strip arising as a result of the transverse distortion have, because of the longitudinal curvature, a resultant perpendicular to the plate surface. This amounts to a load distributed along the strip which at any point is proportional to the deflection of the strip at that point. The problem is therefore analogous to the problem of a beam on an elastic foundation. By considering an element *dx-dy* cut from the deformed plate (Figure 1.6), the governing differential equation for the deflection of the transverse strip is given by

$$\frac{d^4 w}{dy^4} + 4\alpha^4 w = 0 \tag{1.8}$$

where $4\alpha^4 = \frac{12(1-\nu^2)}{R^2 t^2}$ and R is the radius of curvature of the neutral surface in the longitudinal direction. A general solution of equation 1.8 may be written in the form of

$$w = A\cosh\alpha y\cos\alpha y + B\cosh\alpha y\sin\alpha y + C\sinh\alpha y\sin\alpha y + D\sinh\alpha y\cos\alpha y \tag{1.9}$$

Rewriting equation 1.9 in a nondimensional form, and applying the boundary conditions ($[V_y]_{y=\pm b/2} = 0$, $[M_y]_{y=\pm b/2} = 0$), it follows that

$$\frac{w}{t} = \bar{A}\cosh\alpha y\cos\alpha y + \bar{B}\sinh\alpha y\sin\alpha y \tag{1.10}$$

where $\bar{A} = -\frac{\nu}{\alpha^2 Rt}\frac{\sinh(\alpha b/2)\cos(\alpha b/2) - \cosh(\alpha b/2)\sin(\alpha b/2)}{\sinh\alpha b + \sin\alpha b}$,

$$\bar{B} = -\frac{\nu}{\alpha^2 Rt}\frac{\sinh(\alpha b/2)\cos(\alpha b/2) + \cosh(\alpha b/2)\sin(\alpha b/2)}{\sinh\alpha b + \sin\alpha b}.$$

For given Poisson's ratio, the term αb/2 is directly proportional to the dimensionless ratio $\sqrt{b^2/Rt}$ and it is this ratio which determines the mode of transverse deflections. Equation 1.10 shows that no matter how large b^2/Rt becomes, there is always some distortion at the free edges of the plate (Ashwell, 1950; Conway and Nicola, 1964; Bellow et al., 1965). Throughout 3D finite element analysis in the present study, anticlastic bending behavior is taken into consideration and its dependence on thickness and Poisson's ratio are investigated. More detailed results are specified in a later section.

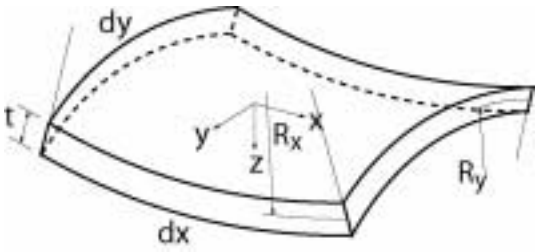

Figure 1.6 Plate element

Chapter 2. EXPERIMENTAL WORK

The tack performance of pressure sensitive adhesives has been investigated experimentally by other researchers. Roberts (1997, 1999) described FINAT test method number 9 for loop tack and compared results of tests. Le et al. (1999) performed loop tack tests on PSA tapes with Mylar or polypropylene backings at Virginia Tech. The loop tack test is used to examine the behavior of a sticky tape consisting of a backing and an adhesive. Two different test methods are usually used. One uses a strip with adhesive on it, and in the other, the adhesive is on the rigid substrate. Once sample preparation steps are done, all types of loop tack test can be performed in the same way. In order to measure mechanical properties of materials used in the loop tack test, various types of tests are carried out. They include uniaxial tensile test, dynamic mechanical analysis test, and Arcan tensile test. Uniaxial tensile test for stainless steel and Mylar strips, and the Arcan tensile test for VHB tape, are described in Appendices B and C. These tests are required to obtain a knowledge of the tensile stress versus strain properties of the strip which forms the tear-drop shape loop of the loop tack test. Especially, the Arcan tensile test for VHB tape shows the force versus displacement relationship in the debonding process.

2.1 Loop Tack Test

Loop tack test experiments were performed by Stacy Coulthard. In the experiments, a strip of stainless steel 12.7mm wide, 0.0254mm-0.1016mm thick (four different thicknesses were used), and 279.4mm long was formed into a loop. The top of the loop was clamped in an Instron tensile testing machine in the Adhesion Mechanics Laboratory. VHB tape was placed on the horizontal platform under the loop where thickness of PSA (h_a) = 1.143mm. The platform was raised at 12mm/min (Figure 1.1). As soon as the contact area reached $25.4\text{mm} \times 12.7\text{mm}$, the platform was lowered at 12mm/min. The force at the clamp was measured, as well as the displacement of the platform, until the loop separated from the adhesive. To obtain consistent results, the test should be conducted under the same environmental conditions (temperature and humidity). Duncan et al. (1999) described specimen preparation and conditioning for the loop tack test. Table 2.1 shows the humidity and the temperature in the laboratory for each experiment.

Throughout the experiments, there are several uncertainties, including the initial position ($h_{initial}$), the contact area ($L_{contact} \times W_{strip}$), the length of the loop (L_{loop}), and alignment of the loop with respect to the substrate plate, where $L_{contact}$ is the length of the contact region in the longitudinal direction, W_{strip} is the width of the strip, and L_{loop} is the length of the loop after it is clamped (Figure 2.1). In the numerical analysis, the initial location is such that the bottom of the teardrop-shape loop contacts only one line through the transverse direction on the adhesive, but in the experiment the initial height of the loop ($h_{initial}$) was usually higher than the numerical one. Therefore, we need to shift the pulling force curve to eliminate initial error. Ideally, the final contact area is fixed as $25.4\text{mm} \times W_{strip}$ at the end of the pushing procedure, but this was not achieved precisely in the experiments, especially for the thinner strips, because measuring the contact length in the experiments only relied on the tester's eye. That is, the pulling procedure started before the contact area reached 25.4mm in some of the experiments. Due to alignment of the loop, the plane of the loop's centroidal curve may not be perfectly normal to the surface plane of the adhesive. Parametric studies have been conducted to understand the effect of experimental uncertainties.

In the numerical analysis, it is assumed that the rigid foundation is stationary and that the clamped top of the loop is moved downward and then upward (Figure 2.1). Figures 2.2, 2.3, 2.4, and 2.5 illustrate curves of the pushing and pulling force (P) versus the displacement at the top of the loop (y_{top}) for different strip thicknesses. The pushing force is plotted as a negative value and the pulling force as a positive value. As was mentioned, tack is defined as the maximum pulling force under conditions of short contact time and low contact force. From the experimental results, it is found that the pushing and pulling force curve trends for different strip thicknesses are similar in that they include an initial transition region, plateau region, and peak force region. However, there are large differences in the maximum pulling force, average pulling force in the plateau region, and area of the pulling zone (Table 2.2-2.5), respectively, even if measured for the same adhesive because of the effect of strip thickness. This is one disadvantage of the loop tack test. Due to experimental uncertainties, the measured curves for each thickness are not identical even though the same strips and adhesives are used. Thus, the repeatability of the experimental results was not very good. At this point one question arises: out of these results for each strip thickness, which result should be chosen to compare with the numerical analysis results? Based on the aver-

age maximum pulling force and area of the pulling zone, one pulling curve is chosen out of the experimental results for each thickness. Figures 2.6, 2.7, 2.8, and 2.9 depict the chosen pulling force curves.

Table 2.1 Environmental conditions during the experiments

Loop thickness, mm	Temperature, °C	Humidity, %	Rate, mm/min
0.0254	22	59-61	12
0.0508	22	56-57	12
0.0762	23	35	12
0.1016	23	23	12

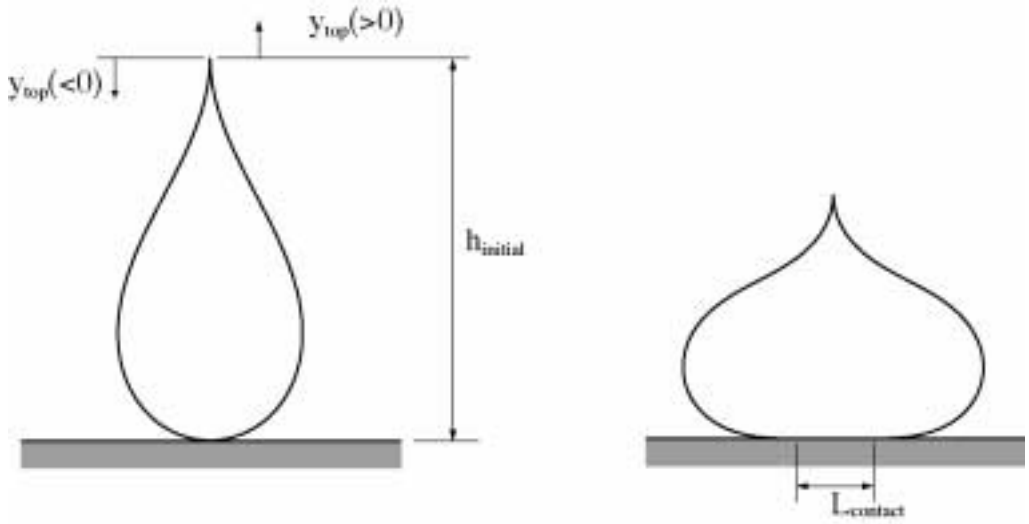

(a) Initial (b) The end of pushing

Figure 2.1 Deformed shape of loop

Table 2.2 Loop thickness = 0.0254mm

Test Number	Minimum y_{top} in Pushing, mm	Maximum y_{top} in Pulling, mm	Maximum Pulling Force, N	$P_{plateau}$, N	Area, mm^2
1	-31	17.58	9.08	no plateau region	32.08
2	-31	17.63	8.94	5.38	23.11
3	-31	18.41	7.81	5.24	29.75
4	-31	18.8	8.64	4.74	34.31
5	-31	18.51	8.35	4.22	27.29
Average			8.56	4.90	29.31

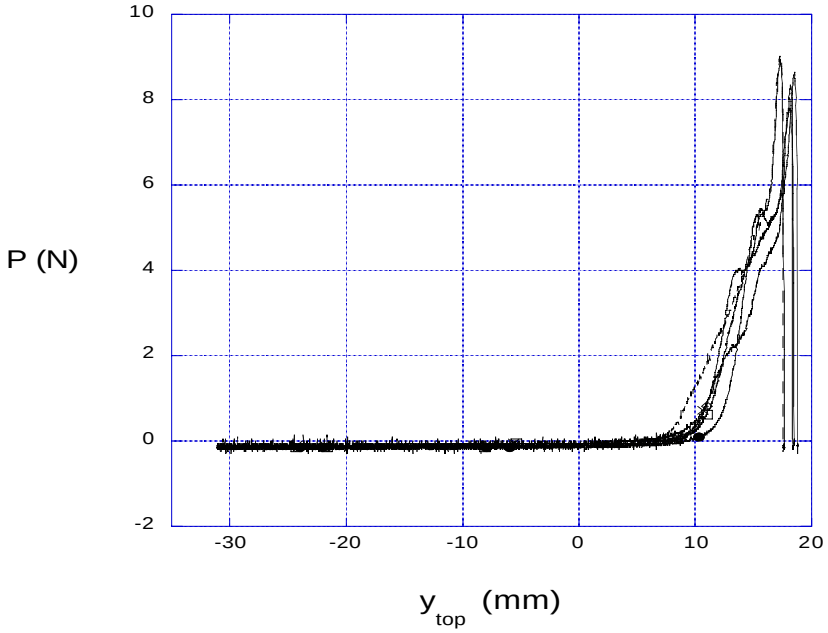

Figure 2.2 Pushing and pulling force vs. y_{top} for loop thickness 0.0254mm

Table 2.3 Loop thickness = 0.0508mm

Test Number	Minimum y_{top} in Pushing, mm	Maximum y_{top} in Pulling, mm	Maximum Pulling Force, N	$P_{plateau}$, N	Area, mm^2
1	-34	19.97	14.84	10.70	80.76
2	-34	19.58	14.60	11.33	82.55
3	-34	20.26	21.73	18.12	123.85
4	-34	19.78	16.94	14.71	103.02
5	-34	20.9	18.07	14.44	113.85
6	-34	19.38	13.87	10.57	70.60
Average			16.68	13.31	95.77

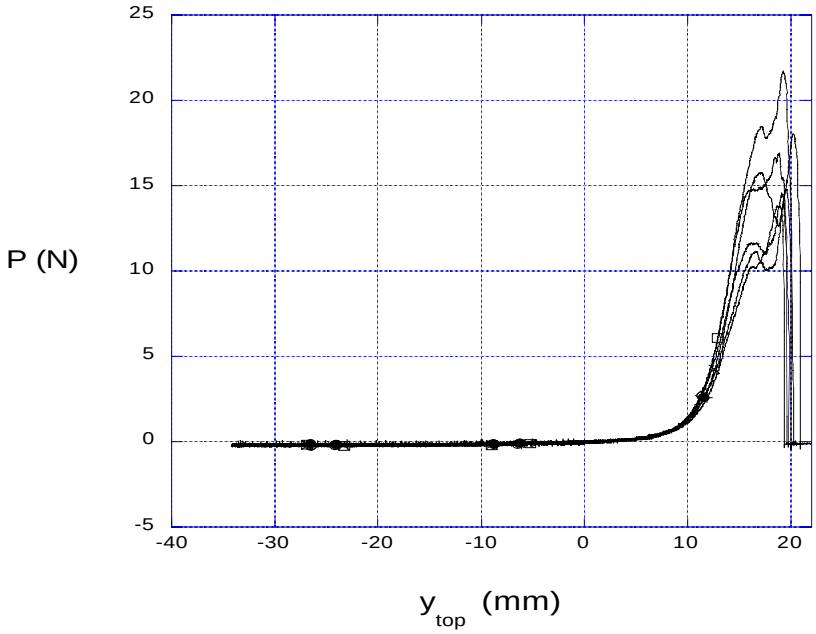

Figure 2.3 Pushing and pulling force vs. y_{top} for loop thickness 0.0508mm

Table 2.4 Loop thickness = 0.0762mm

Test Number	Minimum y_{top} in Pushing, mm	Maximum y_{top} in Pulling, mm	Maximum Pulling Force, N	$P_{plateau}$, N	Area, mm^2
1	-38	23.29	46.48	40.71	390.78
2	-38	19.63	29.49	22.01	205.62
3	-38	21	49.27	38.87	362.99
4	-38	20.8	38.62	30.09	303.03
5	-38	20.07	27.39	16.05	170.52
6	-38	19.24	26.51	20.31	220.88
Average			36.29	28.01	275.64

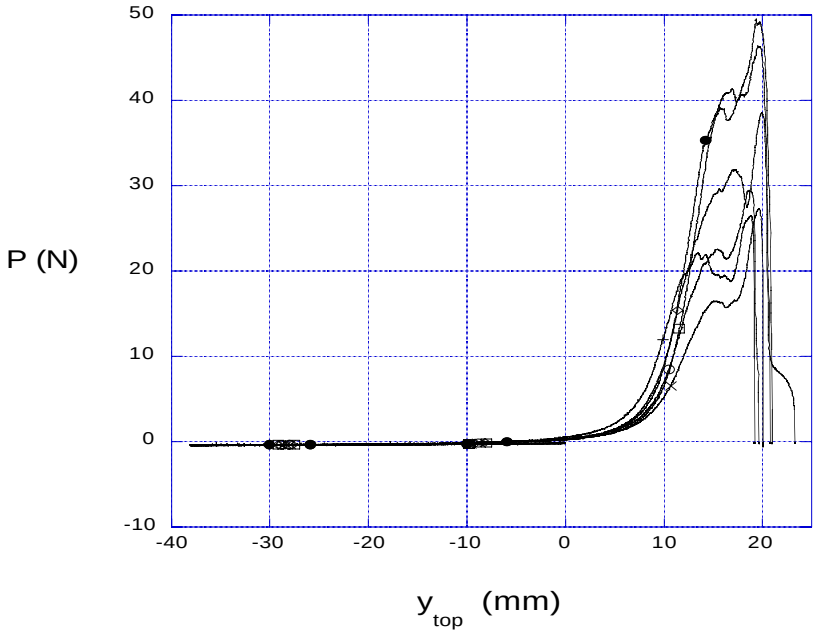

Figure 2.4 Pushing and pulling force vs. y_{top} for loop thickness 0.0762mm

Table 2.5 Loop thickness = 0.1016mm

Test Number	Minimum y_{top} in Pushing, mm	Maximum y_{top} in Pulling, mm	Maximum Pulling Force, N	$P_{plateau}$, N	Area, mm^2
1	-39	18.12	22.12	6.30	100.90
2	-39	18.46	22.22	4.94	93.55
3	-39	18.7	21	5.91	96
4	-39	18.65	17.87	4.43	79.24
5	-39	19.04	17.14	3.72	80.06
6	-39	18.80	18.99	5.21	90.76
Average			19.89	5.08	90.09

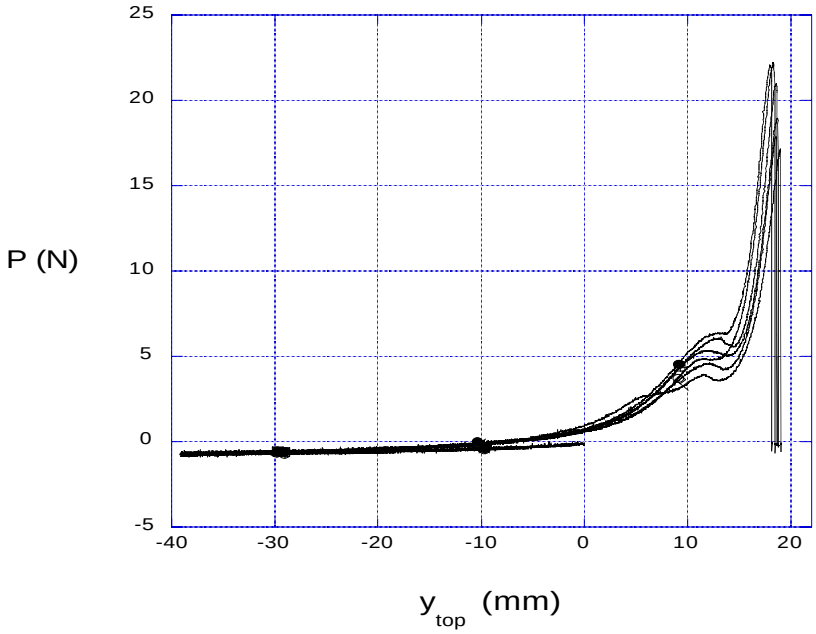

Figure 2.5 Pushing and pulling force vs. y_{top} for loop thickness 0.1016mm

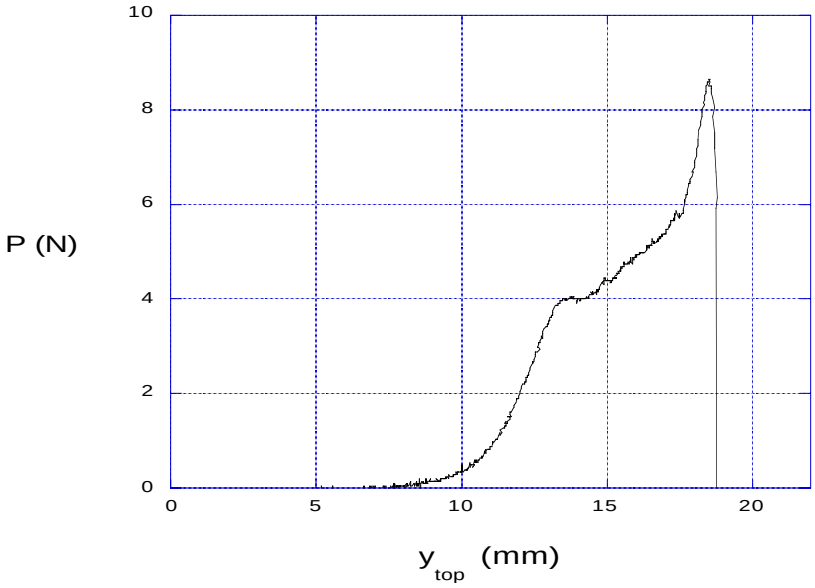

Figure 2.6 Pulling force vs. y_{top} for loop thickness 0.0254mm

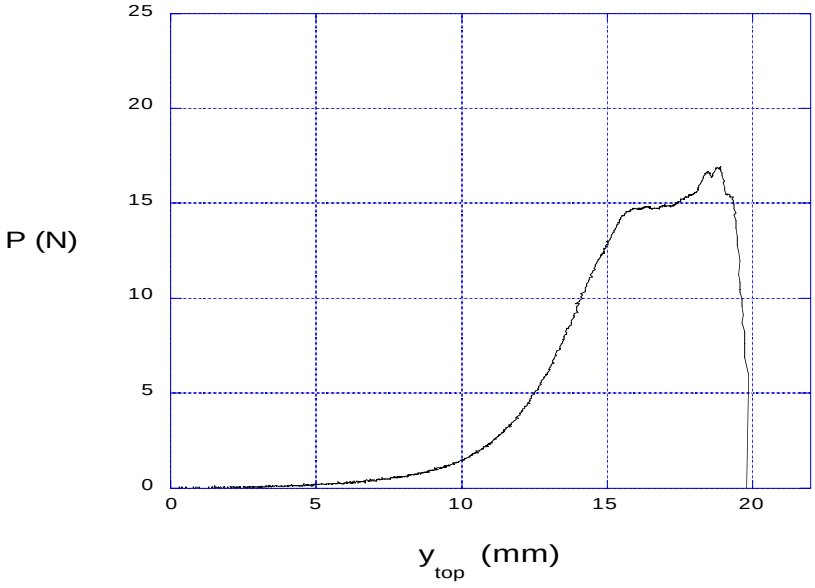

Figure 2.7 Pulling force vs. y_{top} for loop thickness 0.0508mm

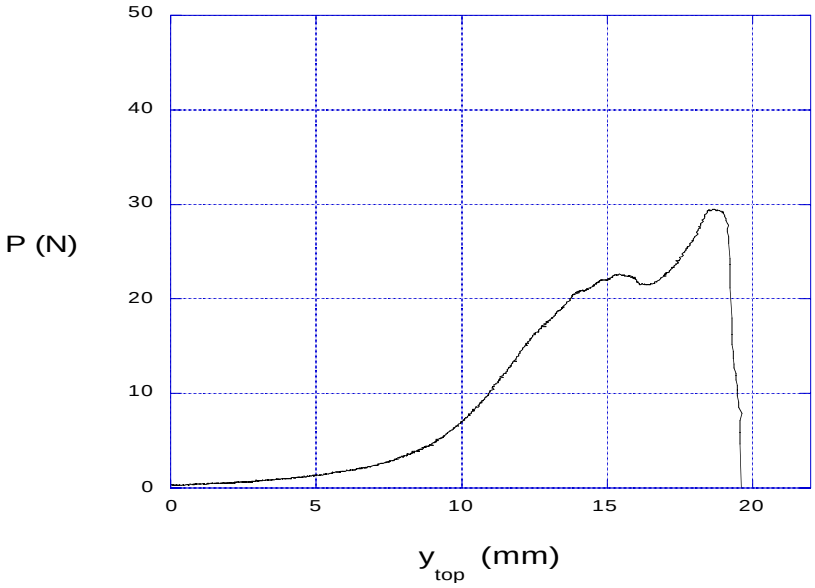

Figure 2.8 Pulling force vs. y_{top} for loop thickness 0.0762mm

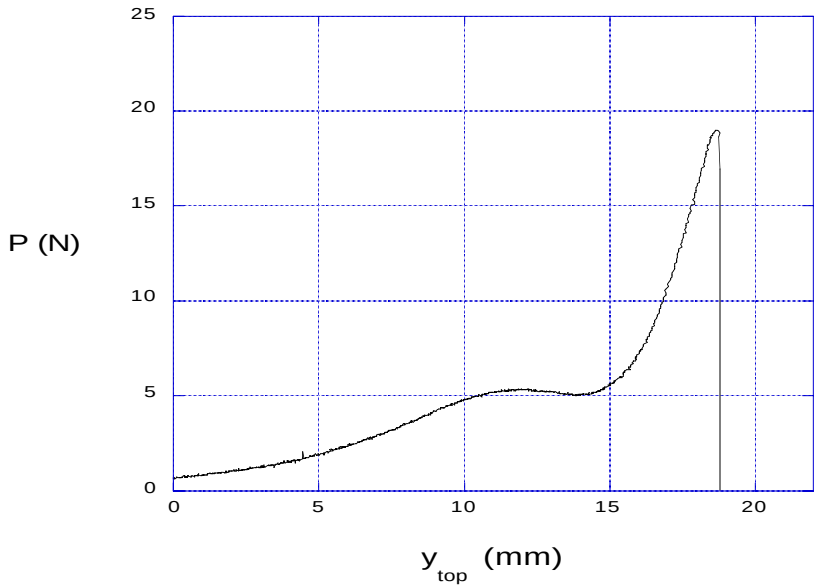

Figure 2.9 Pulling force vs. y_{top} for loop thickness 0.1016mm

2.2 Dynamic Mechanical Analysis Test

Pressure sensitive adhesives are polymers and polymeric materials exhibit viscoelastic properties, that is, they have viscous and elastic properties. The viscoelastic behaviour of the polymers is determined by dynamic mechanical measurements with an instrument with parallel plates as shown in Figure 2.10. Measurements made on a VHB tape in sinusoidal oscillation in shear between parallel plates give stress and strain curves. The stress leads the strain by a phase angle δ. The linear elastic response of the material is proportional to the strain, so it is in-phase with the strain, while the viscous response is proportional to the rate of strain, and it is 90 degrees out-of-phase with the strain. The response can be resolved vectorially into the in-phase component with tensile storage modulus E' and the out-of-phase component with tensile loss modulus E''. Tan δ, the ratio of E'' to E', is called the loss factor (Satas, 1989). The storage modulus E' is associated with energy storage and release during periodic deformation. On the other hand, the loss modulus E'' is associated with the dissipation of energy and its transformation into heat. The ratio $E''/E' = \tan\delta$ is widely used as a measure of the damping capacity of viscoelastic materials. The complex modulus for the mechanical model ($E^* = E' + iE''$) may be detemined by using the constitutive equation of the model.

Dynamic mechanical analysis (DMA) tests were carried out by Lei Zang, who was a graduate student in the Chemistry Department. In Figure 2.11, dynamical mechanical data for VHB tape as a function of temperature are shown. At low temperature in the tensile storage modulus curve, the VHB tape is in the glassy state and it is brittle and stiff, and as the temperature increases, the specimen become flexible and changes into the rubbery state. A plot of the tensile loss modulus has a shape similar to that of tensile storage modulus except for the leftward transition of E'' after it reaches a maximum value as the temperature decreases. The maximum in the tan δ (loss factor) curves in Figure 2.11 (c) occurs at the glass transition temperature (T_g). It is important to note, however, that the position of the peak in the tan δ curve is not only dependent upon temperature, but also upon frequency. Equations for DMA data conversions are specified in Appendix C.

(a)

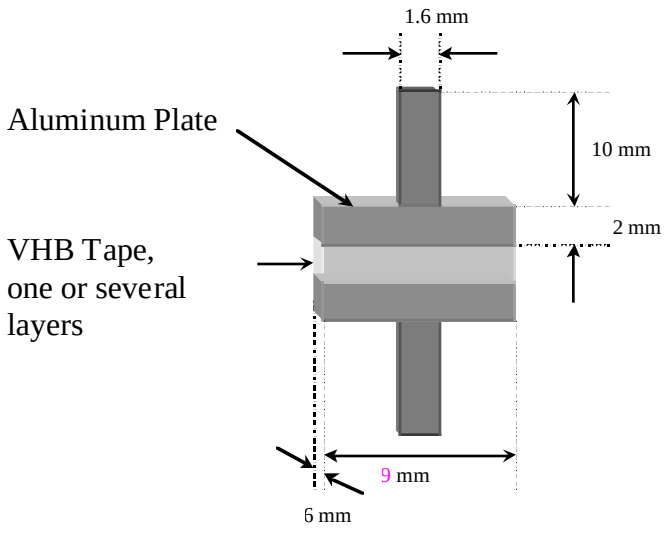

(b)

Figure 2.10 DMA specimen for out-of-plane tensile tests

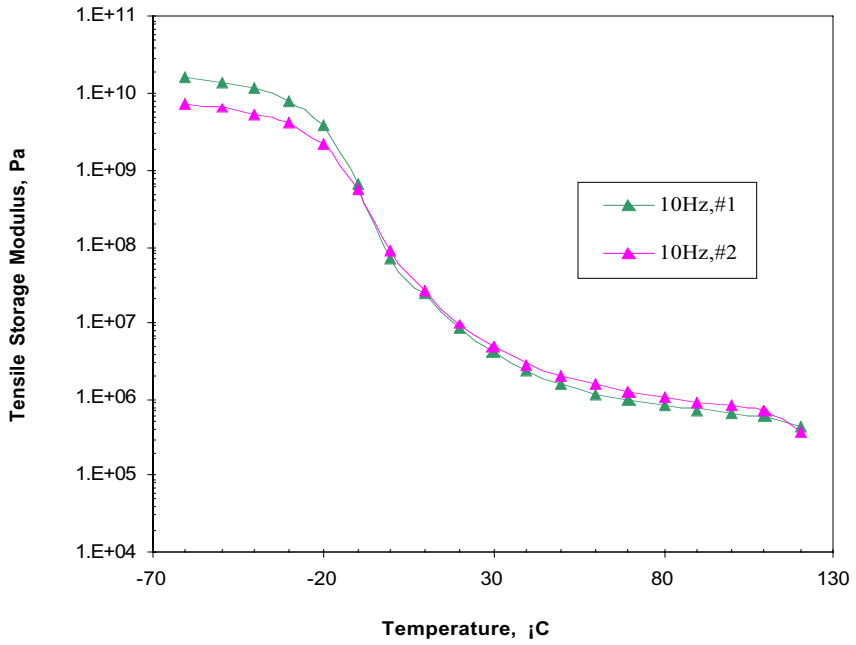

(a) Out-of-plane tensile storage modulus vs. temperature for VHB 4950 1/2”

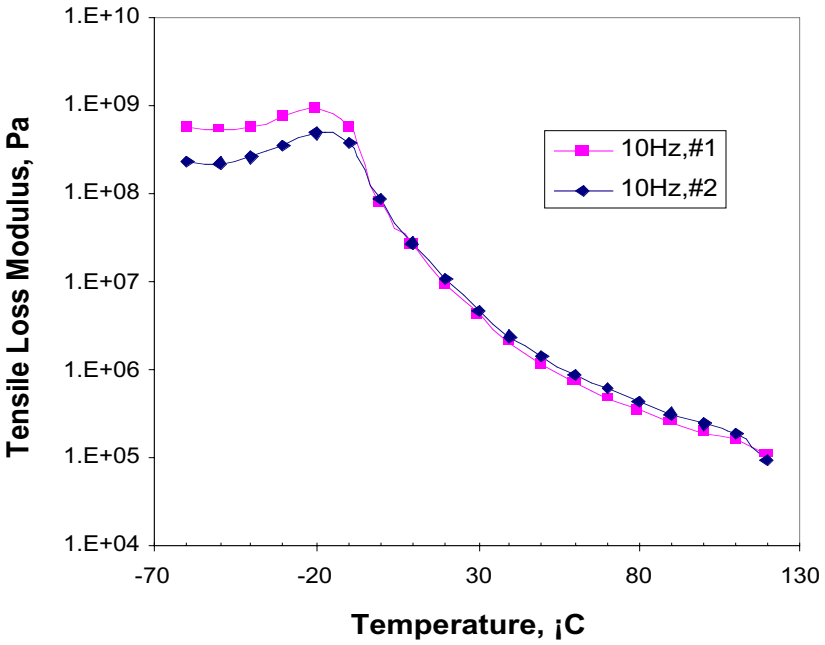

(b) Out-of-plane tensile loss modulus vs. temperature for VHB 4950 1/2”

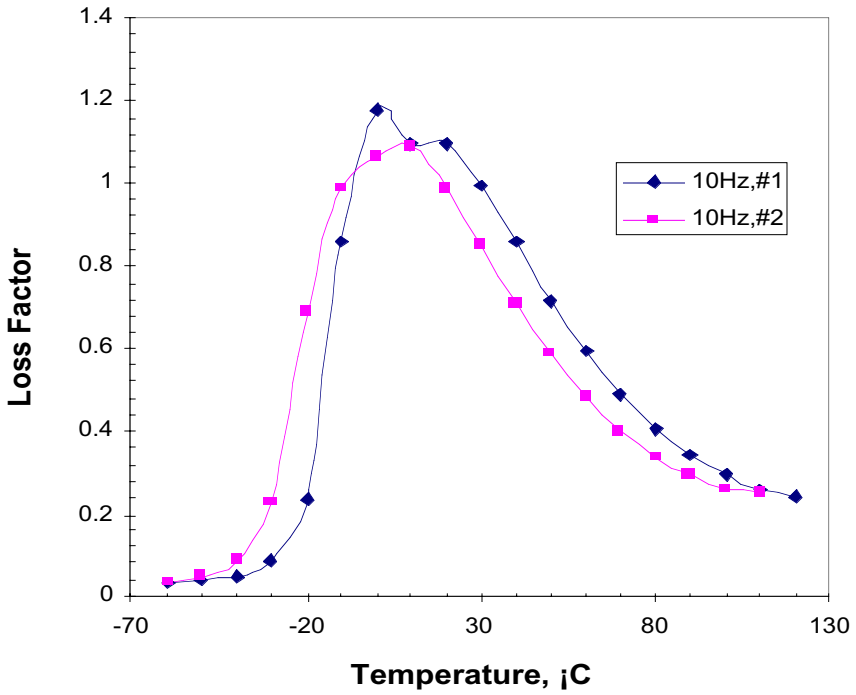

(c) Out-of-plane tensile loss factor vs. temperature for VHB 4950 1/2”

Figure 2.11 DMA test

Chapter 3. NUMERICAL ANALYSIS

In the previous finite element analyses of the loop tack test (Hu et al., 1998; Duncan and Lay, 1999), numerical loop tack test simulation was generated using 2-node, linear, in-plane beam elements. The real test, however, exhibits 3D behavior. Accordingly, a 3D nonlinear finite element analysis is conducted to investigate the 3D behavior of the loop in the initial part of this study. Based on the 3D results, and to save computational time, hybrid beam elements are then used. All simulations of the loop tack test are performed with 3D and 2D finite elements using the commercial finite element program ABAQUS, and it includes a nonlinear problem in several aspects. The loop deformation is large enough that equilibrium equations must be written with respect to the deformed configuration, i.e., it is a geometric nonlinearity problem. The strip material properties are functions of the state of stress or strain, i.e., it is a material nonlinearity problem. ABAQUS is capable of solving problems with both material and geometric nonlinearities.

The model of the strip consists of two materials, stainless steel or Mylar. The Mylar strip model is used to compare anticlastic bending behavior of the loop and the planar deformed shape of the loop throughout the numerical analysis. The pressure sensitive adhesive (PSA) is assumed to be on the substrate as a thin layer, rather than on the loop. The shear stresses in the layer are assumed to be negligible, and the deformation of the PSA is approximated as uniaxial extension of independent adhesive strands. Thus, the adhesive is modeled as a Winkler-type linear elastic foundation or viscoelastic foundation. The strip, considering plasticity, is represented using hybrid beam elements (B21H) or shell elements (S4R). The ABAQUS SPRING1 element is used to define the Winkler-type elastic foundation as a PSA. The vertical stiffness properties of the SPRING1 element are represented by a force-displacement relation which models the bonding and debonding sequence between the strip and the substrate. In the bonding formation, it is assumed that the loop is perfectly bonded to the adhesive and frictionless contact occurs between the loop and the adhesive. To model a Winkler-type viscoelastic foundation, the simplest model, composed of elastic springs and dashpots (Kelvin-Voigt model), is chosen. The ABAQUS SPRING1 and equivalent concentrated load instead of dashpot are considered to describe the Kelvin-Voigt model. Once the strip has formed the teardrop shape, pushing and pulling simulation is conducted by applying the proper displacement to the top of the loop. A parametric study is conducted to investigate the tack of the loop. In Appendix A, using the finite difference method, the 2D no-contact teardrop shape

of the loop is simulated. It is an alternative numerical analysis and only performed for the initial loop formation procedure.

3.1 Modeling of Strip in ABAQUS

For modeling purposes, the strip is represented first using shell elements (S4R) and then using hybrid beam elements (B21H) in ABAQUS. Due to symmetry, a quarter of the loop and a half of the loop were analyzed in three-dimensional and two-dimensional simulations, respectively (Figure 3.1). To consider the plasticity effect of the stainless steel strip or Mylar strip material, stress versus strain curves are idealized by a bilinear elastic-plastic relationship (Figure 3.2) from uniaxial tensile test results. The unloading process occurs in the now-debonded peel strip away from the peel front. Figure 3.3 illustrates transition of the maximum von Mises stress during the loop tack test simulation. More detail results about the plasticity effect are presented in chapter 5. Uniaxial tension tests were conducted to obtain the tensile stress versus strain properties of the material (Appendix B). ABAQUS requires the use of the true stress versus the logarithmic plastic strain relationship for the inclusion of the material nonlinearity. This must be determined from the engineering stress-strain relationship using $\sigma_{true} = \sigma_{eng}(1 + \varepsilon_{eng})$ and $\varepsilon_{\ln} = \ln(1 + \varepsilon_{eng})$. Large-strain conditions were used, with the von Mises yield criterion, isotropic strain-hardening, and associated plastic flow.

Hybrid beam elements are provided for use in cases where it is numerically difficult to compute the axial and shear forces in the beam by the usual finite element displacement method. This problem arises most commonly in geometrically-nonlinear analysis when the beam undergoes large rotations and is very rigid in axial and transverse shear deformation, such as a flexing long pipe or cable. The problem in such cases is that slight differences in nodal positions can cause very large forces which, in turn, cause large motions in other directions. The hybrid elements overcome this difficulty by using a more general formulation in which the axial and transverse shear forces in the elements are included, along with the nodal displacements and rotations, as primary variables. Although this formulation makes these elements more computationally expensive, they generally converge much faster when the beam's rotations are large and, therefore, are more efficient overall in such cases (ABAQUS, 1997). Thus, the hybrid beam element is more suitable than the normal

beam element in the case of geometric nonlinear problems. However, the calculations were terminated, even when using hybrid beam elements, after the peak pulling force was reached. This computational difficulty may be posed by ill-conditioning, that is, large stiffness differences between loop and springs that occur after a certain top displacement of the loop. However, it occurs after the peak pulling force has been achieved, and is not critical problem.

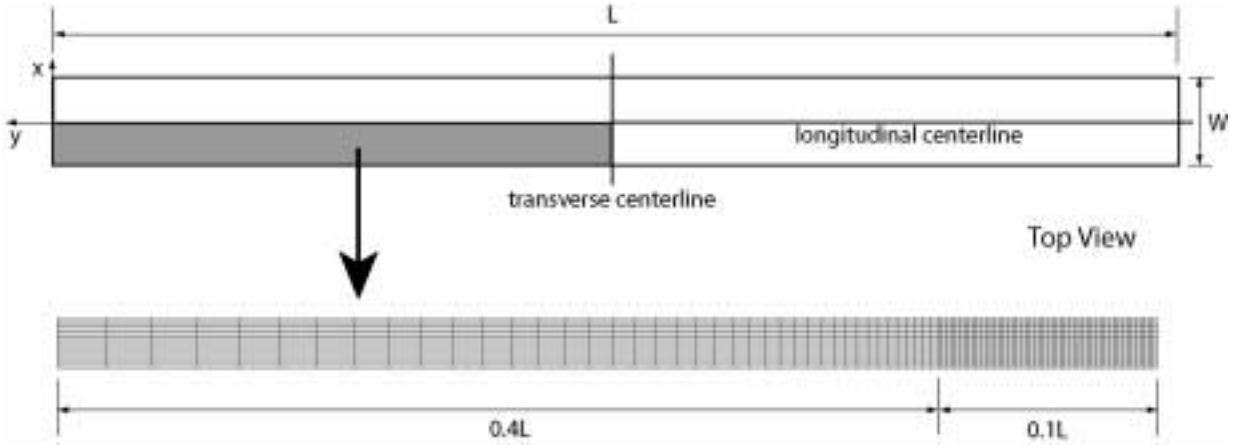

(a) 3D modeling

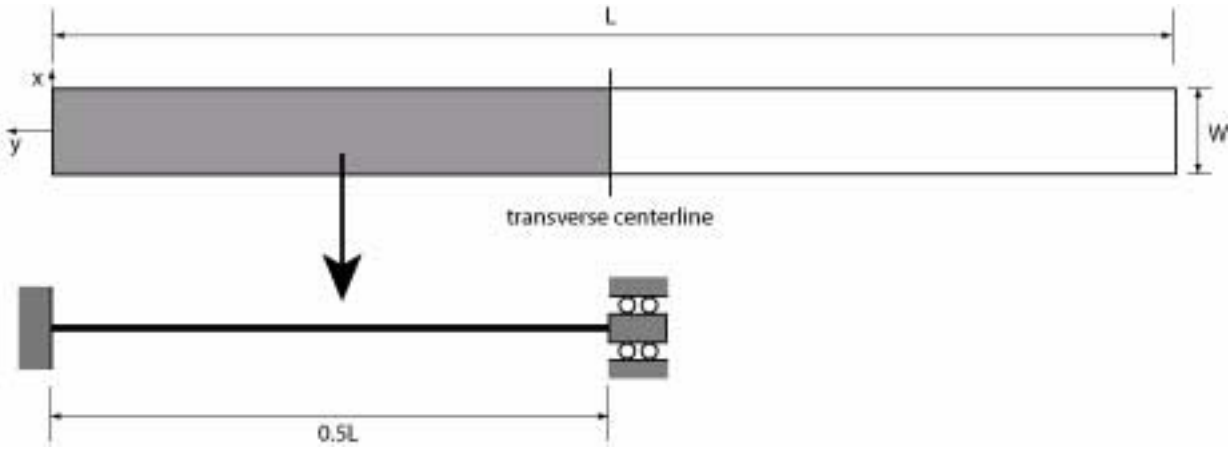

(b) 2D modeling

Figure 3.1 3D and 2D strip modeling

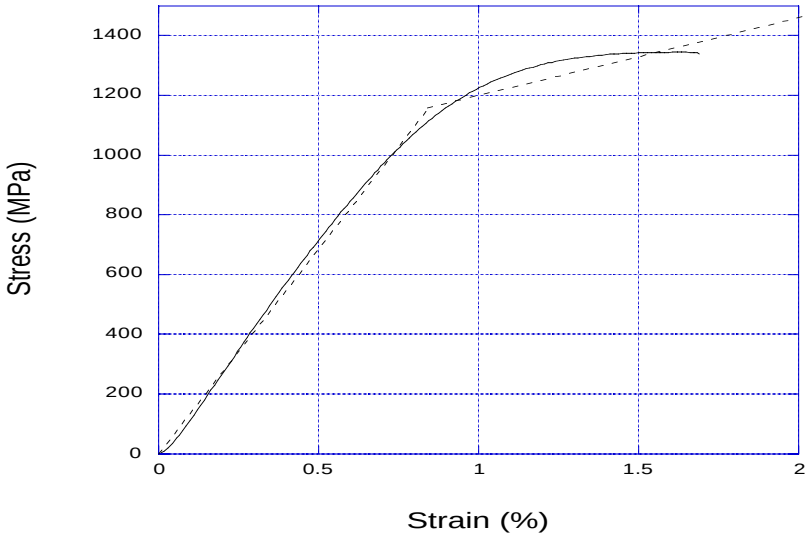

(a) Stainless steel

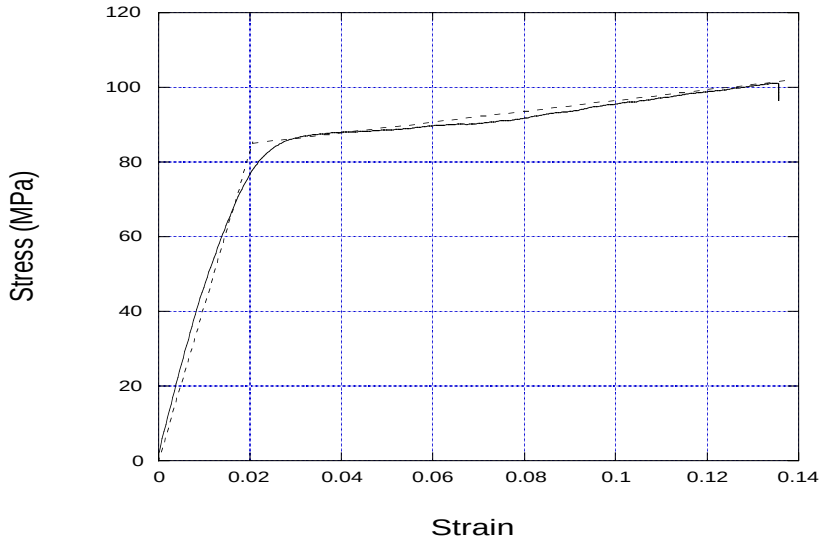

(b) Mylar

Figure 3.2 Stress versus strain curves; Dashed line: approximate bilinear relationship

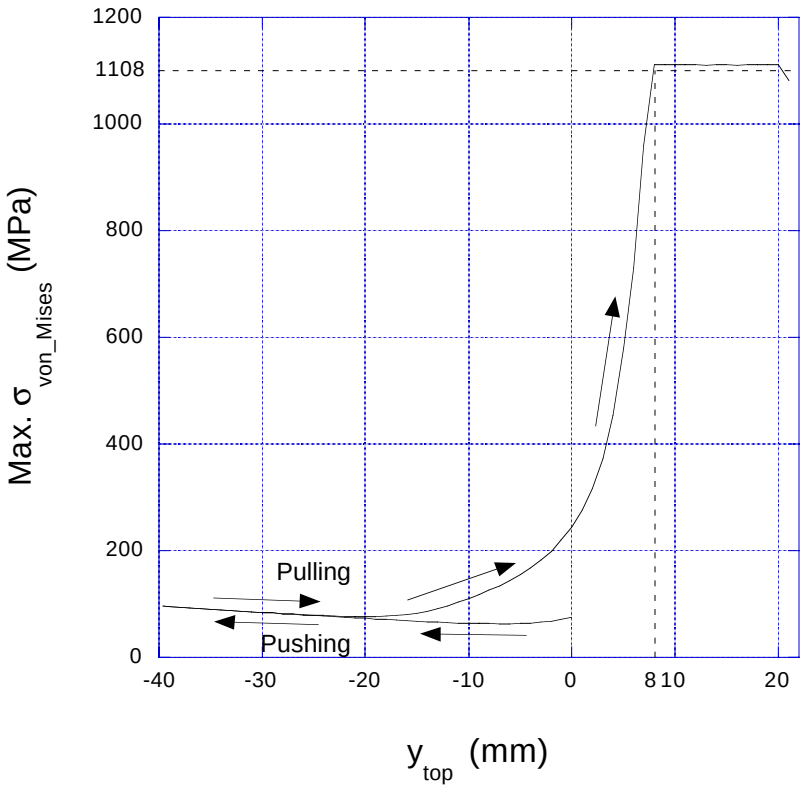

Figure 3.3 Maximum von Mises stress versus y_{top} curve for stainless steel strip (0.0254mm)

3.2 Simulation of Teardrop Shape: Loop Formation in ABAQUS

In order to form the teardrop shape of the loop from the initial flat strip, the following process is used in the finite element simulation, shown in Figure 3.4. The displacement control method is used through the numerical analysis. Recently, Qi (2000) used this method to develop her simulation in ABAQUS. The initial boundary conditions are shown in Figure 3.1(b). In the 3D analysis, the boundary condition along the left end is clamped, the longitudinal centerline has a symmetric boundary condition, and the transverse centerline is allowed to have y direction translation. In the 2D analysis, the left end is clamped and the right end is only allowed y direction translation because of symmetry. The 3D loop model consists of a total of 1911 nodes and 1800 shell elements (S4R) as shown in Figure 3.1(a). The 2D loop model includes a total of 91 nodes and 90 hybrid beam elements (B21H). A finer mesh is created in an area of $0.1L \times \frac{W}{2}$ near the transverse centerline to capture the localized curvature and contact with the adhesive. To avoid abrupt changes in element size, the spacings of the nodes are gradually changed from the left end to 0.4L (Figure 3.1(a)) where L is the total length of the initial flat strip. Even if element aspect ratios are satisfactory for an abrupt element size change, a disturbance appears in the gradient field in the neighborhood of the abrupt change. The element size in the fine mesh part is $0.5588\text{mm} \times 0.3175\text{mm}$.

At first, a certain amount of rotation is applied to the right end until the angle of the right end support is $90°$ from the initial boundary condition ($=0°$), as shown in Figure 3.5. Applying displacements in a simulation procedure, we must control step increments to avoid errors in ABAQUS. Even though ABAQUS controls step increments in nonlinear finite element analysis by itself, the user should assign appropriate values to achieve satisfactory results. Once the strip has formed the teardrop shape, a displacement is applied to the top of the teardrop shape loop until a contact length of 25.4mm is reached. Then a displacement is applied to the top of the loop in the opposite direction until the loop pulls off the substrate. Since the contact pattern depends on the thickness and elasticity modulus of the strip, in order to define nonlinear springs in accordance with contact of each node, the displacement increment of the top of the loop (dy_{top}) in the pushing procedure is not constant. However, the displacement increment of the top of the loop (dy_{top}) in the pulling procedure is constant, for example, dy_{top} = 1mm up to y_{top}=0 and dy_{top} = 0.1mm until the loop pulls off the substrate. Figure 3.4 shows the deformed shape at three steps during applica-

tion of rotation to the right end (transverse centerline) in 3D finite element analysis. Only a quarter of the strip is shown because of symmetry. Figure 3.4(c) is the last configuration in the loop formation procedure, which has achieved a quarter teardrop shape of the loop.

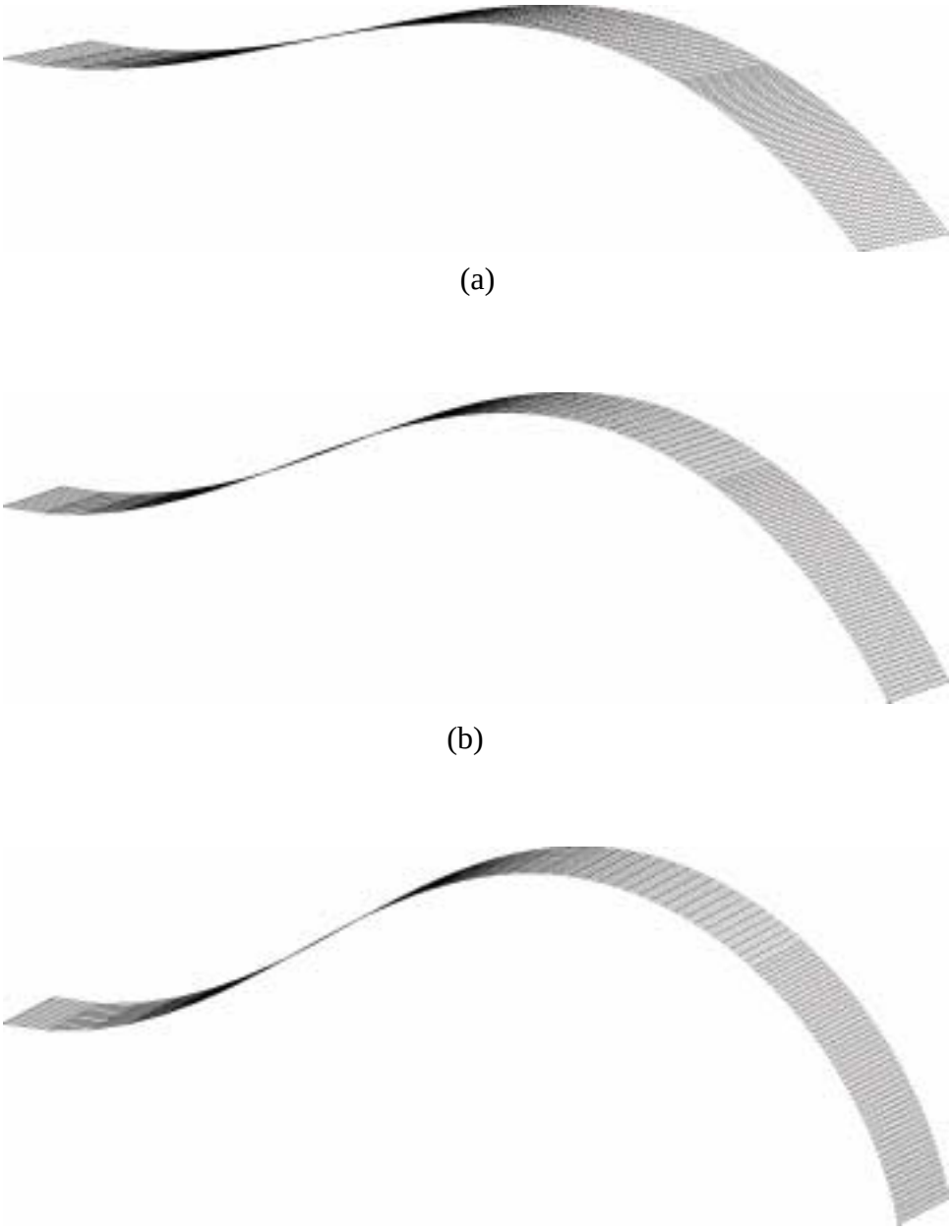

(a)

(b)

(c)

Figure 3.4 Simulation of forming the loop in ABAQUS (3D)

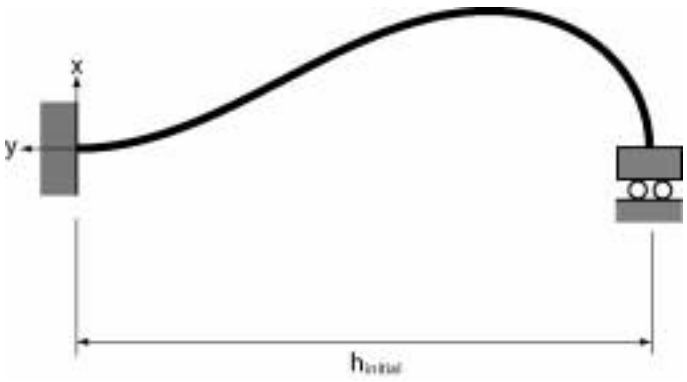

Figure 3.5 Formed loop in ABAQUS (2D)

3.3 Modeling of Pressure Sensitive Adhesive in ABAQUS

3.3.1 Elastic springs

The adhesive is replaced by Winkler-type elastic or viscoelastic foundations. For the elastic case, the assumed force-displacement relationship for each nonlinear spring is illustrated in Figure 3.6. Throughout the numerical analysis, the tensile force-displacement relationship for each elastic spring has the same form as that adopted by several researchers (e. g., Wei and Hutchinson, 1998; Yang et al., 2000; Kafkalidis et al., 2000; and Yang and Thouless, 2001). Wei and Hutchinson (1998) employed a traction-separation relation to model the interface as a condition linking continuum descriptions of the film and the substrate in the peel test. Yang et al. (2000) conducted a numerical 2-D study of the symmetrical $90°$ peel test using ABAQUS. In that study, the interface was replaced by user-defined elements that simulated a similar traction-separation relationship. Kafkalidis et al. (2000) also used a trapezoid shape traction-separation law to model the adhesive layer for plastically-deforming, ahesively-bonded joints. The results of the Arcan tensile test (see Appendix C) also show a similar trend.

The force-displacement relationship is made up of a compression zone defining bonding formation and a tension zone defining debonding of the adhesive. In the compression zone, it is assumed here that the deflection of the spring into the foundation should not be greater than 20% of the thickness of the adhesive. The force of the spring in the compression zone is defined as follows:

$$Force = E(y_{spring})\frac{y_{spring}}{h_a}\mathrm{A}_1 \tag{3.1}$$

where A_1 is the tributary area at the node. Usually $\mathrm{A}_1 = 7.097\mathrm{mm}^2$ in the 2D analysis, but at the right end nodes it is half of this value (A_2) because of symmetry. In the case of 3D analysis it is necessary to consider three different tributary areas, which are $\mathrm{A}_1 = 0.1774\mathrm{mm}^2$ (for nodes at the inside of the strip), $\mathrm{A}_2 = 0.0887\mathrm{mm}^2$ (for nodes at the x-y centerline), and $\mathrm{A}_3 = 0.0444\mathrm{mm}^2$ (for nodes at the corner).

The function $E(y)$ in the compression zone is chosen to approach infinity as $y \to -d$ and to be almost constant for small negative values of *y*. Based on this, $E(y)$ is chosen as follows:

$$E(y) = E_{01}\left[1 + \frac{c_1 y^{2n}}{(d^2 - y^2)^m}\right] \tag{3.2}$$

For example, in the case of adhesive thickness h_a=1.143mm, we use n=2, m=2, c_1=1, d=0.2h_a, y=y_{spring}:

$$E(y_{spring}) = E_{01}\left[1 + \frac{y_{spring}^4}{\{(0.2h_a)^2 - y_{spring}^2\}^2}\right] \tag{3.3}$$

Figure 3.7 (a) shows a plot of equation 3.2 and Figure 3.7 (b) presents the force versus displacement relationship of the nonlinear spring in the compression zone.

The initial slope of the tension field is assumed to be the same as the initial slope of the compression zone, i.e., it is the same as the elasticity modulus (E_{01}) of the PSA at y=0. The elasticity modulus (E_{01}) is determined from DMA test results. As shown in Figure 3.6 and equation 3.4, the failure criterion for debonding assumes that the adhesive will debond when it reaches a certain length ($(\beta_1 + \beta_2 + \beta_3)h_a$). The force-displacement curve from the Arcan tensile test (see Appendix C) offers a way to characterize debonding (the formation and growth of fibrils) quantitatively. However, the behavior of the PSA from the Arcan tensile test and the loop tack test may be different because of the different experimental methods. Therefore, the Arcan tensile test may just suggest a trend of the load versus displacement curve and rough β_1, β_2, and β_3 values.

In the 2D analysis the PSA is modeled with 24 spring elements (SPRING1) in the y direction and springs are attached to nodes throughout the contact length (25.4mm). The 480 spring elements (SPRING1) are taken into account in the contact area ($25.4\text{mm} \times 6.35\text{mm}$) for 3D analysis. The number of springs is dependent upon the number of nodes in the contact area; that is, if the mesh is refined further, then more springs will be needed. Figure 3.8 illustrates the pushing and pulling procedure with the Winkler-type elastic foundation in 2D finite element analysis. The shear deformation in the adhesive is disregarded. Instead of using contact simulation in ABAQUS, contact between loop and adhesive is defined by a different process, as given in Figure 3.9. First all springs at nodes in the subsequent contact area are defined together and they are inactivated. Then, in the bonding procedure, each spring activates as soon as the node on the loop at the top of the spring reaches the substrate. In the debonding procedure, activated springs work continuously until the total spring elongation reaches $(\beta_1 + \beta_2 + \beta_3)h_a$.

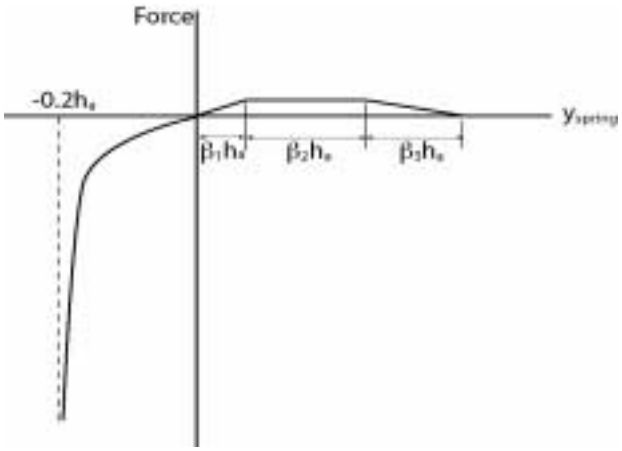

Figure 3.6 Nonlinear spring function in ABAQUS

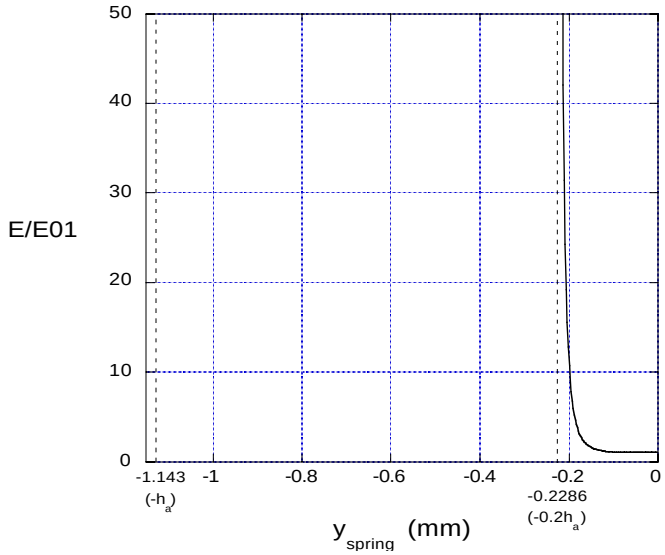

(a) $E(y_{spring})/E_{01}$ vs. y_{spring}

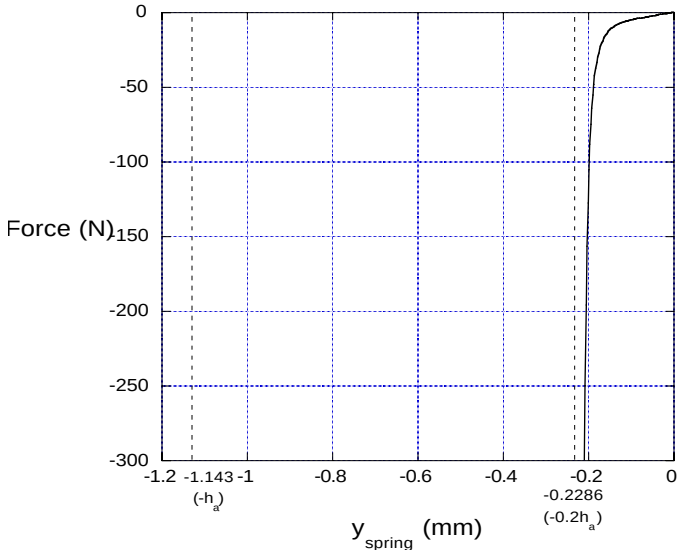

(b) Force vs. y_{spring}

Figure 3.7 $E(y_{spring})$ and force correspond to y_{spring}

The algorithm of how the nonlinear spring works is presented as follows:

$$F = \begin{cases} E(y_{spring})\dfrac{y_{spring}}{h_a}\mathrm{A}_1 & if \;\; -0.2h_a < y_{spring} < 0 \\ \alpha y_{spring} & if \;\; 0 \le y_{spring} < \beta_1 h_a \\ \alpha\beta_1 h_a & if \;\; \beta_1 h_a \le y_{spring} < (\beta_1+\beta_2)h_a \\ -\dfrac{\alpha\beta_1}{\beta_3}\{y_{spring} - (\beta_1+\beta_2+\beta_3)h_a\} & if \;\; (\beta_1+\beta_2)h_a \le y_{spring} < (\beta_1+\beta_2+\beta_3)h_a \\ 0 & if \;\; (\beta_1+\beta_2+\beta_3)h_a \le y_{spring} \end{cases} \tag{3.4}$$

where $E(y_{spring}) = E_{01}\left[1 + \dfrac{y_{spring}^4}{\{(0.2h_a)^2 - y_{spring}^2\}^2}\right]$ and $\alpha = \dfrac{\mathrm{A}_1 E_{01}}{h_a}$.

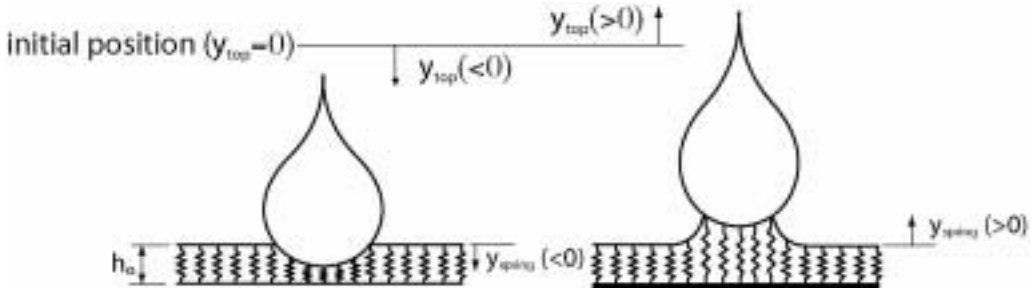

Figure 3.8 Pushing and pulling phases with Winkler-type elastic foundation

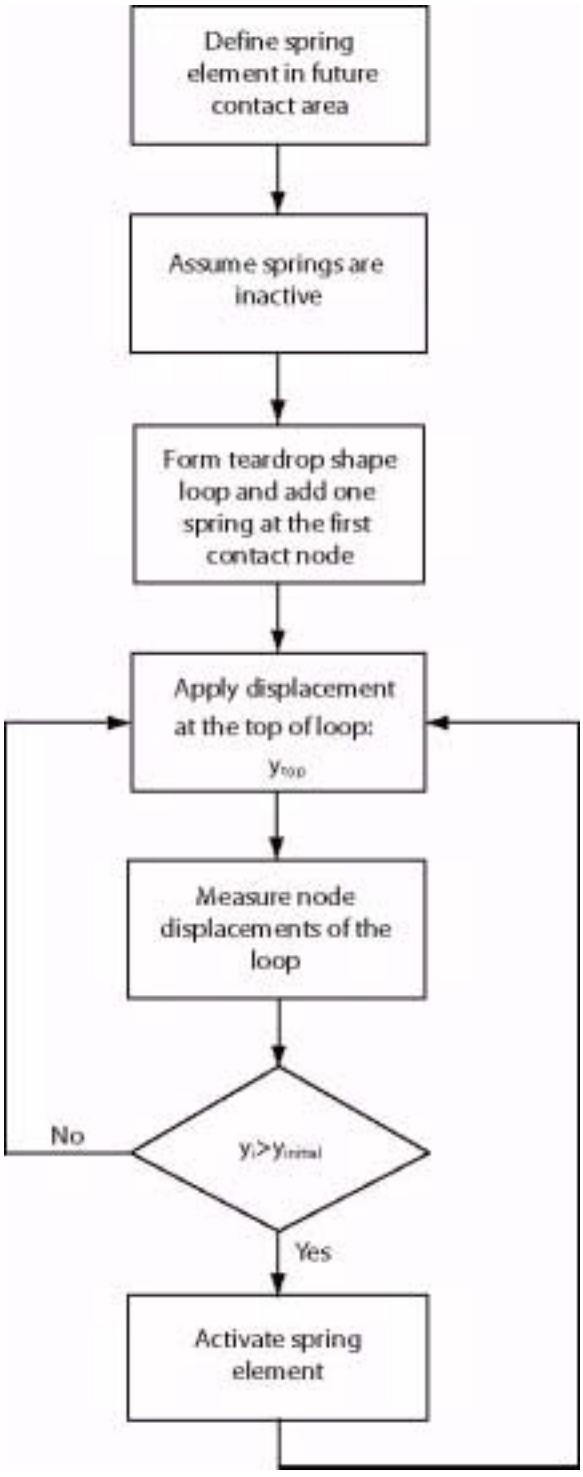

Figure 3.9 Flowchart for elastic springs

3.3.2 Viscoelastic Model

Various mechanical models have been suggested to describe the behavior of pressure sensitive adhesives in peel. Hata (1985) suggested that the deformation of the PSA is approximated as uniaxial extension of independent adhesive strands. Using a set of parallel Maxwell elements the adhesive's rheological properties were modeled. He assumed that the failure criterion for debonding of these extended adhesive strands from the substrate is based on reaching a critical value of the stored elastic energy density in the strand. More recently, Mizumachi (1985), Hatano (1989), and Tsukatani (1989) have applied Hata's method, using the two-element model and treating the parameters of the Maxwell element models, to the problem of predicting the rolling friction coefficient of PSAs as a function of speed and temperature, and have provided modifications to account for the bonding process as well as the debonding process (Yarusso, 1999). Yarusso (1999) also followed Hata's suggestion and employed a generalized Maxwell model description of the adhesive rheology to the prediction of peel force versus peel rate master curves for PSAs, obtaining the parameters of the model from the measured dynamic mechanical properties.

We assume that mechanical behavior of the pressure sensitive adhesive can be described by Winkler-type viscoelastic foundations. A Kelvin-Voigt model is adopted, as shown in Figure 3.10. This model consists of a spring and viscous dashpot in parallel. The constitutive equation of a Kelvin-Voigt model is

$$\sigma = E\varepsilon + \eta\dot{\varepsilon} \tag{3.5}$$

The viscoelastic properties of VHB tape were measured in DMA tests as presented in Chapter 2.2. Through the use of complex variables, a viscoelastic material which is subjected to the strain history $\varepsilon(t) = \varepsilon_0 \sin\omega t$ has the stress response

$$\sigma(t) = E'(\omega)\varepsilon_0 \sin\omega t + E''(\omega)\varepsilon_0 \cos\omega t \tag{3.6}$$

where E' is the tensile storage modulus and E'' is the tensile loss modulus. Since $\dot{\varepsilon} = \varepsilon_0 \cos\omega t$, equation 3.6 can be written as

$$\sigma(t) = E'(\omega)\varepsilon + \frac{E''(\omega)}{\omega}\dot{\varepsilon} \tag{3.7}$$

A comparison of equation 3.5 with equation 3.7 suggests the association with the spring constant E and the viscosity η as follows:

$$E = E' \text{ and } \eta = \frac{E''}{\omega} \tag{3.8}$$

In the present study, for the Kelvin-Voigt model, the same nonlinear elastic spring element is attached at the node for the spring element and the dashpot is replaced by an equivalent load instead of attaching a dashpot element. The equivalent dashpot force is generated as follows:

$$F = A\eta\dot{\varepsilon} = A\eta\frac{d\Delta}{dt}\frac{1}{h_a} = c\dot{\Delta} \tag{3.9}$$

where $\dot{\Delta} = \frac{d\Delta}{dt}$ is the elongation rate, $c = \frac{A\eta}{h_a}$ is the damping coefficient, A is the tributary area at the node (it is the same as in the elastic spring case), and h_a is the adhesive thickness. Substituting $dt = \frac{|dy_{top}|}{v_{top}}$ into equation 3.9, the following equivalent dashpot force is obtained:

$$F_{i+1} = cv_{top}\frac{d\Delta}{|dy_{top}|} = cv_{top}\frac{(y_{i+1} - y_i)}{|(y_{top})_{i+1} - (y_{top})_i|} \tag{3.10}$$

where i is the step number. In applying y_{top}, the dashpot force is updated at every step. The failure criterion of the dashpot is the same as for the elastic spring, i.e., when the elastic spring debonds, the dashpot will be released simultaneously. Figure 3.11 shows the algorithm of how the equivalent dashpot force is applied.

The behavior of most real viscoelastic materials cannot be described very well by Kelvin or Maxwell models (which have only two parameters). More complicated models with larger numbers of adjustable parameters should be used to approximate more closely the behavior of real materials.

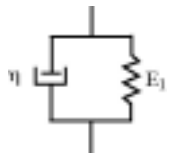

Figure 3.10 Kelvin model

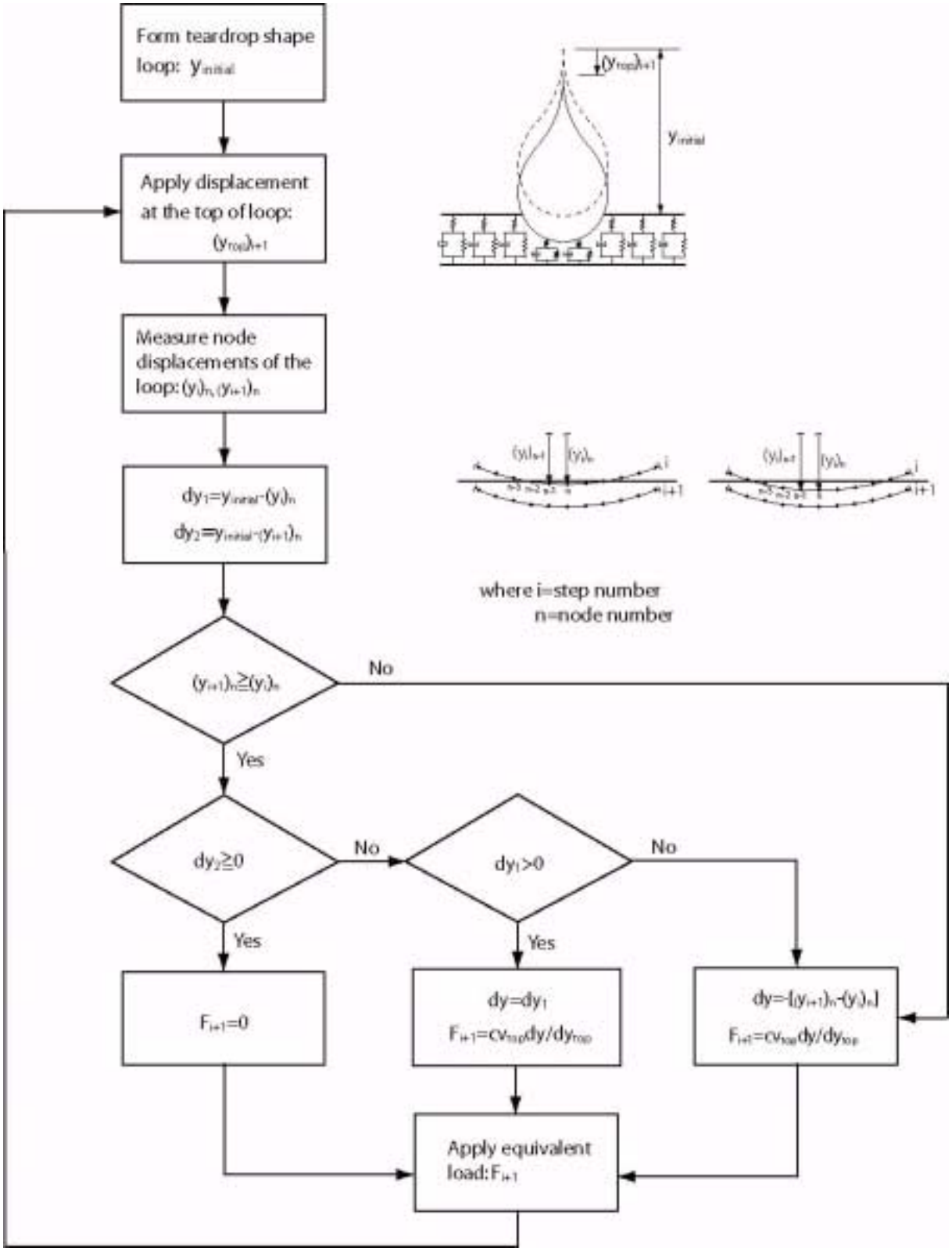

Figure 3.11 Flowchart for viscoelastic model

Chapter 4. PARAMETRIC STUDY

The pulling force curve is considered for several cases, using the 2D analysis, after the displacement at the top of the loop (y_{top}) reaches the initial location during the pulling procedure. Figure 4.1 shows a typical pulling force curve. It is classified in three regions, which are the initial transition region, plateau region, and peak pulling force region, respectively. The pulling force at each value of y_{top} is generated by the total forces in the springs. The maximum force reached as the loop is pulled off the substrate is called the tack or pull-off force. Unlike the results of Williams (2000), the pulling force versus top displacement (y_{top}) of the loop shows a plateau and a final sharp peak in the present numerical results, as in the experimental results. The existence of fibrils during debonding, and stretching of the loop during pulling, may cause a plateau region to occur before the peak pulling force is reached. As each result shows, even though the trend of the pulling force versus top displacement of the loop agrees approximately with the experimental results, there are still differences between the numerical and experimental results. Therefore, it is necessary to do a parametric study in order to show how each parameter contributes to the pulling force curve.

Different parameters considered to investigate the tack of the pressure sensitive adhesive are: (1) nonlinear spring function parameters β_1, β_2, and β_3; (2) contact area ($L_{contact} \times W_{strip}$); (3) length of loop ($L_{loop}$); and (4) strip thickness (t_{strip}). Details of the parameters are specified in Tables 4.1 and 4.2. The size of the stainless steel strip is the same as used in the experiments. The mechanical properties of the strip are $E = 153\text{GPa}$, $\nu = 0.27$, and the yield stress is taken to be $\sigma_y = 1108.8\text{MPa}$. The adhesive is spread as a Winkler-type elastic foundation and the modulus of elasticity (E_{01}) is kept equal to 8MPa in the parametric study. This value is obtained from the DMA test for VHB tape when the laboratory temperature is $23°C$. The influence of different moduli of elasticity (E_{01}) in the springs is studied in next chapter. Throughout the parametric study, the displacement at the top of the loop, the peak pulling force, area of the pulling zone, and average pulling force in the plateau region are quantified and graphically depicted. The area of the pulling zone represents the energy required to separate the adhesive from the loop. It is related to peel and tack. The pushing force curve is identical, even though different nonlinear spring functions are selected in the numerical analysis. So the total spring force curves in the pushing phase

are not specified in the parametric study. However, the pushing force curves are variable according to different thicknesses with the same nonlinear spring function, as given in section 4.4.

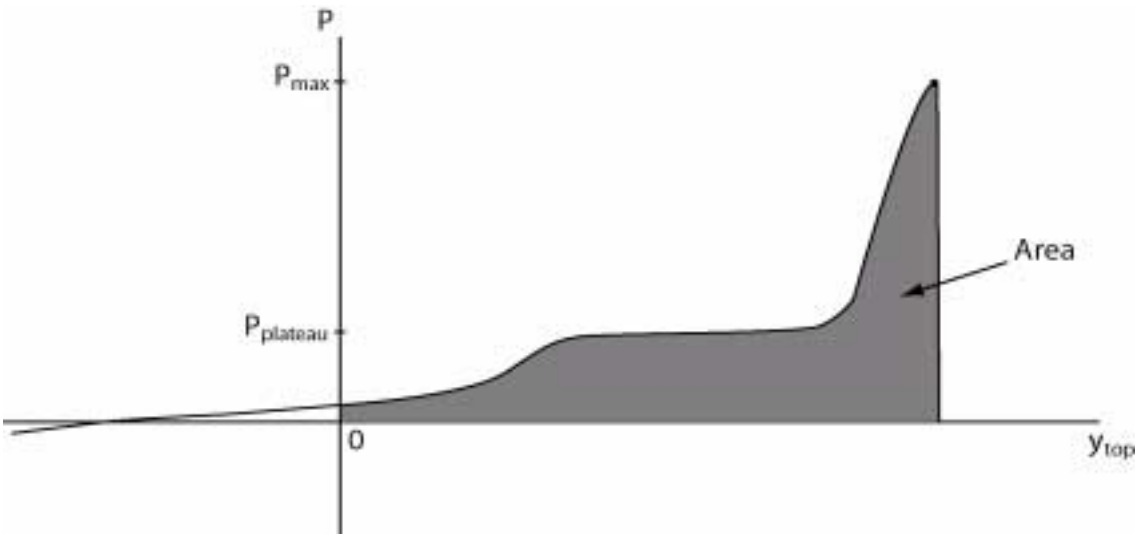

Figure 4.1 Pulling force (tack) curve

4.1 Nonlinear spring function parameters

The effect of the nonlinear spring function parameters β_1, β_2, and β_3 on the pulling curve is investigated. From the results, it can be seen that the pulling force curve is sensitive with respect to the nonlinear spring function. As presented in the previous chapter, the nonlinear spring element (SPRING1) is used to model the pressure sensitive adhesive in the Winkler-type elastic foundation. The nonlinear spring behavior in the tension zone is defined by pairs of force-displacement values using parameters β_1, β_2, and β_3 (Figure 4.2) and the compression zone is described by E(*y*) in section 3.3.1. The nonlinear spring function in the tension zone as shown in Figure 4.2 models the debonding process, plotted as positive values. Throughout the numerical analysis for the effect of the nonlinear spring function parameters, other parameters are fixed: the strip thickness (t_{strip}) is 0.0762mm, the contact area is $25.4\text{mm} \times 12.7\text{mm}$, and the length of the loop is 279.4mm.

4.1.1 β_1

The parameter β_1 defines the length of the ascending part of the curve. The initial slope is determined by the initial slope of the compression zone (Equations 3.4). It is equal to $A_1 E_{01} / h_a$. Because the maximum vertical force of the spring is determined by β_1, it is expected that β_1 is the most important factor in the nonlinear spring function. Other parameters are fixed as $\beta_2 = 2$ and $\beta_3 = 0.5$ in this section. As β_1 is increased, the following points are observed from Table 4.3 and Figures 4.3 and 4.4:

1. The initial slope of the pulling force curve increases.
2. Overall the pulling force curve is higher.
3. The displacement at the top of the loop (y_{top}) increases at the point when the maximum pulling force occurs.

The straight lines in Figure 4.4 indicate that the maximum pulling force and the area of the pulling force curve vary almost linearly with β_1. Compared to the other parameters (β_2, β_3), the rates of increase with β_1 are the largest. This result show

Table 4.1 Details of parameters investigated

Parameters		
Contact area ($L_{contact} \times W_{strip}$), mm^2	Length of Loop (L_{loop}), mm	Strip thickness, mm
25.4×12.7	279.4	0.1016
17.88×12.7	269.4	0.0762
16.76×12.7	259.4	0.0508
14.53×12.7		0.0254

Table 4.2 Details of nonlinear spring function parameters investigated

Nonlinear spring function parameters								
β_1	β_2	β_3	β_1	β_2	β_3	β_1	β_2	β_3
0.01	2	0.5	0.02	1	0.5	0.02	2	0.05
0.02	2	0.5	0.02	2	0.5	0.02	2	0.1
0.03	2	0.5	0.02	3	0.5	0.02	2	0.2
0.04	2	0.5	0.02	4	0.5	0.02	2	0.3
0.05	2	0.5	0.02	5	0.5	0.02	2	0.4
						0.02	2	0.5
						0.02	2	1
						0.02	2	2
						0.02	2	3

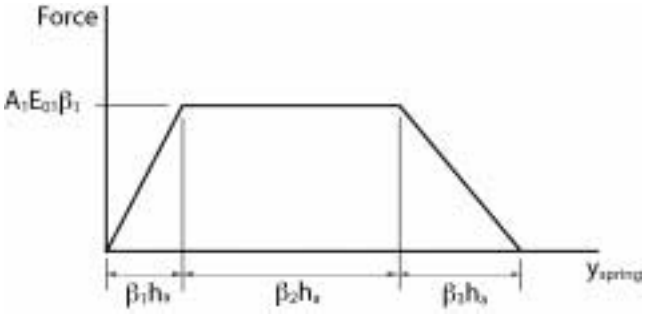

Figure 4.2 Nonlinear spring function in the tension zone

Table 4.3 $\beta_2 = 2$, $\beta_3 = 0.5$, $t_{strip} = 0.0762$mm

β_1	P_{max}, N	Area, mm^2	$P_{plateau}$, N
0.01	9.51	67.45	4.78
0.02	17.35	133.92	10.21
0.03	23.94	204.86	15.78
0.04	30.38	274.46	21.82
0.05	36.42	389.68	27.61
expt	29.49	185.76	21.92

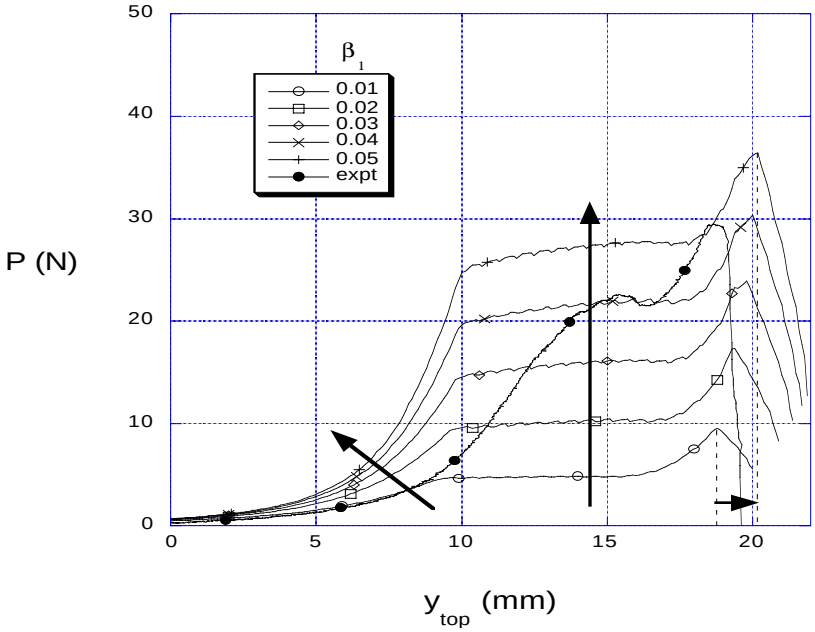

Figure 4.3 Pulling force curves for different β_1

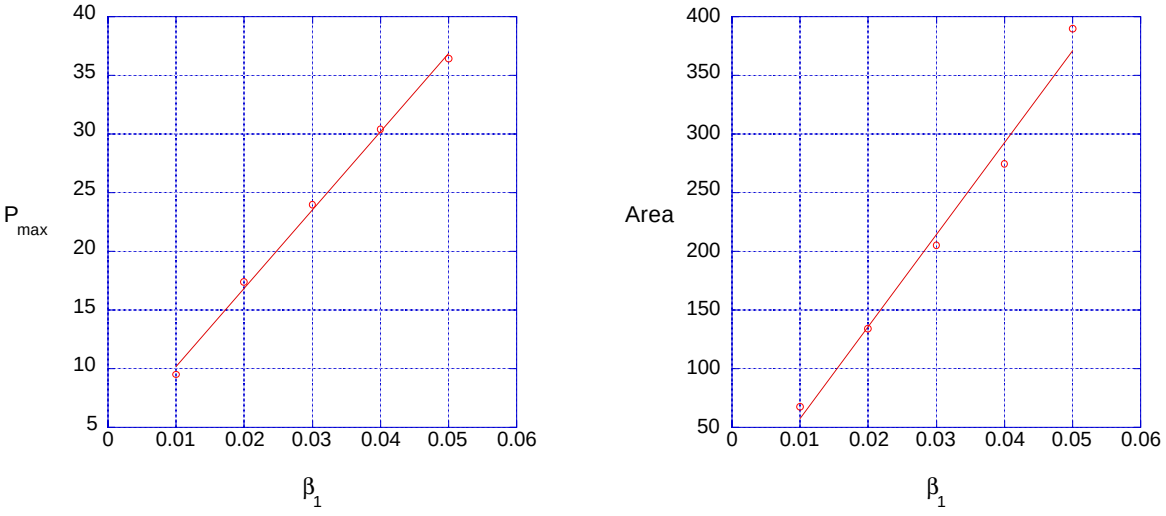

(a) P_{max} vs. β_1 (b) Area vs. β_1

Figure 4.4 Effect of β_1

4.1.2 β_2

The effect of β_2 on the pulling force curve is studied. The parameter β_2 specifies the length of the horizontal part in the spring characteristic in Figure 4.2. This region represents fibril deformation of the adhesive. From the Arcan tensile test result, it is verified that β_2 should be the largest parameter of the nonlinear spring function parameters. The following points can be observed from Table 4.4 and Figures 4.5 and 4.6 as β_2 increases:

1. The initial slope of the pulling curve does not change.
2. From Figure 4.4, it is seen that the length of the plateau region decreases.
3. Like the β_1 case, the pulling force curve increases overall but the amount of increase is smaller than for the β_1 case.
4. The maximum pulling force increases almost linearly and the area of the pulling zone increases approximately quadratically (a quadratic curve is fit with the data).

Table 4.4 $\beta_1 = 0.02$, $\beta_3 = 0.5$, $t_{strip} = 0.0762$mm

β_2	P_{max}, N	Area, mm^2	$P_{plateau}$, N
1	12.01	83.36	5.40
2	17.35	133.92	10.19
3	22.10	174.19	14.68
4	26.86	211.03	19.37
5	31.57	240.00	23.79
expt	29.49	185.76	21.92

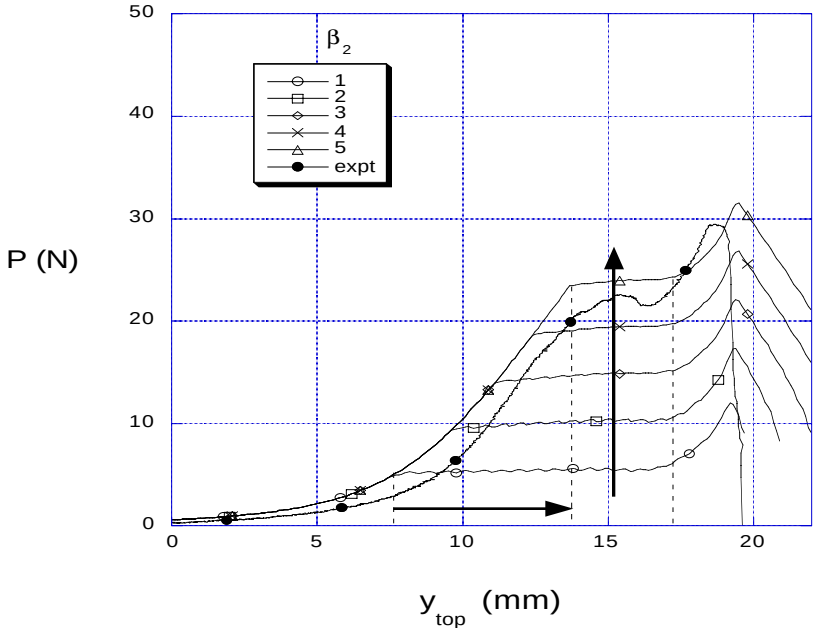

Figure 4.5 Pulling force curves for different β_2

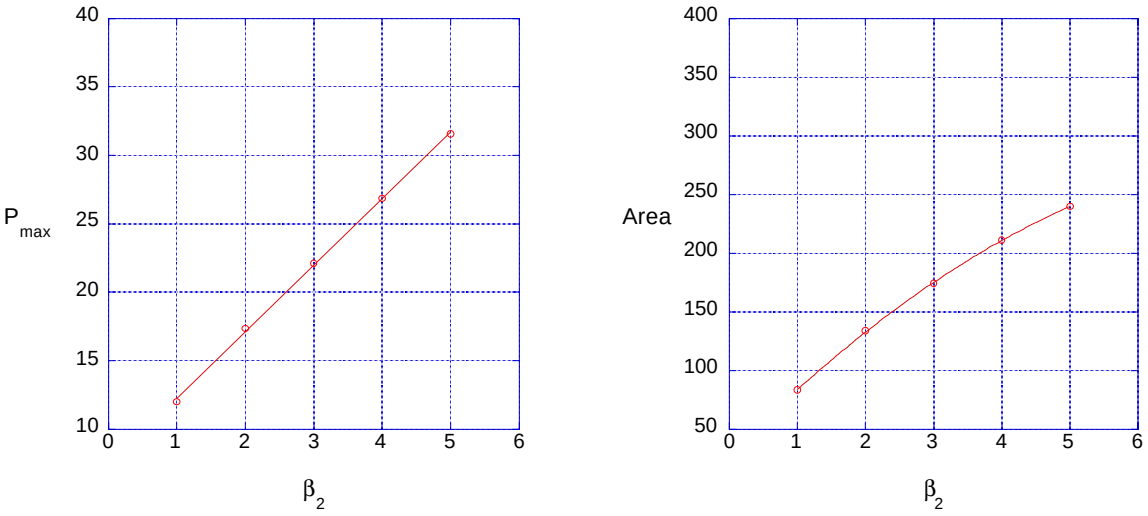

(a) P_{max} vs. β_2 (b)Area vs. β_2

Figure 4.6 Effect of β_2

4.1.3 β_3

The length of the falling branch is defined by β_3. From the numerical results, an oscillating pulling force in the pulling force curve is observed after y_{top} reaches the plateau region. This behavior was observed in the experiment, but the main cause is different. According to Satas (1989, 1999), as the peel rate increases the relatively smooth peel is transformed to a “slip-stick” failure and the pattern of peel-force variation depends on the mode of failure in the peel test. In the range of cohesive failure, the peel force varies greately in a random manner around some mean value. The peel force is usually higher than that observed in adhesive failure. In the region of slip-stick peel failure, the force starts to fluctuate periodically. In the numerical analysis, as soon as the springs at the peel front reach the specified critical elongation, they become inactive. Because of this inactivation of springs, the total spring force decreases at the next step and oscillation occurs in the plateau region. Additionally, there are different sources increasing oscillation in the pulling force curve. A small value of β_3 and the large mesh size of the contact part cause the oscillation of the tack curve in the numerical analysis. If the slope of the β_3 region in Figure 4.2 is steep (that is, β_3 is small), the oscillation will increase. Except for the bottom curve, for $\beta_3 = 0.05$, there is not much oscillation in Figures 4.7 and 4.8. Especially, if β_3 is larger than 0.5 it would not show oscillation (Figure 4.8). Figure 4.9 illustrates increased peak pulling force and area of pulling curve with increae in β_3. When increasing β_3, the following observations are made:

1. The oscillation of the pulling force curve grows after the pulling force reaches the plateau region.
2. The plateau length decreases.
3. The whole pulling force curve increases but the amount of increase is obviously smaller than for the β_1 and β_2 cases.

From Figure 4.10, it is seen that the wavelength and the amplitude of the pulling force curve increase with increasing β_2 if β_1=0.02 and β_3=0.1 and if β_1=0.05 and β_3=0.2. In particular, in the second case, with larger β_1 and β_3, the oscillation is much larger as shown in Figure 4.10. The strip thickness and elasticity modulus of PSA also affect the oscillation, as shown in chapter 4.4 (Figure 4.15) and chapter 5.6 (Figure 5.16). Thus, oscillation of the pulling force in the numerical analysis is not dependent upon one parameter. Use of a more refined mesh in the contact area is able to decrease the oscillation in the numerical results.

Table 4.5 $\beta_1 = 0.02$, $\beta_2 = 2$, $t_{strip} = 0.0762$mm

β_3	P_{max}, N	Area, mm^2	$P_{plateau}$, N
0.05	16.84	122.71	9.07
0.1	16.84	123.61	9.17
0.2	17.06	127.45	9.43
0.3	17.17	129.55	9.64
0.4	17.22	131.75	9.87
0.5	17.35	133.92	10.23
1	18.57	144.41	11.33
2	20.92	163.76	13.71
3	23.25	181.12	16.04
expt	29.49	185.76	21.92

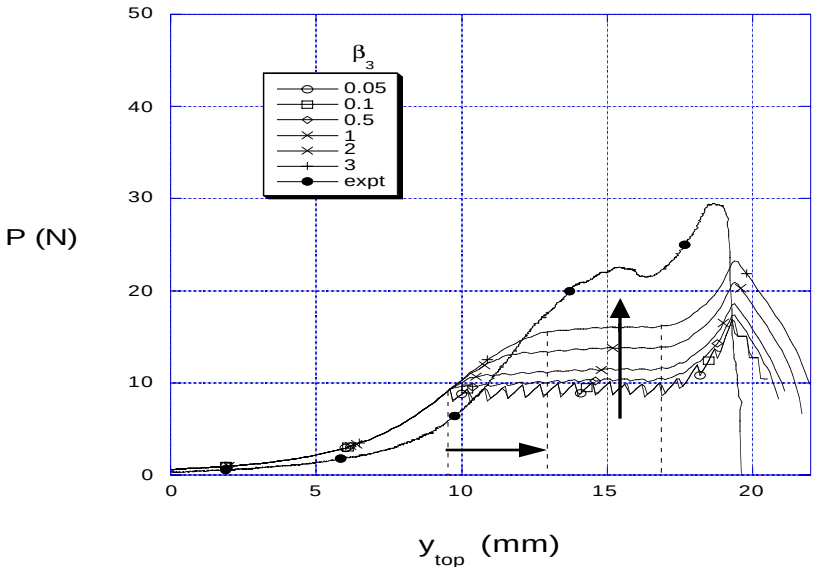

Figure 4.7 Pulling force curves for different β_3 (=0.05, 0.1, 0.5, 1, 2, 3)

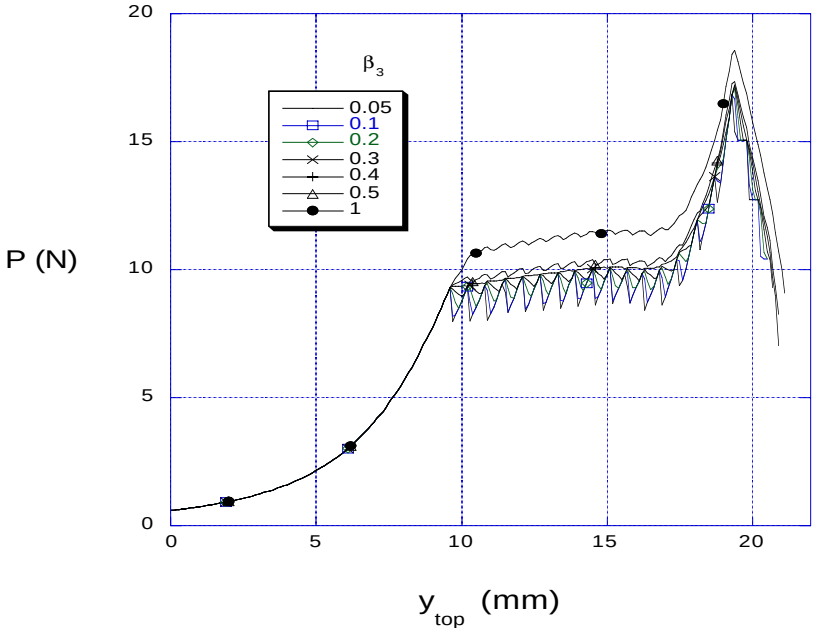

Figure 4.8 Pulling force curves for different β_3 (=0.05, 0.1, 0.2, 0.3, 0.4, 0.5, 1)

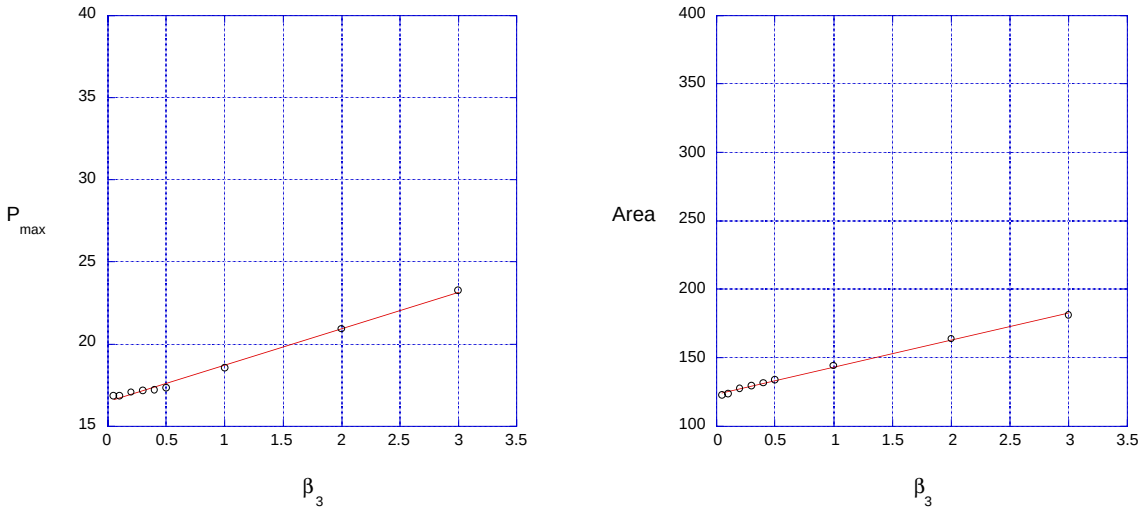

(a) P_{max} vs. β_3 (b) Area vs. β_3

Figure 4.9 Effect of β_3

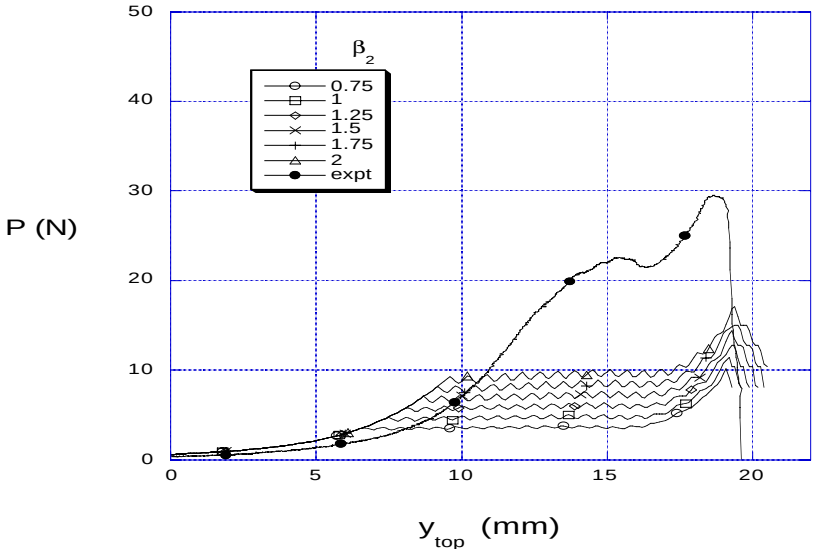

(a) β_1=0.02, β_3=0.1

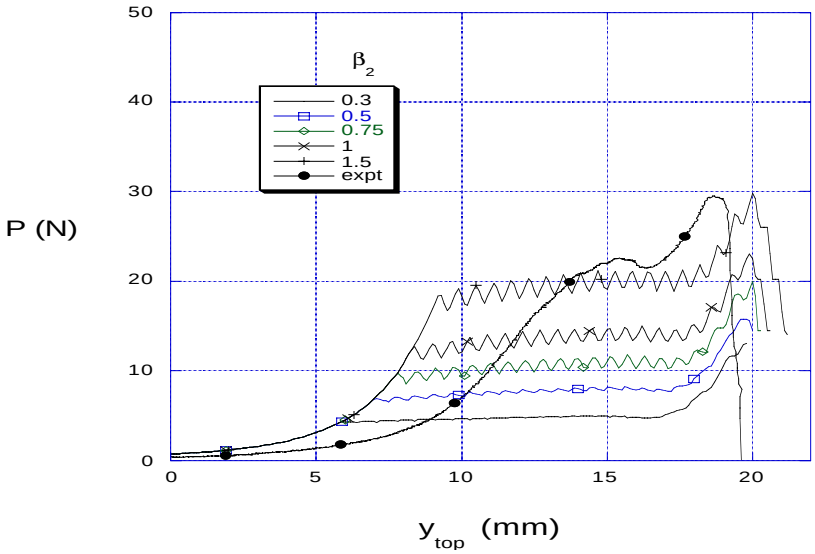

(b) β_1=0.05, β_3=0.2

Figure 4.10 Pulling force curves for different β_2 (t_{strip} = 0.0762mm)

4.2 Contact Area

Since the numerical pulling force curve is determined by 2D finite element analysis, the effect of anticlastic bending is ignored. Accordingly, the contact length in the longitudinal direction is only taken into account and the contact length in the transverse direction is assumed to be the width of strip (W_{strip}) in 2D analysis. The influence of the contact area is presented in Table 4.6 and Figure 4.11. Parameters are fixed as $\beta_1 = 0.02$, $\beta_2 = 0.75$, $\beta_3 = 0.5$, strip thickness t_{strip}=0.0254mm, and length of loop L_{loop}=279.4mm. Throughout the loop tack test, the contact area at the end of the pushing phase is kept equal to $25.4\text{mm} \times 12.7\text{mm}$, but due to experimental uncertainties it is hard to accomplish. Table 4.7 shows that the contact area for various strips in the experiments did not achieve this value. A comparison of the pushing displacement between ABAQUS and the experimental results is given in Table 4.7. Values of contact area with respect to experimental y_{top} in Table 4.7 are numerical analysis results and it presents how much contact area may have occurred in the experiments. A thinner loop needs to be pushed down further to achieve the same contact area. Thus, the numerical analysis result is used as the benchmark of the contact area for different thicknesses. The effect of contact area is as follows:

1. The plateau length increases with an increase of the contact area (Figure 4.8). Since the starting point of the plateau region in the pulling force curve occurs when the first peel front springs fail (i.e., reach critical elongation), the plateau region starts early as the contact length increases.
2. The initial slope of the pulling force curve, peak pulling force, and average pulling force in the plateau region of the pulling force curve are the same.

Table 4.6 $\beta_1 = 0.02$, $\beta_2 = 0.75$, $\beta_3 = 0.5$, t_{strip} = 0.0254mm

$L_{contact}$, mm	y_{top}, mm	P_{max}, N	Area, mm^2	$P_{plateau}$, N
14.53	-33	7.01	41.06	4.72
16.76	-34	7.01	43.78	4.72
17.88	-35	7.01	49.29	4.72
25.4	-39.54	7.01	65.80	4.72
expt	-31	8.64	34.45	4.55

Table 4.7 Comparison of the pushing displacement at the top of the loop

Strip thickness, mm	y_{top} (ABAQUS results), mm	Contact area w. r. t. ABAQUS y_{top}, mm^2	y_{top} (Experimental results), mm	Contact area w. r. t. experimental y_{top}, mm^2
0.0254	-39.59	25.4×12.7	-31	11.18×12.7
0.0508	-39.12	25.4×12.7	-34	17.88×12.7
0.0762	-38.66	25.4×12.7	-38	22.35×12.7
0.1016	-38.24	25.4×12.7	-39	25.4×12.7

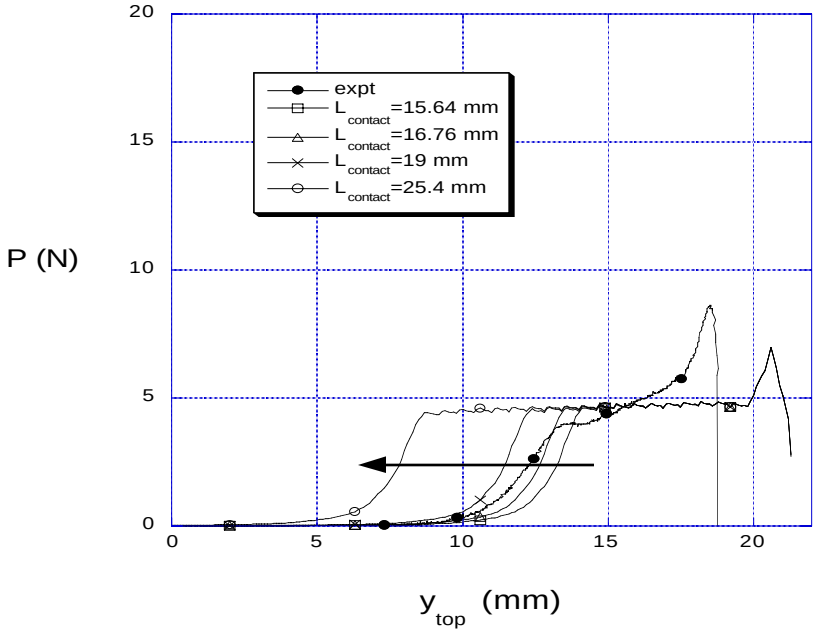

Figure 4.11 Pulling force curves for different contact length ($L_{contact}$)

4.3 Length of Loop

While the strip is clamped in the forming procedure in the experiment, it is hard to keep the length the same every time because of human error in the taped part in Figure 4.12. Even though this uncertainty occurs, it is assumed that the range of error does not go beyond 20mm (this is the total taped length of the left and right ends of the strip, therefore the taped length on each end of the loop is less than half of this). To study the effect of the loop length, three cases are taken into account as given in Table 4.8. Parameters are fixed as $\beta_1 = 0.02$, $\beta_2 = 0.75$, $\beta_3 = 0.5$, strip thickness=0.0254mm, and contact area = $19.0\text{mm} \times 12.7\text{mm}$, respectively. The position of the pulling force curve shifts leftward overall as shown in Figure 4.13, but the maximum pulling force and the average force in the plateau region do not change much (slightly increase as seen in Table 4.8) as the loop length decreases. Since the change of the loop length causes the variation of the initial loop height after forming, overall the pulling force curve moves leftward or rightward depending upon an increase or decrease of the length of the loop. Thus, the effect of the length of the loop is important compared to other parameters.

Figure 4.12 Teardrop shape of the loop

Table 4.8 $\beta_1 = 0.02$, $\beta_2 = 0.75$, $\beta_3 = 0.5$, $t_{strip} = 0.0254$mm

L_{loop}, mm	P_{max}, N	Area, mm^2	$P_{plateau}$, N
279.4	7.01	49.28	4.69
269.4	7.10	49.22	4.85
259.4	7.42	49.52	5.06
expt	8.64	34.45	4.55

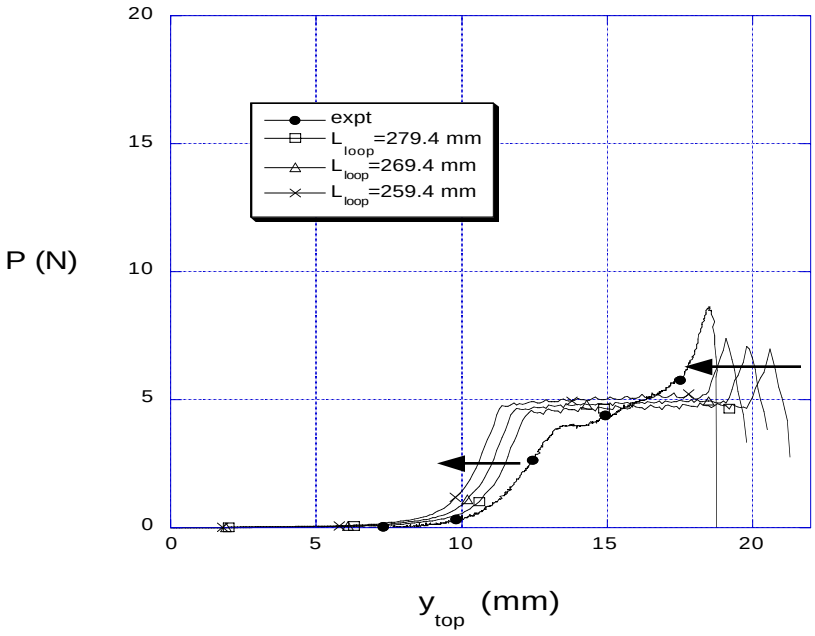

Figure 4.13 Pulling force curve for different length of loop (L_{loop})

4.4 Strip Thickness

The strip thickness has an effect on the pulling force. An investigation of the loop tack test including the effect of strip thickness using finite element analysis has been reported by Hu et al. (1999) and Duncan and Lay (1999) previously. Their results show that the measured tack force decreases as the strip thickness increases. In their simulation, however, they did not include modeling of the adhesive layer (they just used the *SURFACE BEHAVIOR routine in ABAQUS); that is, they did not take into account the physical properties of the adhesive. This does not consider the higher contact pressures produced by the stiffer tapes that would tend to increase the measured tack. Le et al. (1999) show the effect of backing thickness throughout the loop tack test. In their report, the transition of the peak pulling force with respect to three different thicknesses is similar to that in Stacy Coulthard's results (Figure 4.14a) at the 12mm/min rate, but at a higher rate (310mm/min) the peak pulling force increases with increasing thickness.

In the present study, the dependence upon thickness in the experiments is shown in Figure 4.14. The numerical analysis results depend upon which nonlinear spring function is adopted, and choosing the nonlinear spring function is based on the experimental results. Therefore, comparison of the influence of the strip thickness effect with numerical results is meaningless if the nonlinear spring function is selected from the experimental results for each thickness case. The experimental results correspond to four different thicknesses compared with each other at the same debonding rate (12mm/min), temperature ($23°$), and adhesive (VHB tape) in Figure 4.14. All trends of characterized quantities are the same, but they do not show good repeatability, especially for the 0.0762mm strip. A larger thickness of the strip will require a larger pushing force to achieve the same contact area and then, as pointed out by Creton and Leibler (1996), better contact (complete wetting) will occur. Accordingly, because of good contact, the overall pulling force curve should increase with increasing thickness. However, Stacy Coulthard's results do not show an ascending trend of the peak pulling force, plateau pulling force, and area of the pulling zone with increasing thickness, as shown in Figure 4.14.

Table 4.9 and Figures 4.15 and 4.16 show the effect of strip thickness in the numerical analysis for a given same nonlinear spring function. Parameters are fixed as $\beta_1 = 0.02$, $\beta_2 = 0.75$, $\beta_3 = 0.5$, the contact area = $25.4\text{mm} \times 12.7\text{mm}$, and length of loop L_{loop}=279.4mm. As increasing strip thickness, the position of the pulling force curve moves leftward overall and the

peak pulling force increase (Figure 4.15). Figure 4.16 shows increase rate of the pulling force and area of the pulling zone. Since the bending stiffness of thicker loop is larger than thin one, the pushing force curve increase overall as increasing strip thickness (Figure 4.17).

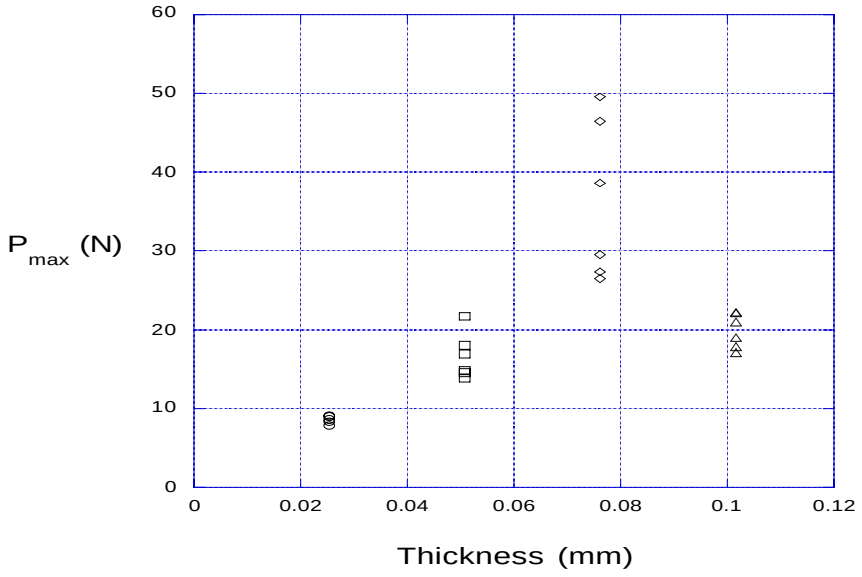

(a) Maximum pulling force vs. thickness

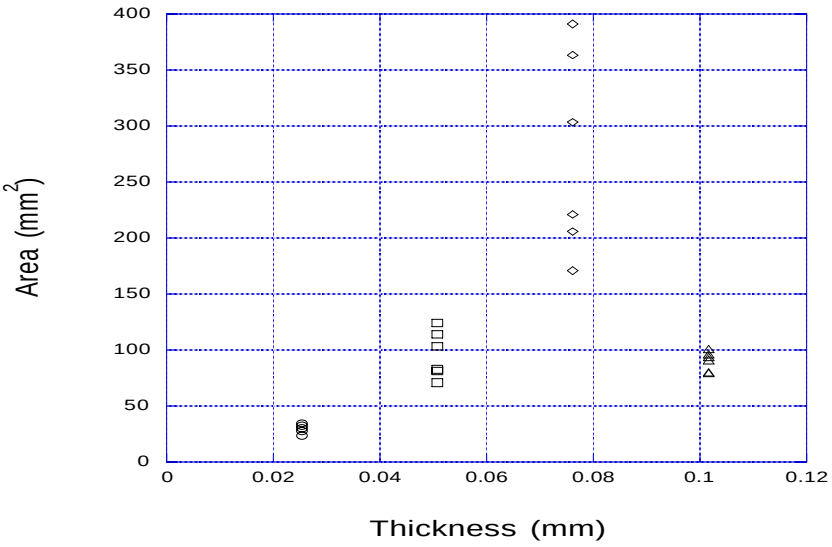

(b) Area of pulling zone vs. thickness

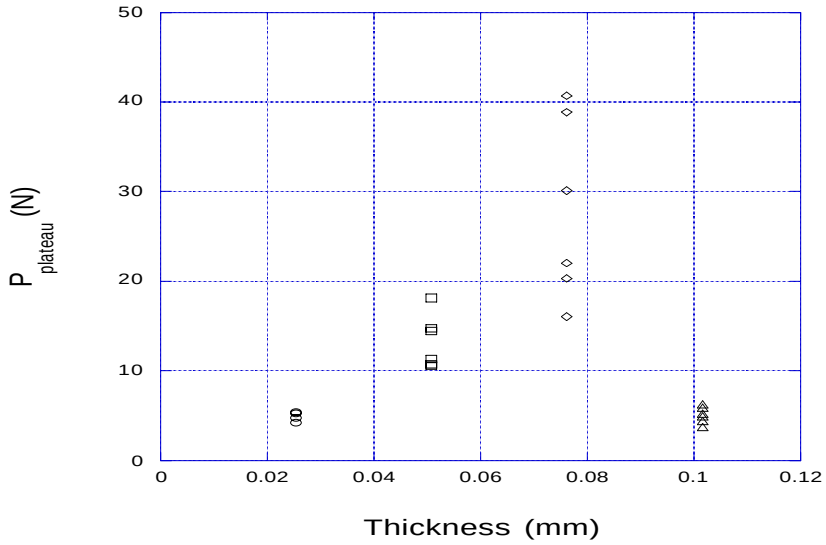

(c) Average pulling force in the plateau region vs. thickness

Figure 4.14 Experimental results

Table 4.9 $\beta_1 = 0.02$, $\beta_2 = 0.75$, $\beta_3 = 0.5$

Thickness, mm	P_{max}, N	Area, mm^2	$P_{plateau}$, N
0.0254	7.01	65.46	4.64
0.0508	9.18	68.92	4.53
0.0762	10.85	72.33	4.26
0.1016	12.26	77.34	4.07

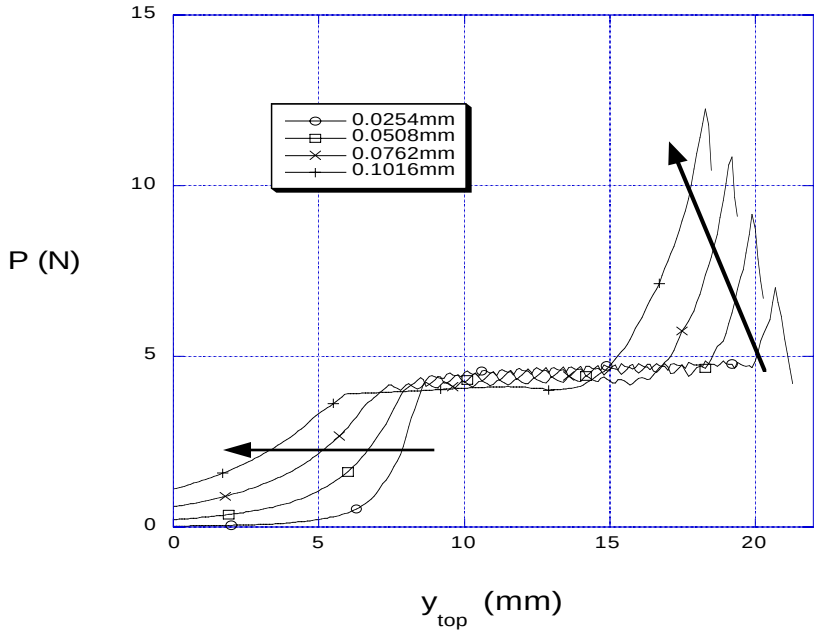

Figure 4.15 Numerical results for pulling phase

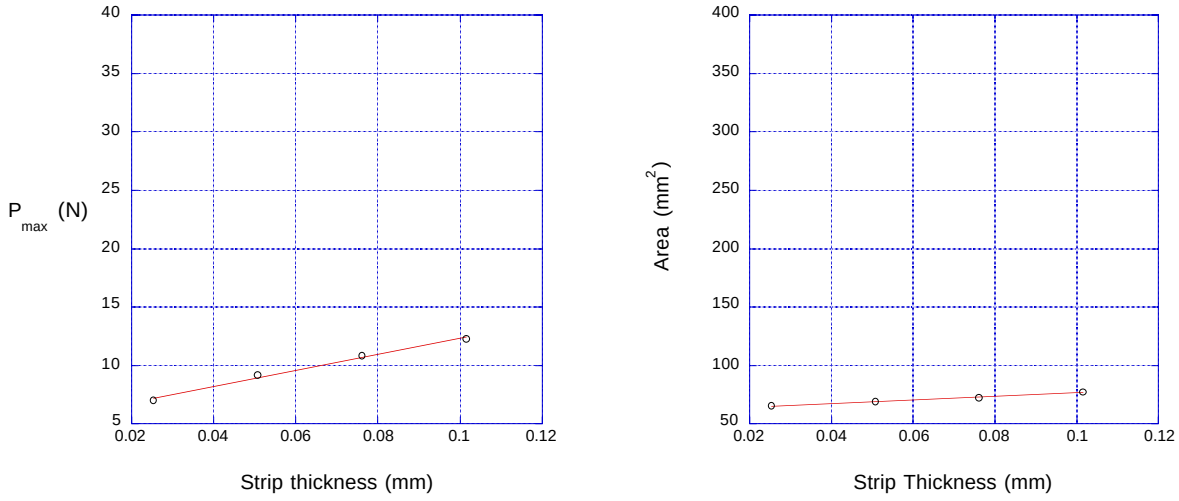

(a) P_{max} vs. strip thickness (b) Area vs. strip thickness

Figure 4.16 Effect of strip thickness

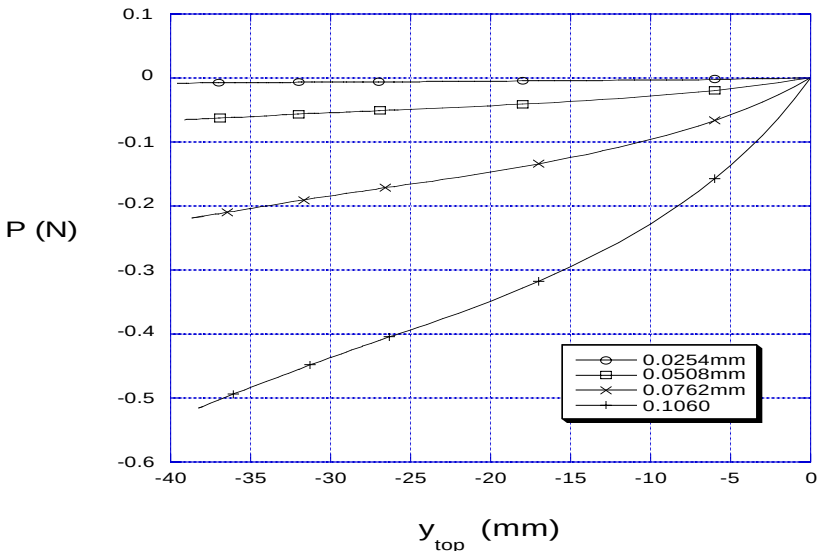

Figure 4.17 Numerical results for pushing process

Chapter 5. RESULTS AND DISCUSSION

5.1 Loop Behavior

Plaut et al. (1999) investigated the behavior of an elastica loop pushed onto a flat rigid surface using either a shooting method or an integral formulation. Williams (2000) presented the behavior of pressure sensitive adhesive tapes in the loop tack test using a shooting method. In her study, the loop is modeled as an inextensible elastica and some assumptions are made. As mentioned previously, her results do not show good agreement for the behavior of the loop at the end of the pulling phase. Due to highly geometrical and material nonlinearities, this problem is solved here numerically by the finite element method. As the strip is pushed down onto the adhesive, and then pulled up, the variations of the deflected shapes of the loop are obtained using ABAQUS. The dimensions of the stainless steel strip are the same as used in the experiments. The sizes of the Mylar strip are 38.1mm wide, 0.0254mm-0.1016mm thick (four different thickness were used), and 195.6mm long. The elastic constants of the Mylar strip are $E = 4.6\text{GPa}$, $\nu = 0.37$. The yield stress of the strip is taken to be $\sigma_y = 140\text{MPa}$, and the experimentally determined uniaxial stress-strain curve and idealized bilinear stress-strain curve are shown in Figure 3.2. The contact areas for the stainless steel strip and Mylar strip are $25.4\text{mm} \times 12.7\text{mm}$ and $25.4\text{mm} \times 38.1\text{mm}$, respectively, but in the 3D analysis the contact area is not made perfectly in the transverse direction (more detailed description is given in section 5.3). The lengths of the loops (L_{loop}) for the stainless steel strip and Mylar strip are 279.4mm and 195.6mm, respectively, throughout this section. Even though spring elements are not visualized in all figures they exist during the analysis.

5.1.1 2D Analysis Results

The effect of anticlastic bending is ignored in this section. The planar deformed shapes of the loop during pushing and pulling are presented with respect to two different thickness and different material in Figures 5.1- 5.3. In this analysis, the final contact length is fixed at 25.4mm and VHB tape is modeled by a Winkler-type elastic foundation where $\beta_1 = 0.05$, $\beta_2 = 1.5$, and $\beta_3 = 0.5$ for t_{strip}= 0.0254m and t_{strip}=0.1016mm as mentioned before, i.e., the viscoelastic model is not considered. During pushing, the behavior of different thickness stainless steel strips and Mylar

strips are nearly the same, but due to different stiffnesses and Poisson's ratio the behavior of the two strips during pulling shows much different results after y_{top}>10. At the peel front, a large localized curvature is illustrated as in the experiments; that is, the loop shapes are nearly triangular, especially for thinner stainless steel strips and Mylar strips. As mentioned, although deformed shapes of the loop in the pushing phase are similar, to achieve the same contact length, the tops of thinner strips and more flexible strips should be pushed more.

Even though it cannot be seen in Figures 5.1-5.3, the curvature of the strip along the longitudinal direction is not constant in the contact region. Figure 5.4 shows an exaggerated planar deformed shape of the loop for the contact region in the middle of the bottom put of the loop. It illustrates how contact spreads in the longitudinal direction with respect to varying top displacement of the loop in the pushing procedure. Figure 5.5 shows the pulling force versus y_{top} and corresponding behavior of the loop. Figure 5.6 shows the variation of the left-half spring forces along the contact region. The plateau region starts when the first peel front spring reaches the specified critical elongation. The distribution curve of spring forces in Figure 5.6 exhibits oscillation. It was found that after the strip starts to debond, the positive spring force area and the absolute value of the negative spring force area remain constant as the peel angle increases. Because of this, the pulling force curve exhibits a plateau region until the absolute value of the negative area decreases. When the negative area of the spring forces disappears, the maximum pulling force occurs. The behavior may be more similar to that of a probe test than a peel test when the loop becomes thin and the sides are almost vertical, and this may explain the occurrence of a peak just before the loop separates from the substrate.

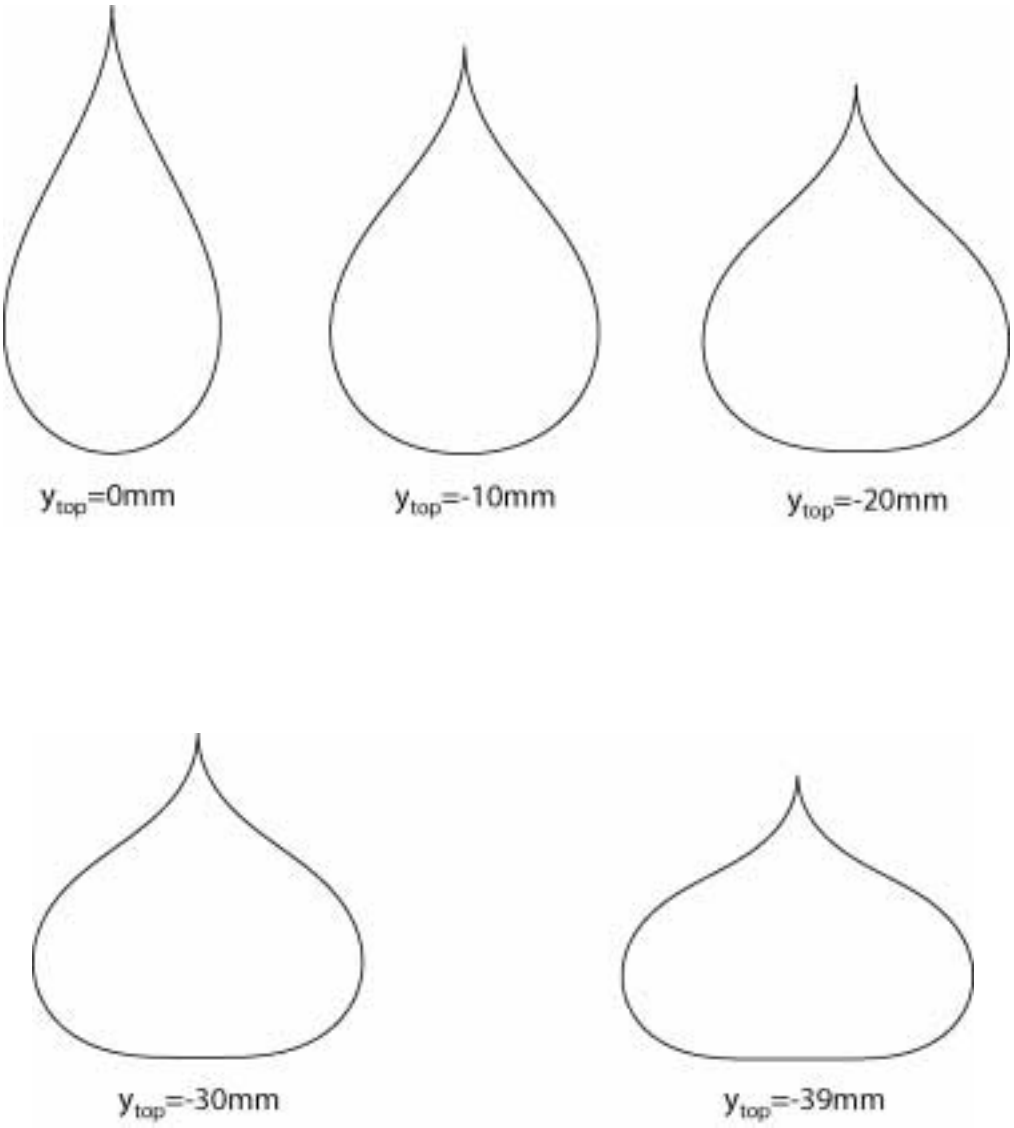

(a) Deflected shape of the loop in pushing procedure (t_{strip}=0.0254mm)

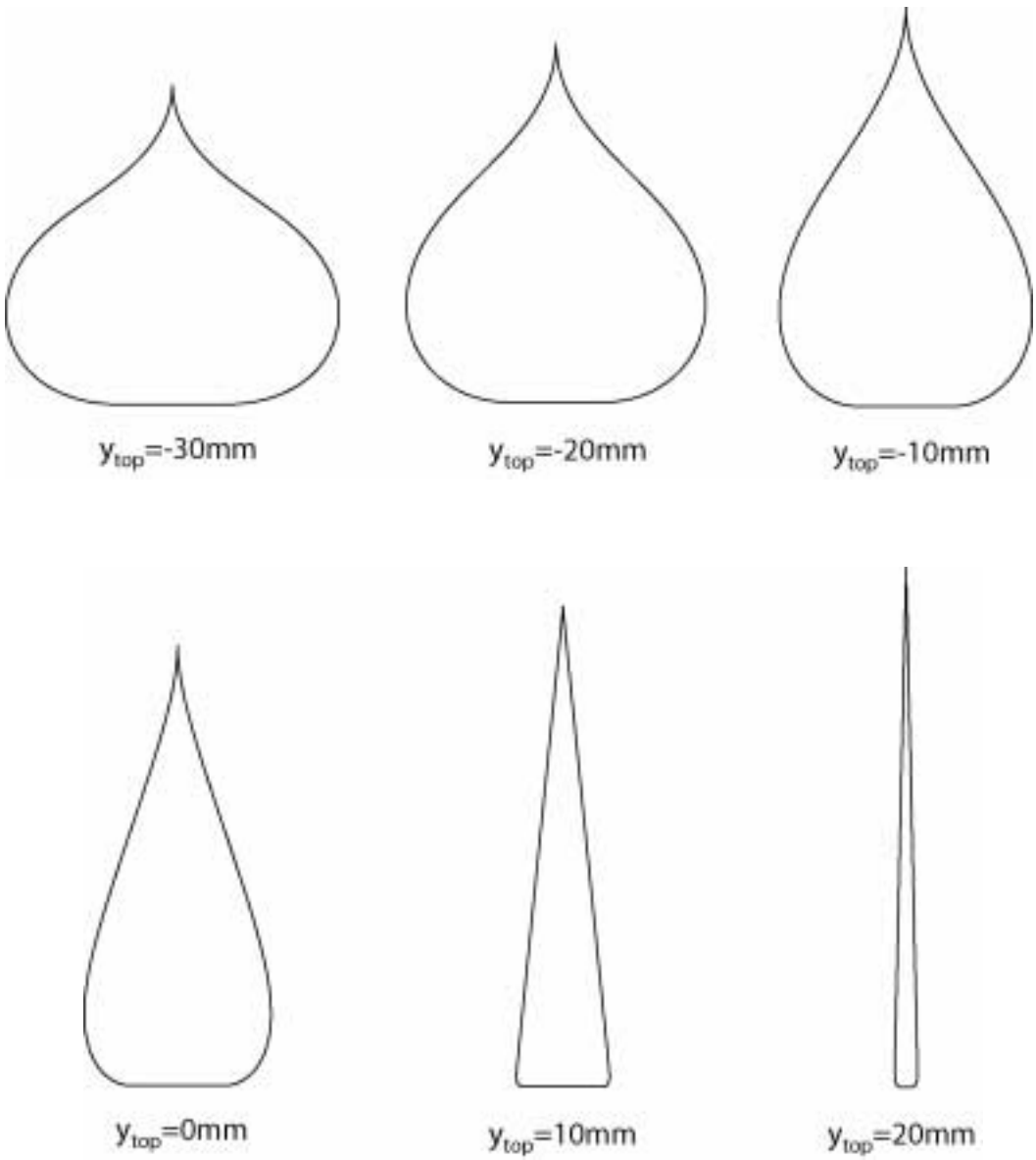

(b) Deflected shape of the loop in pulling procedure (t_{strip}=0.0254mm)

Figure 5.1 Deflected shapes of the loop for stainless steel strip (t_{strip}=0.0254mm)

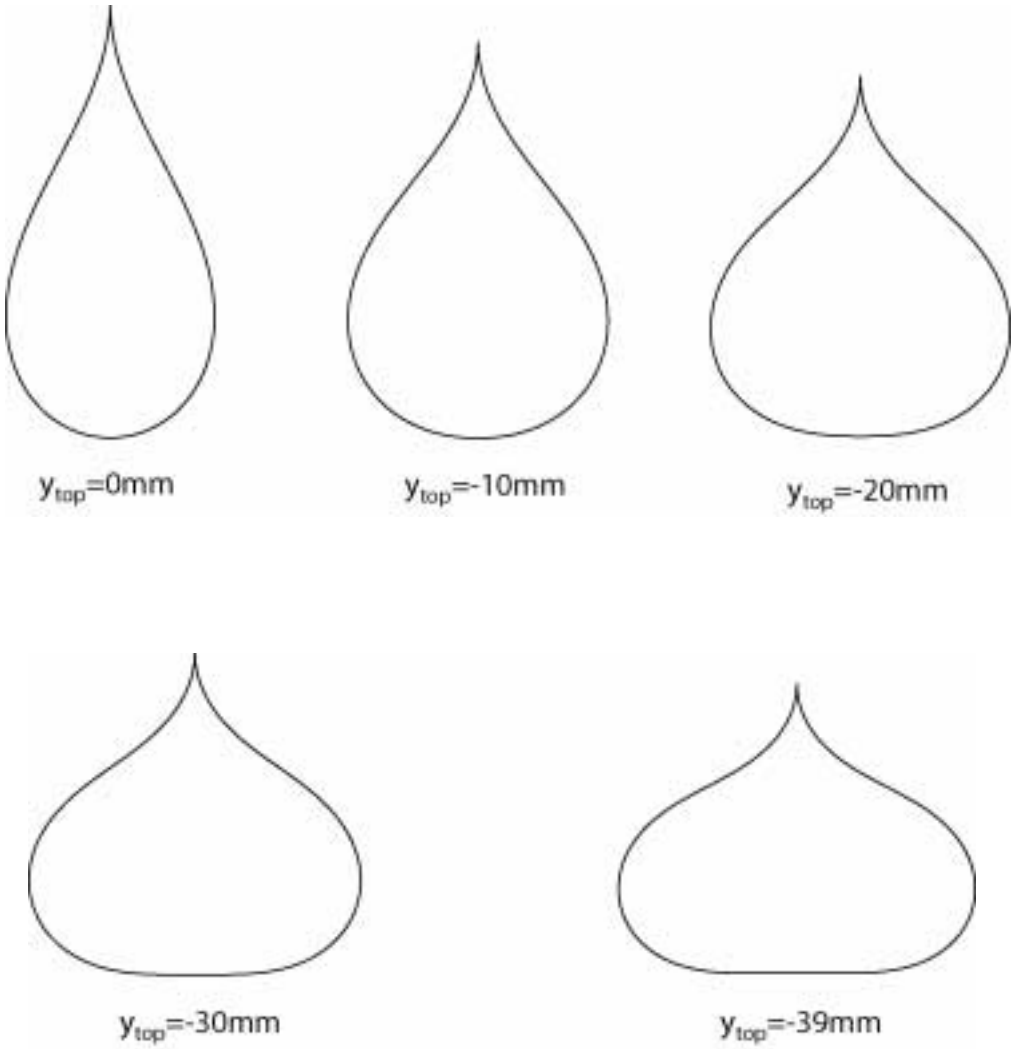

(a) Deflected shape of the loop in pushing procedure (t_{strip}=0.1016mm)

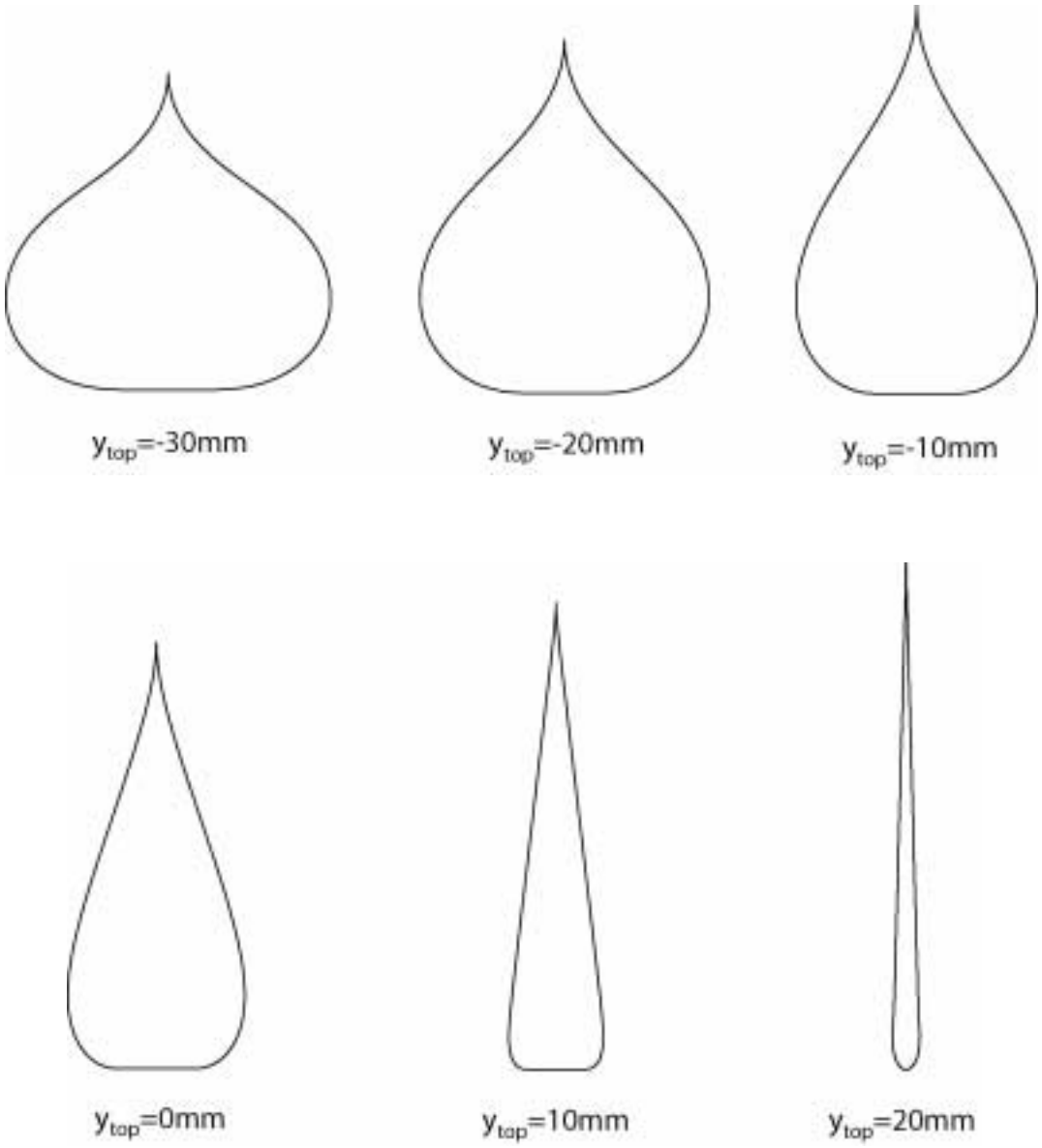

(b) Deflected shape of the loop in pulling procedure (t_{strip}=0.1016mm)

Figure 5.2 Deflected shapes of the loop for stainless steel strip (t_{strip}=0.1016mm)

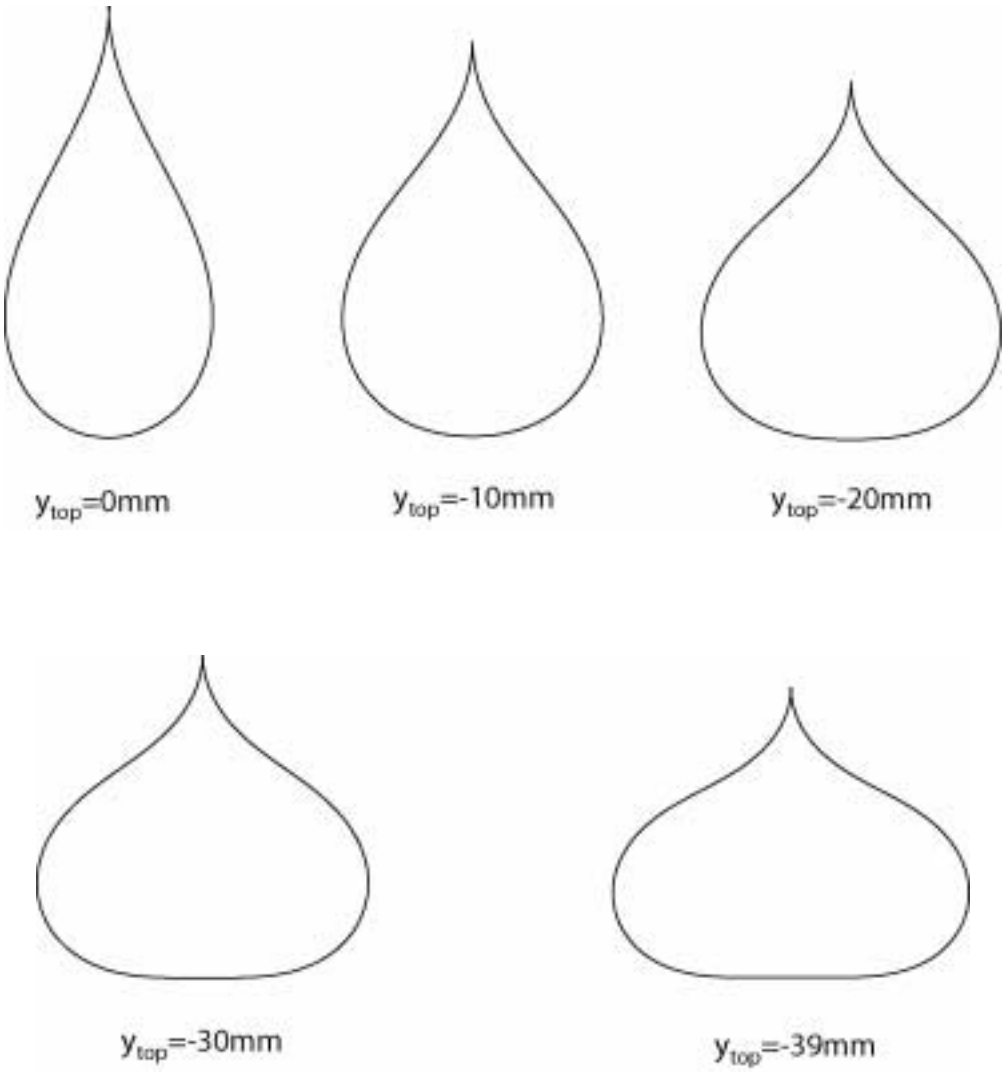

(a) Deflected shape of the loop in pushing procedure (t_{strip}=0.0508mm)

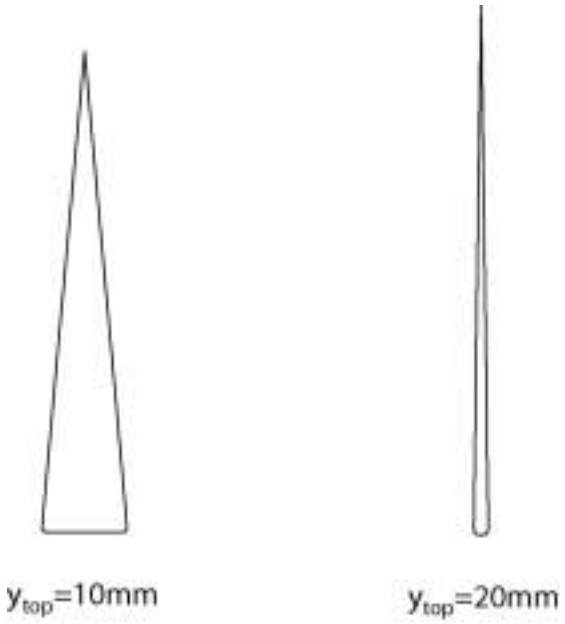

(b) Deflected shape of the loop in pushing procedure (t_{strip}=0.0508mm)

Figure 5.3 Deflected shapes of the loop for Mylar strip (t_{strip}=0.0508mm)

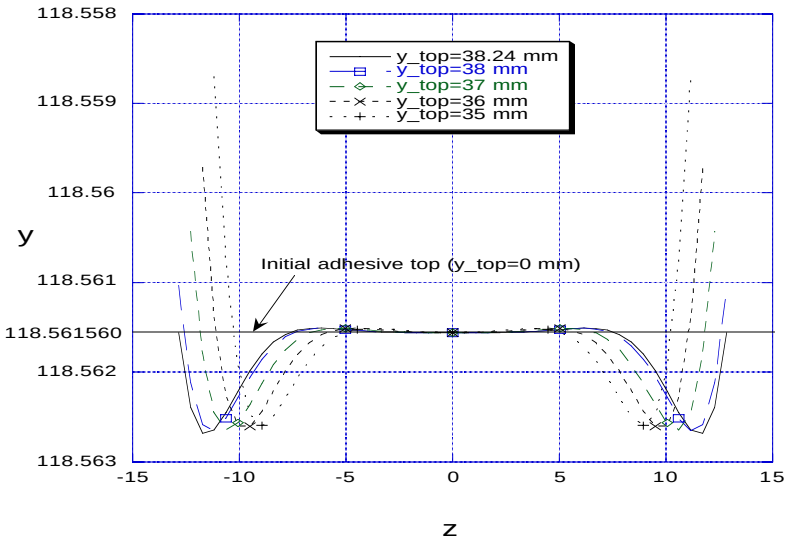

(a) t_{strip}=0.1016mm

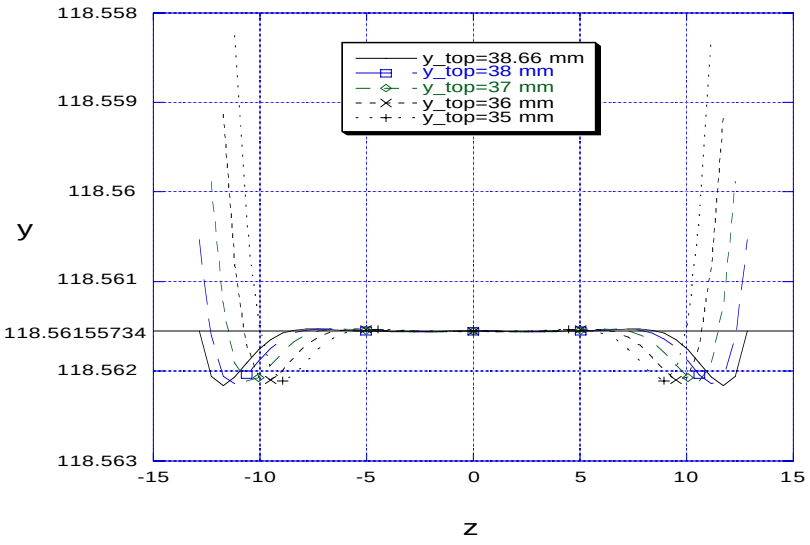

(b) t_{strip}=0.0762mm

Figure 5.4 Variation of deformed loop shape on contact part

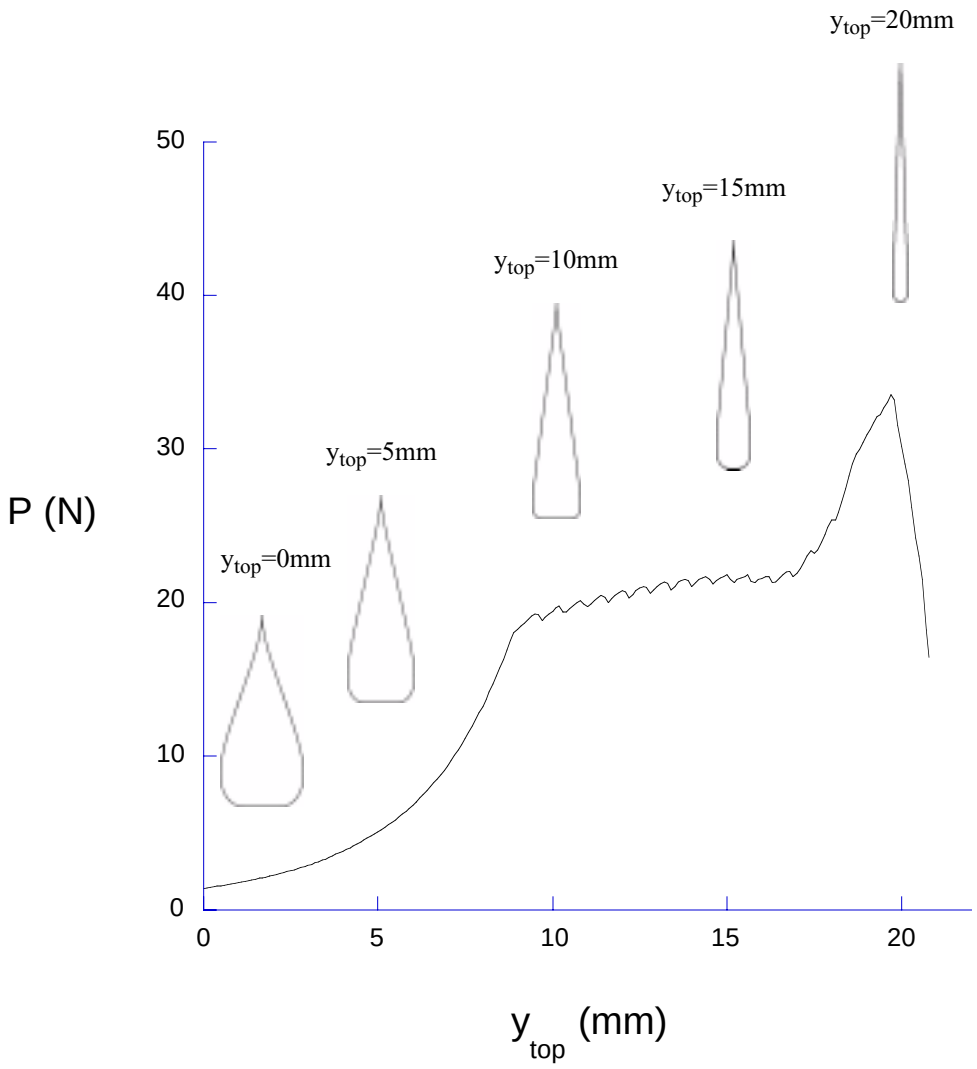

Figure 5.5 Pulling force vs. y_{top} and corresponding behavior of the loop (t_{strip}=0.1016mm, β_1=0.05, β_2=1.5, β_3=0.5)

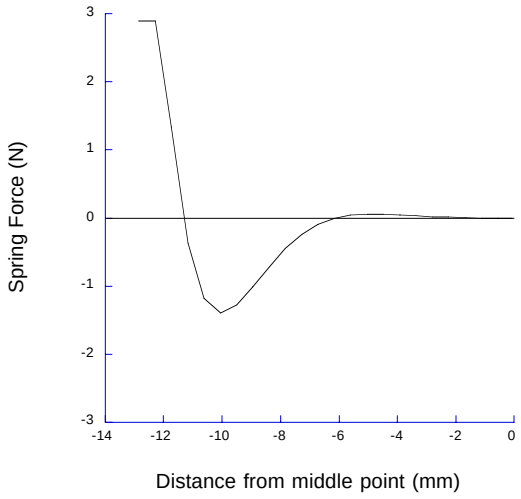

(a) y_{top}=0mm

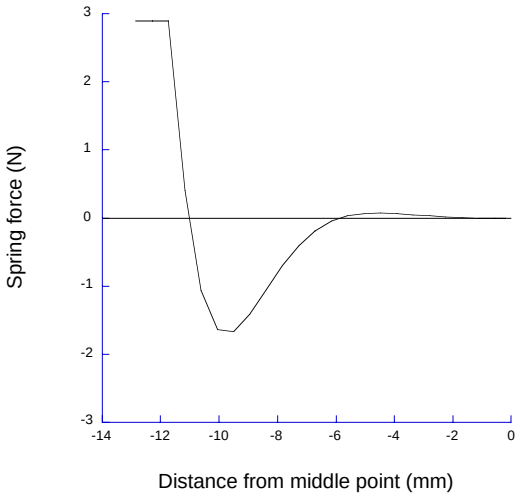

(b) y_{top}=2.5mm

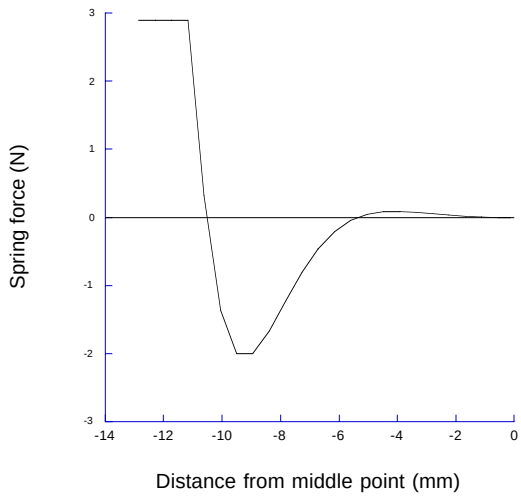

(c) y_{top}=5mm

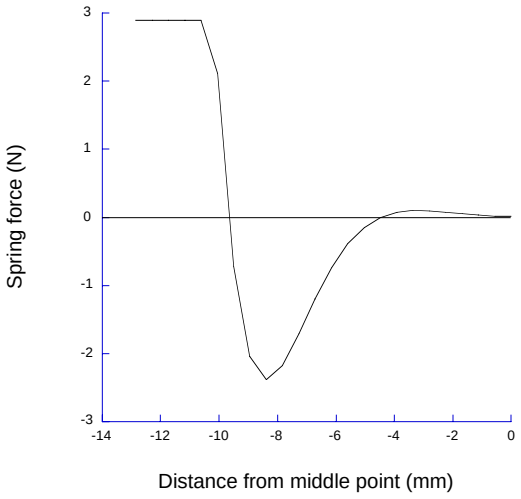

(d) y_{top}=7.5mm

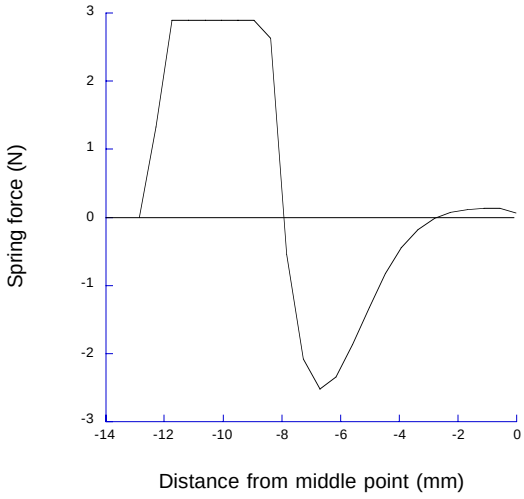

(e) y_{top}=10mm

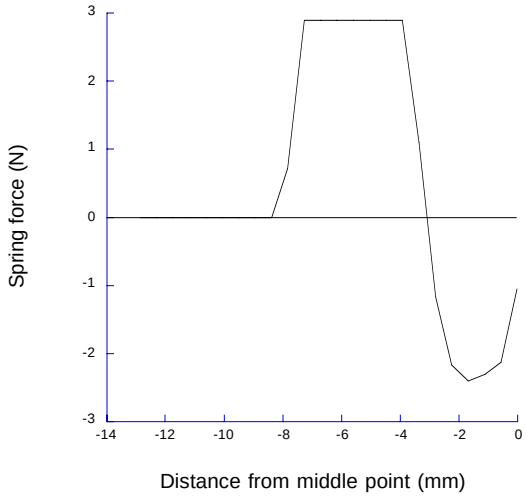

(f) y_{top}=15mm

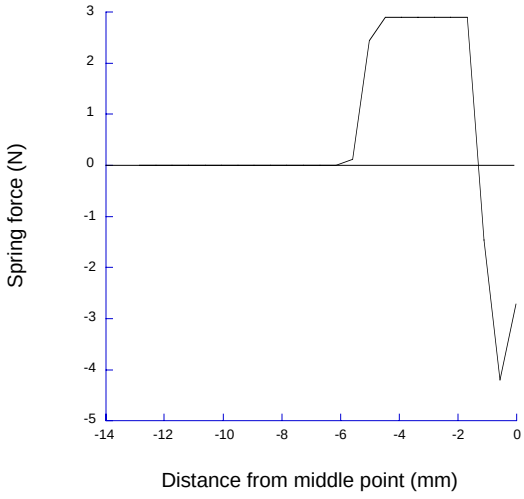

(g) y_{top}=17.5mm

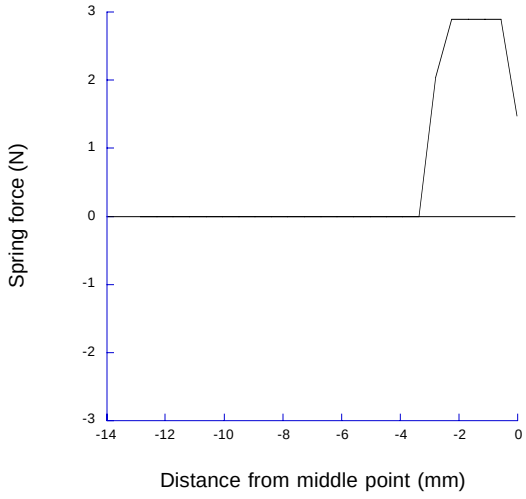

(h) y_{top}=20mm

Figure 5.6 Variation of the left-half spring forces along the contact area

5.1.2 3D Analysis Results

Now consider 3D analysis using shell elements where the nonlinear elastic spring function parameters are $\beta_1 = 0.03$, $\beta_2 = 1.5$, and $\beta_3 = 0.2$. Only a quarter-strip is generated and the anticlastic bending effect is taken into account in 3D finite element analysis. Figure 5.7 shows the variation of the von Mises stress contour as well as the 3D deformed loop shape for the quarter loop corresponding to top displacement of the loop where t_{strip} = 0.1016mm. The red region represents the maximum von Mises stress region at each y_{top} and it is in accord with the region where the maximum curvature occurs. The part of the loop that deforms plastically is shown in red in Figure 5.7j. For better understanding of the overall loop configuration, the planar deformed shape of the loop is also illustrated in Figure 5.7. Figure 5.8 depicts the deformed shape at the bottom center of the loop in the transverse direction for different thicknesses of the loop. From the numerical analysis results (Figure 5.8), it is seen that the strip deforms more into a cylindrical shape than into a saddle shape as described previously. For decreasing thickness, it becomes flatter, but in the case of a very thick strip, as presented in Figure 5.8b, anticlastic deformation of the cross section takes place. Figure 5.9 shows the detailed 3D deformed loop shape. Figure 5.10 shows the Mylar strip deformed shape along the transverse direction. Poisson's ratio of stainless steel and Mylar are 0.27 and 0.37, respectively. Due to different Poisson's ratio, their anticlastic bending behavior is a little different, even for the same thickness. We can predict how the contact pattern between the adhesive and adherend will be established. Contact first takes place at the edge of the loop, and contact next occurs at the middle of the loop, and then spreads across the width to the edge. However, this behavior depends on the thickness, width, and Poisson's ratio of the backing, so that we should take into account their relationship to anticipate the behavior of the thin strip. The contact pattern in 3D analysis will describe later section.

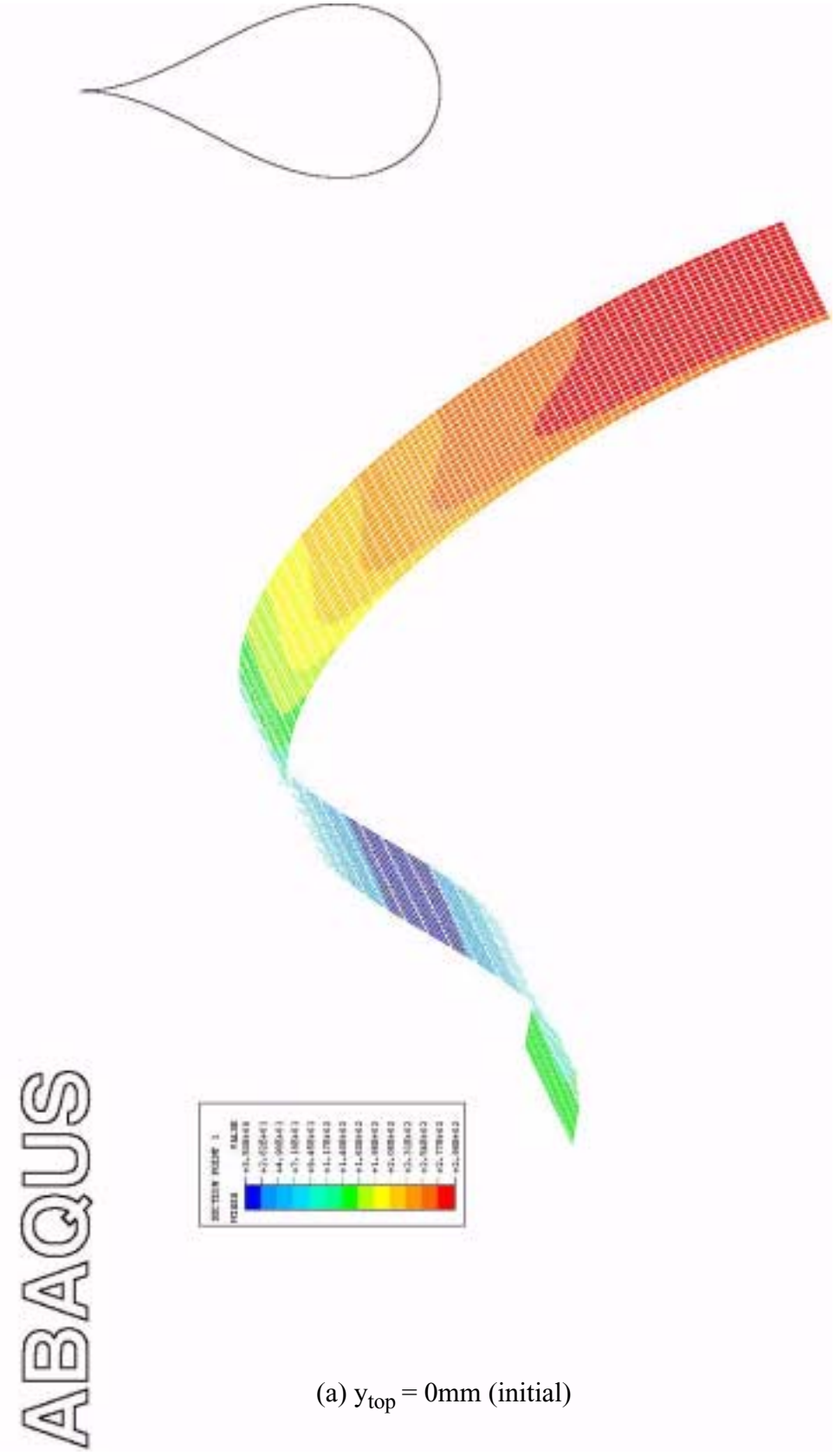

(a) y_{top} = 0mm (initial)

(b) y_{top} = -20mm (pushing)

(c) $y_{top} = -30$ (pushing)

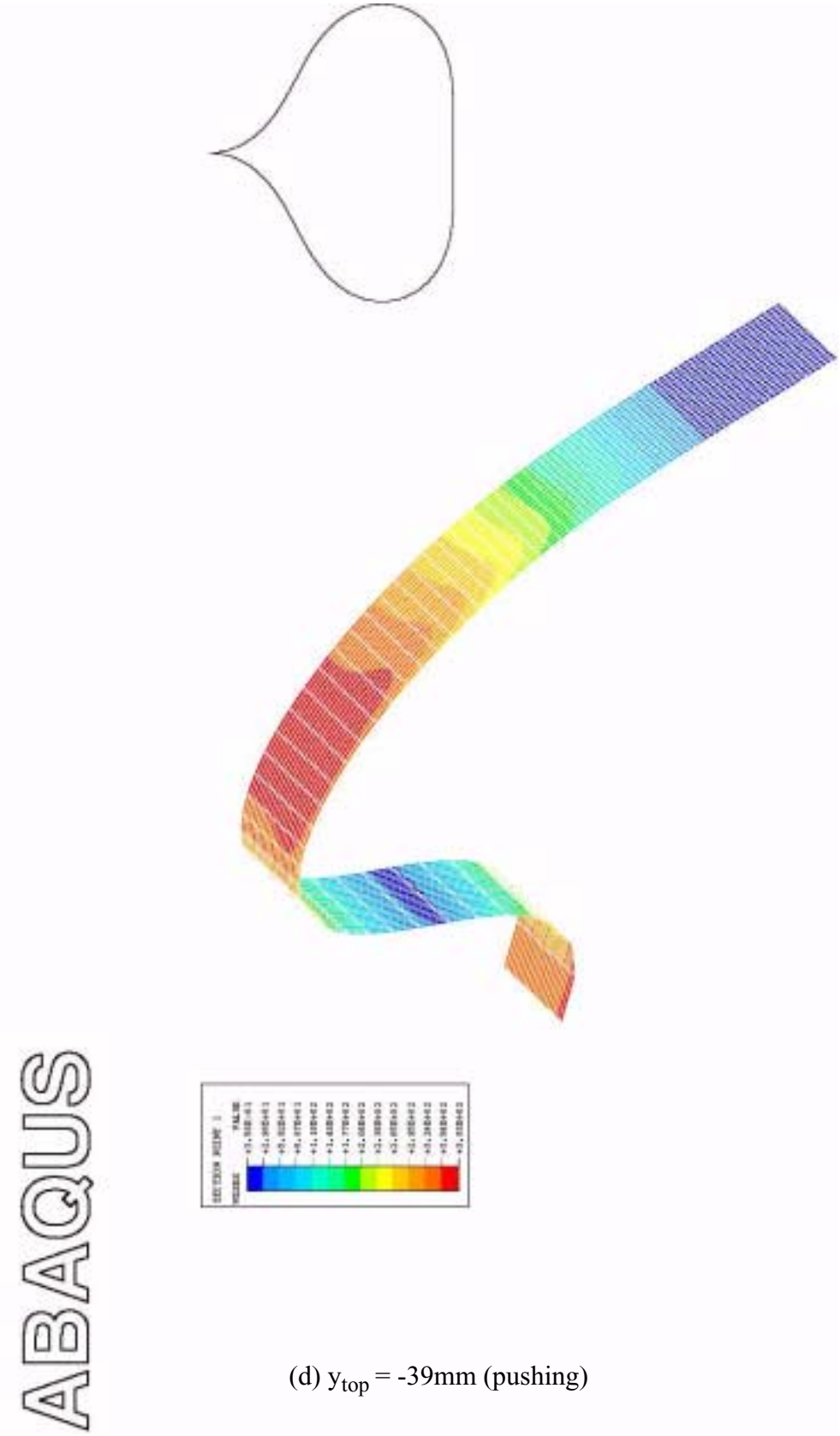

(d) y_{top} = -39mm (pushing)

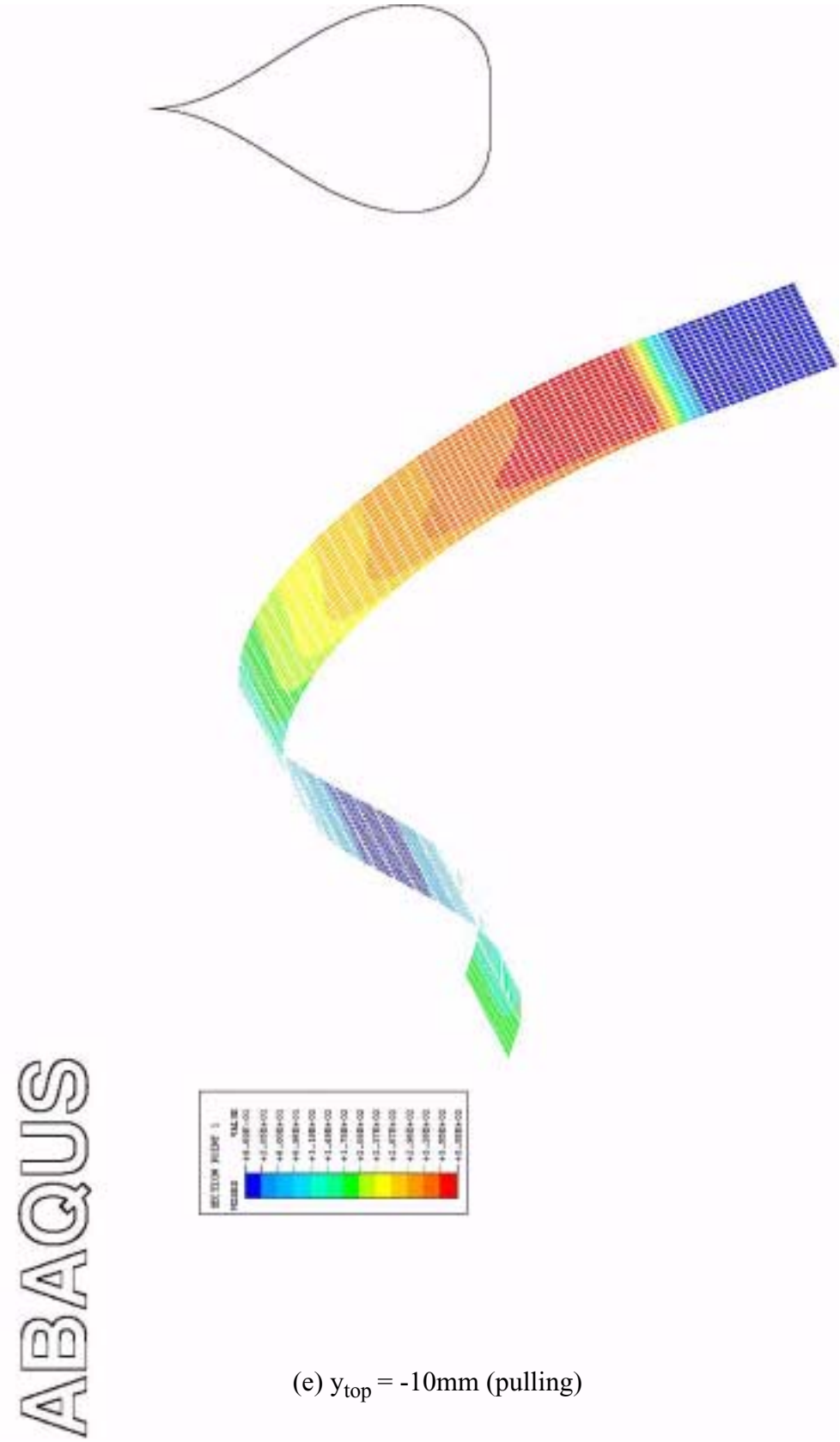

(e) y_{top} = -10mm (pulling)

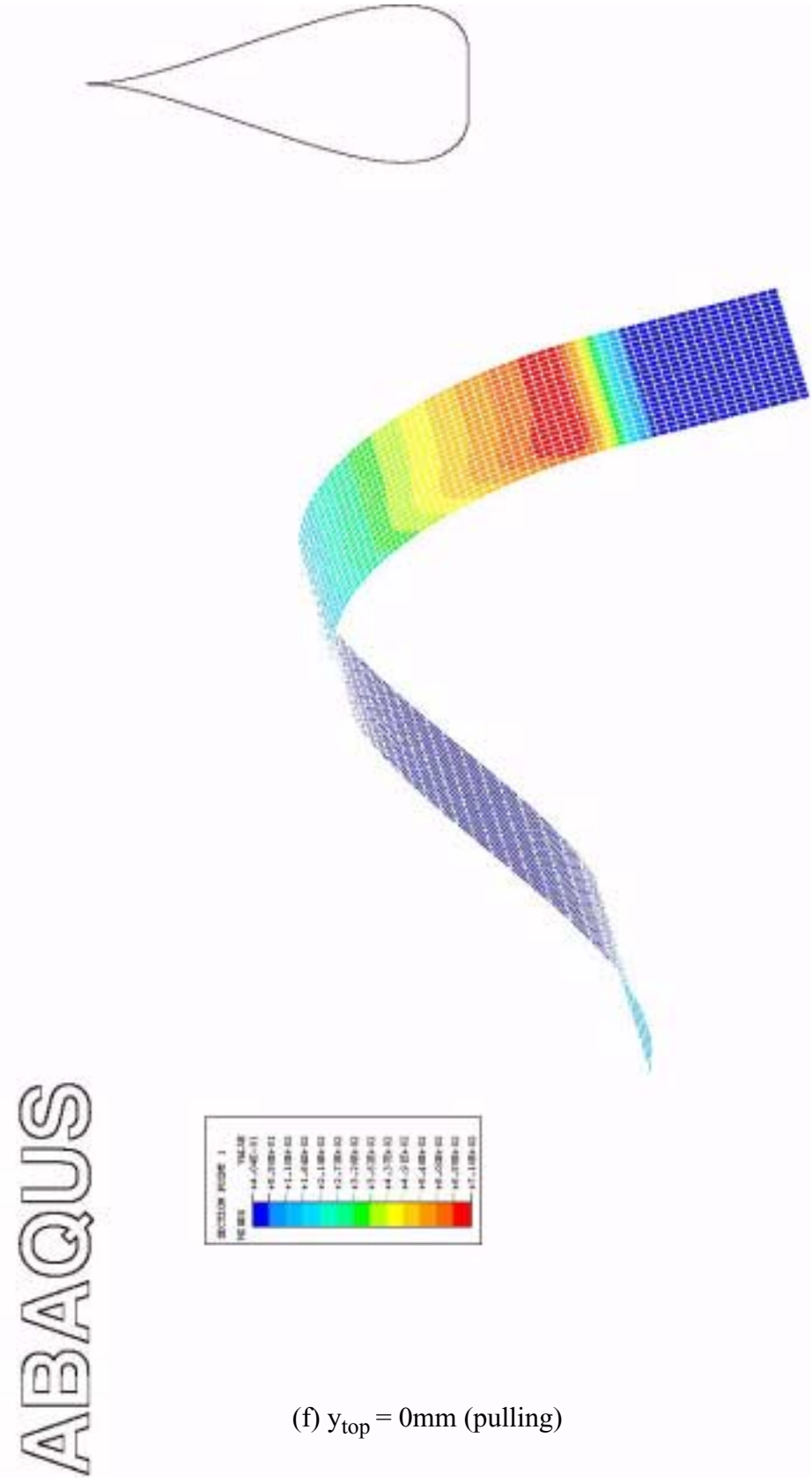

(f) y_{top} = 0mm (pulling)

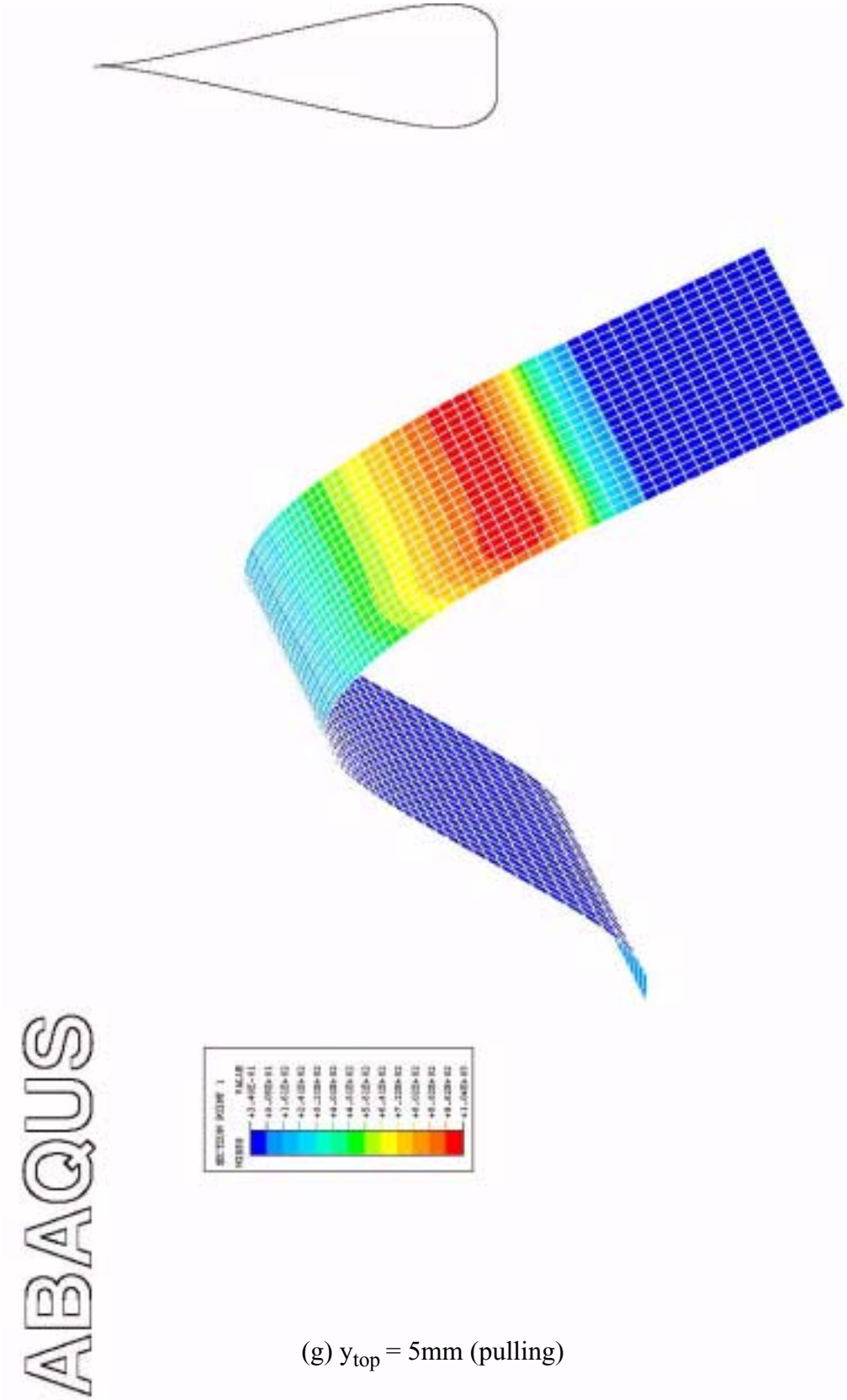

(g) y_{top} = 5mm (pulling)

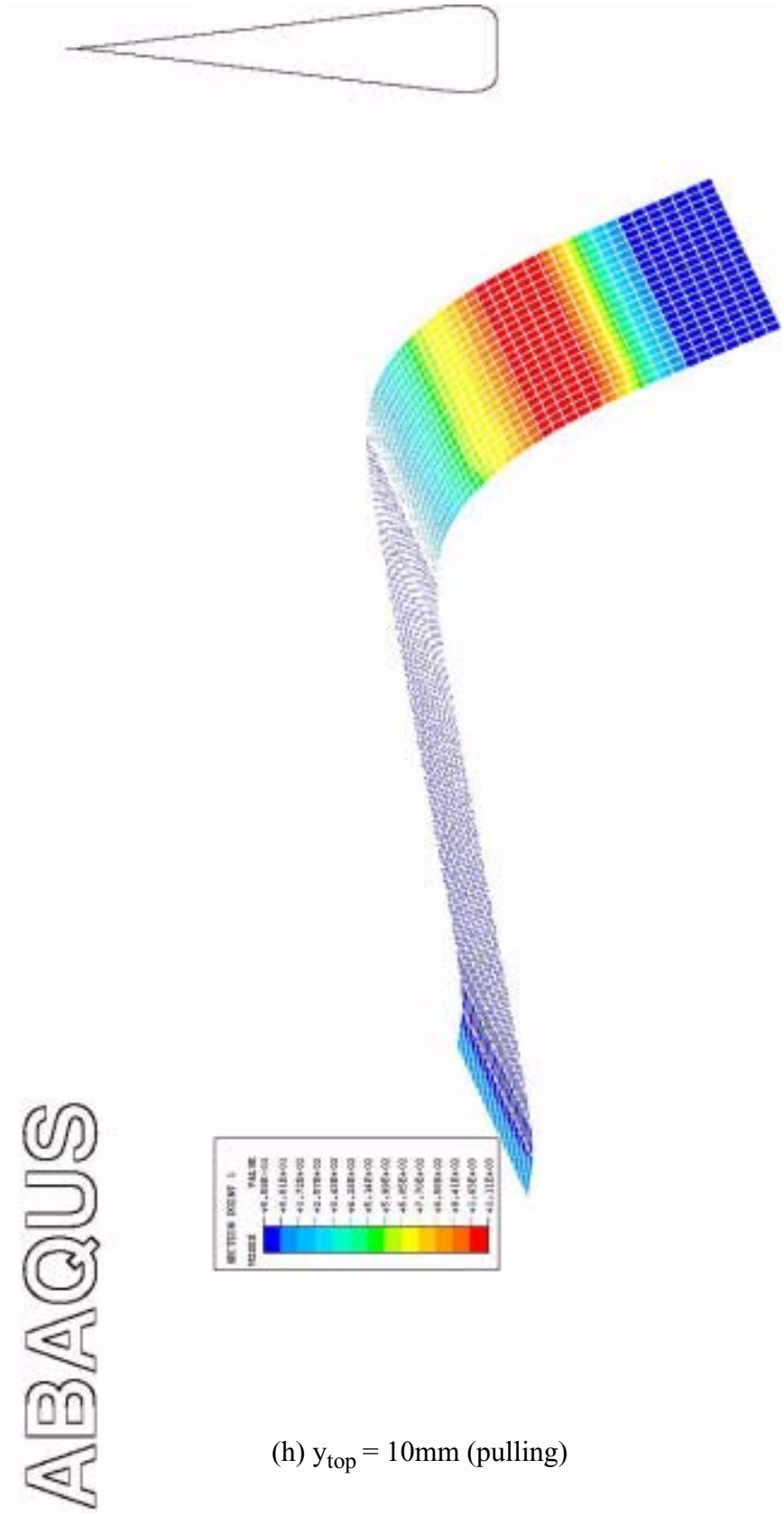

(h) y_{top} = 10mm (pulling)

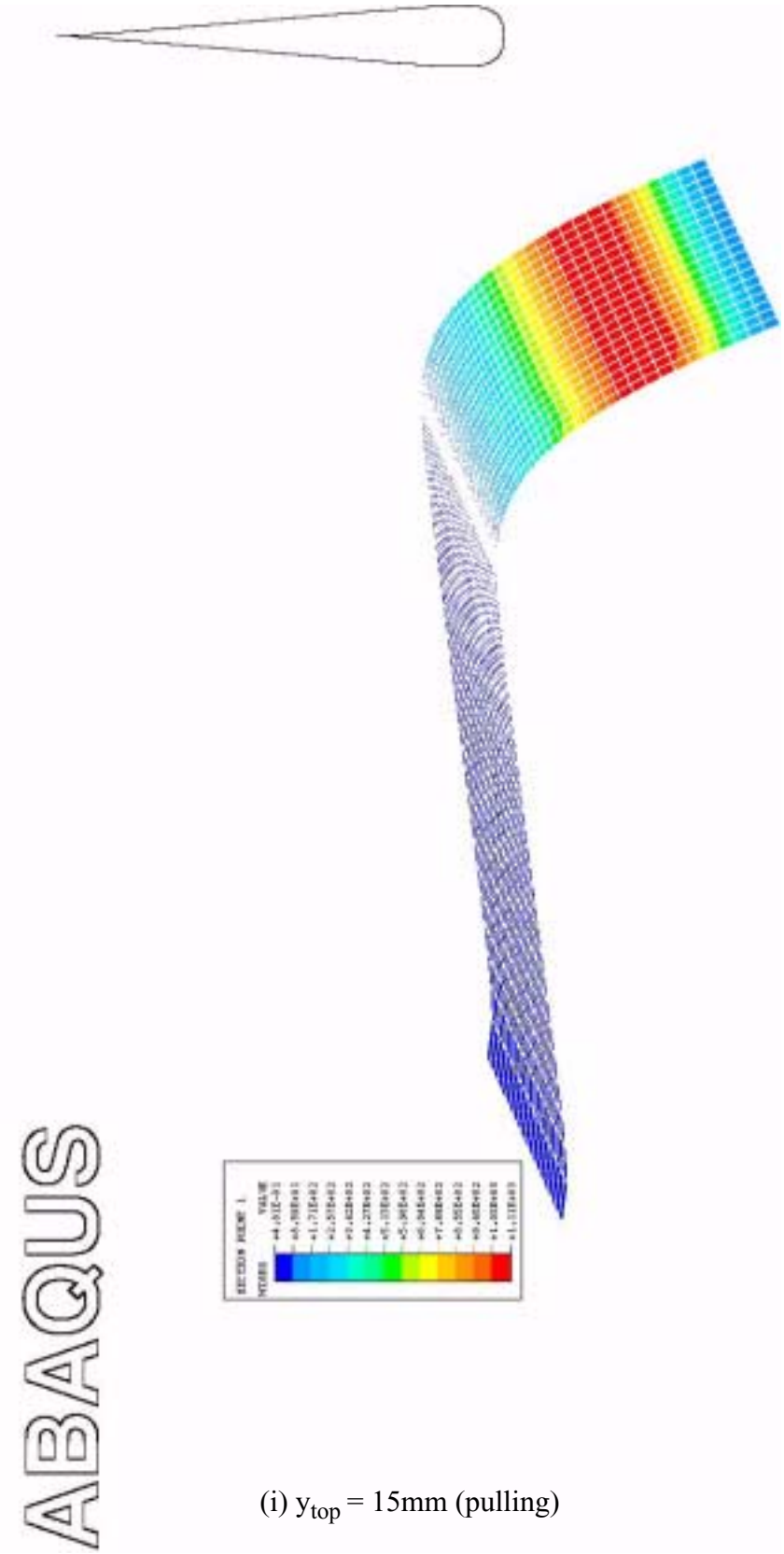

(i) y_{top} = 15mm (pulling)

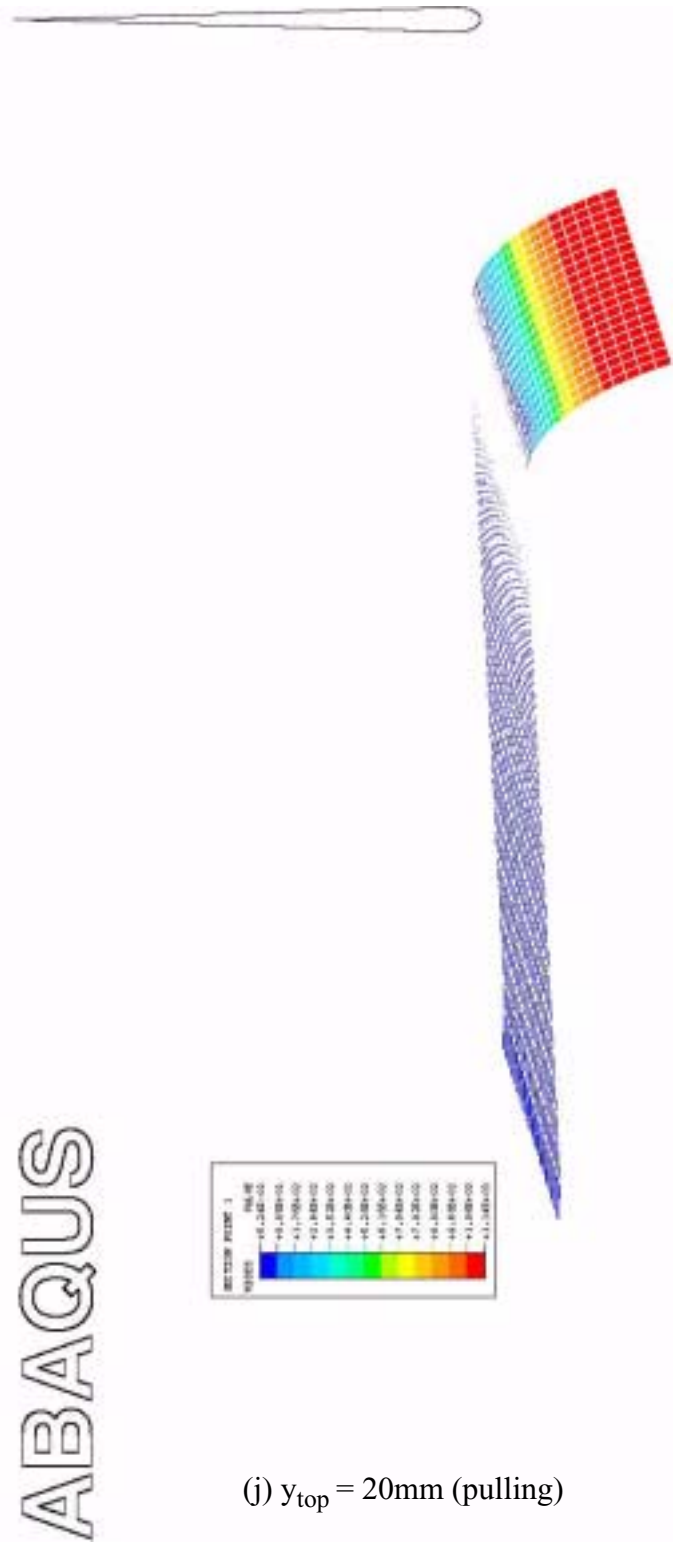

(j) y_{top} = 20mm (pulling)

Figure 5.7 von Mises stress contour in loop tack test

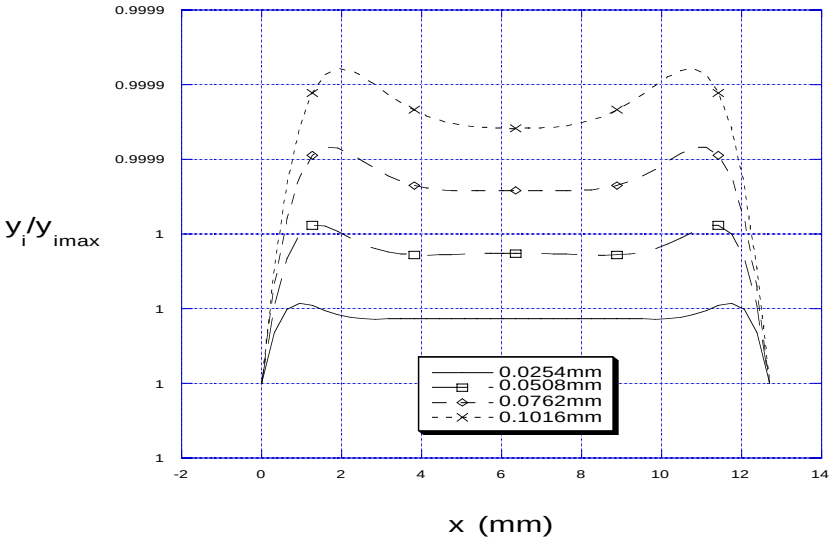

(a) t_{strip}=0.0254mm, 0.0508mm, 0.0762mm,0.1016mm

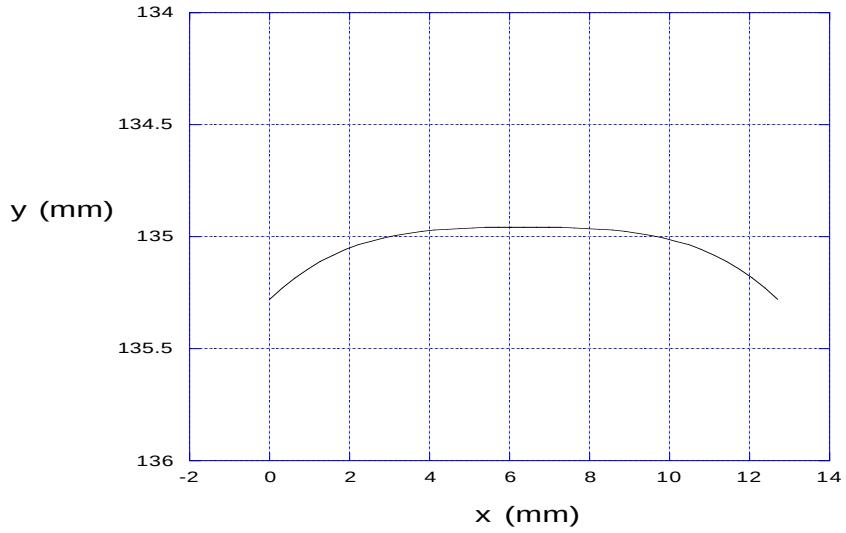

(b) t_{strip}=2.54mm

Figure 5.8 Anticlastic bending behavior for stainless steel strip

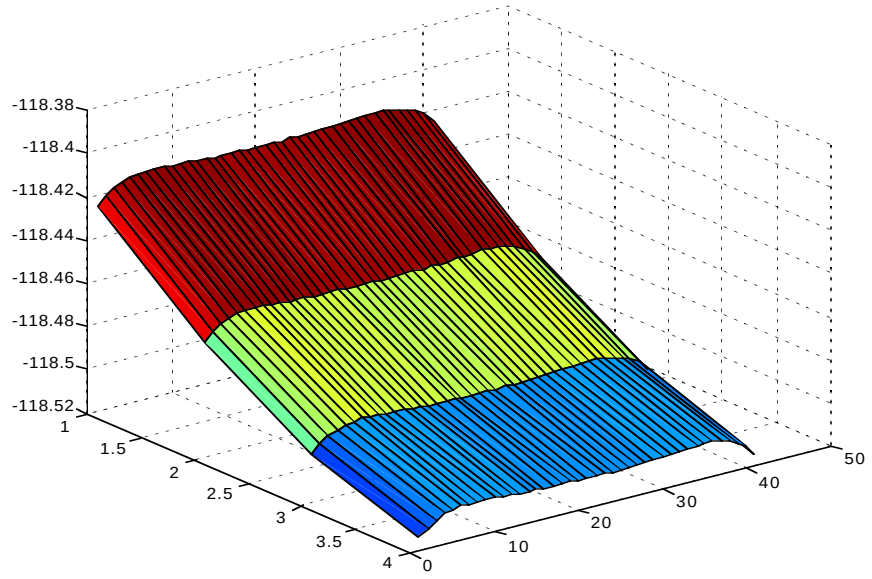

(a) t_{strip}=0.1016mm

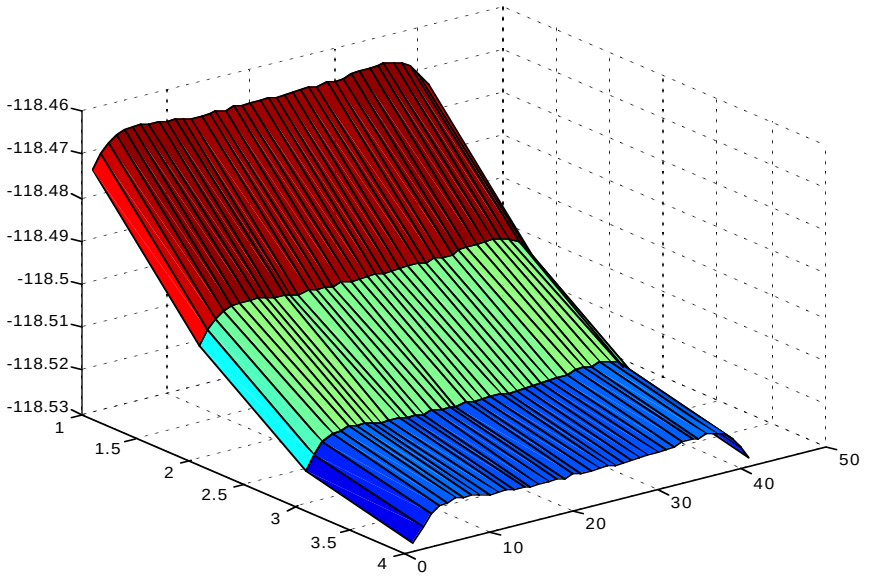

(b) t_{strip}=0.0762mm

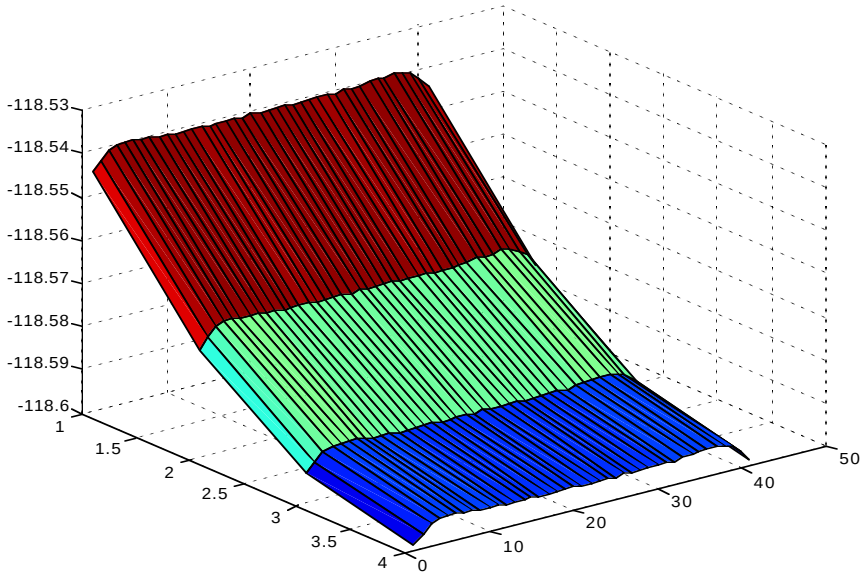

(c) t_{strip}=0.0508mm

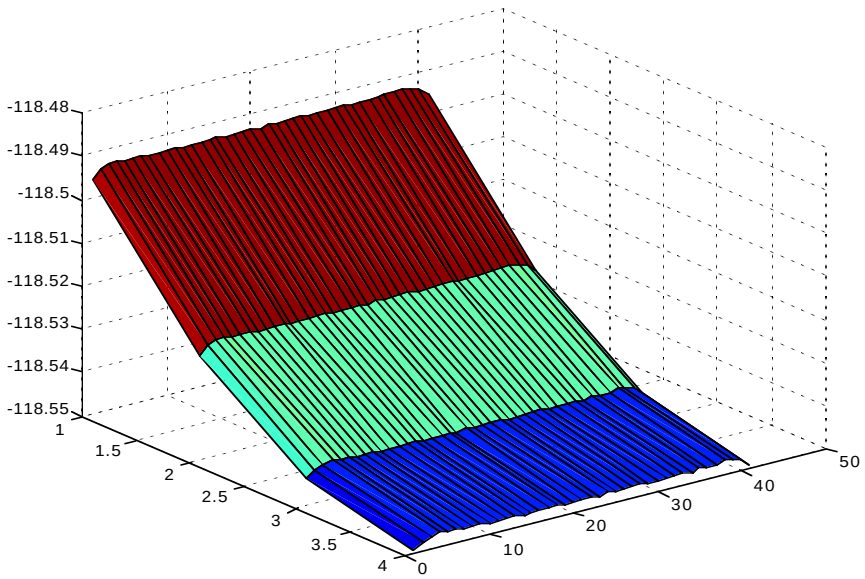

(d) t_{strip}=0.0254mm

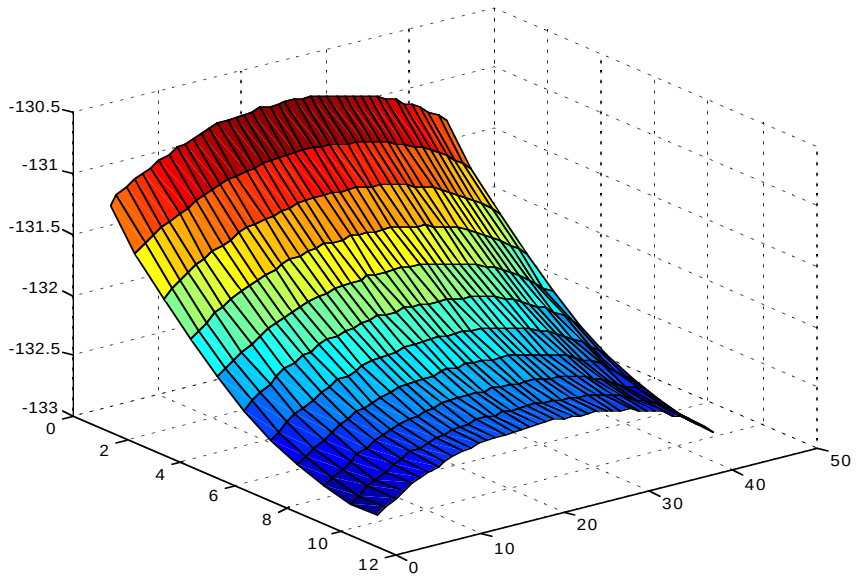

(e) t_{strip}=2.54mm

Figure 5.9 3D anticlastic bending behavior for stainless steel strip

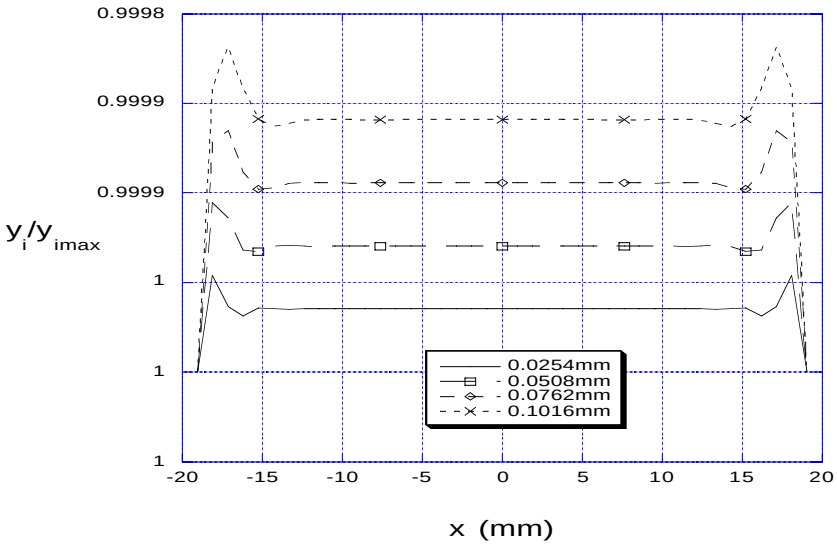

(a) t_{strip}=0.0254mm, 0.0508mm, 0.0762mm,0.1016mm

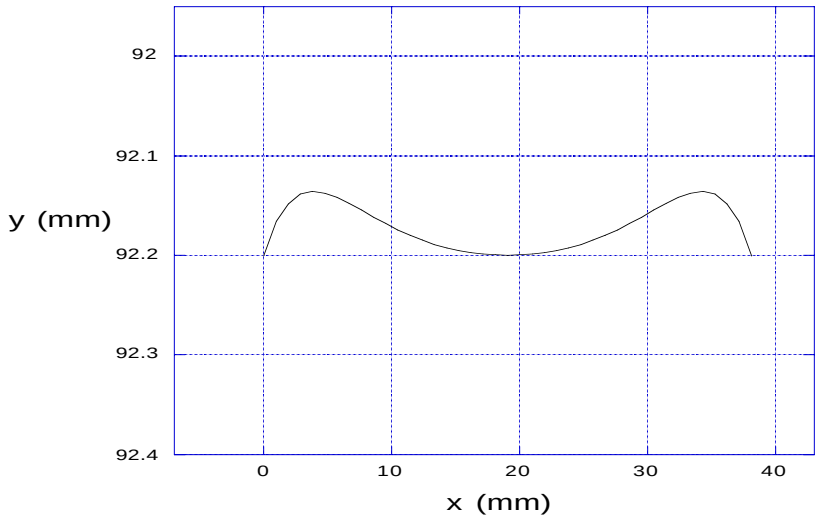

(b) t_{strip}=2.54mm

Figure 5.10 Anticlastic bending behavior for Mylar strip

5.2 Plasticity Effect of Strip

As mentioned in the review section, after the test strip is curled, a plastic hinge may be observed at the middle of the loop. This observation indicates that the strip is plastically deformed during the loop tack test. Therefore, consideration of the plastic behavior of the strip is required. The effect of plasticity of the strip is investigated throughout the 2D finite element analysis (Figures 5.11 and 5.12) and 3D finite element analysis (Figure 5.7). The elastic constants of the stainless steel strip are $E = 153\text{GPa}$, $\nu = 0.27$. The yield stress of the strip is taken to be $\sigma_y = 1108.8\text{MPa}$ (dash lline in Figure 5.11), and the experimentally determined uniaxial stress-strain curve and idealized bilinear stress-strain curve for the strip are shown in Figure 3.2. The nonlinear spring function parameters are $\beta_1 = 0.02$, $\beta_2 = 0.75$, and $\beta_3 = 0.5$, and the contact length at the end of the pushing process is 25.4mm. The length of loop (L_{loop}) is 279.4mm.

Figure 5.11 shows the calculated maximum von Mises stress as a function of the vertical top displacement of the loop. First leftward arrows in Figure 5.11 indicate transition of the maximum von Mises stress during the pushing procedure and the rightward arrows show transition of the maximum von Mises stress during the pulling procedure. It is possible to predict yielding position at the top displacement of the loop. As shown in these figures, the maximum von Mises stress approaches the yield stress as the top displacement of the loop reaches 8mm, 8mm, 18mm, and 16mm for each strip thickness, respectively. Figure 5.12 shows a comparison of the elastic and plastic pulling force curve results. For the same PSA, a thin strip yields earlier, but the total energy dissipated will be small because the thickness is small. Therefore, the contribution of plastic yielding to the pulling force is smaller than for a thicker strip.

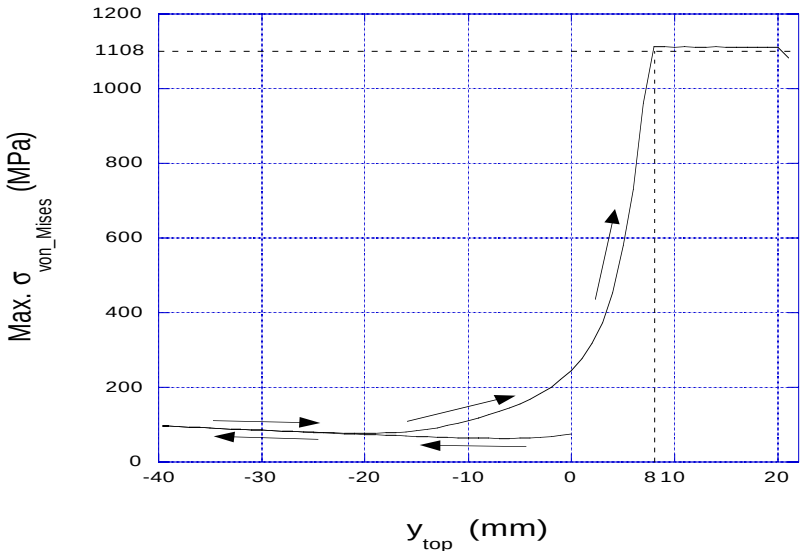

(a) t_{strip}=0.0254mm

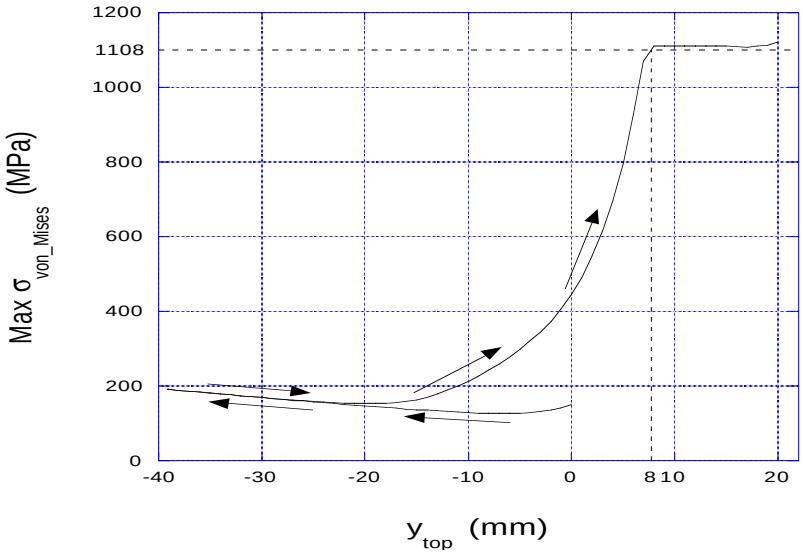

(b) t_{strip}=0.0508mm

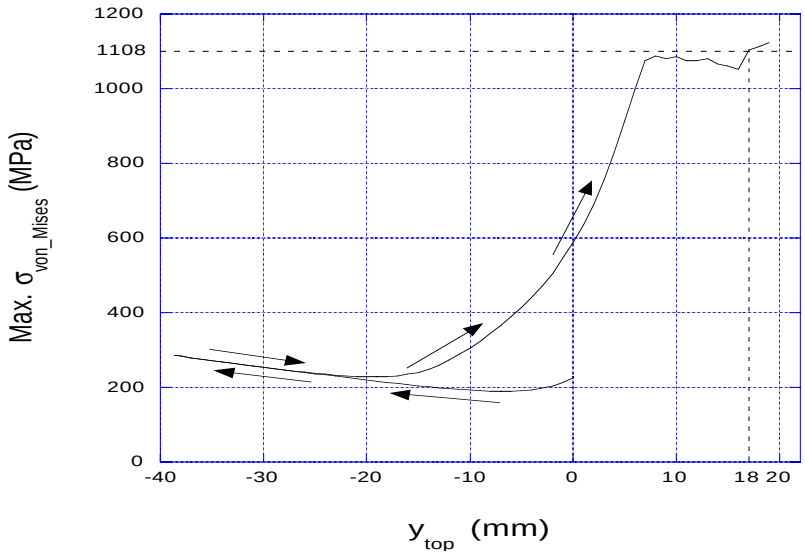

(c) t_{strip}=0.0762mm

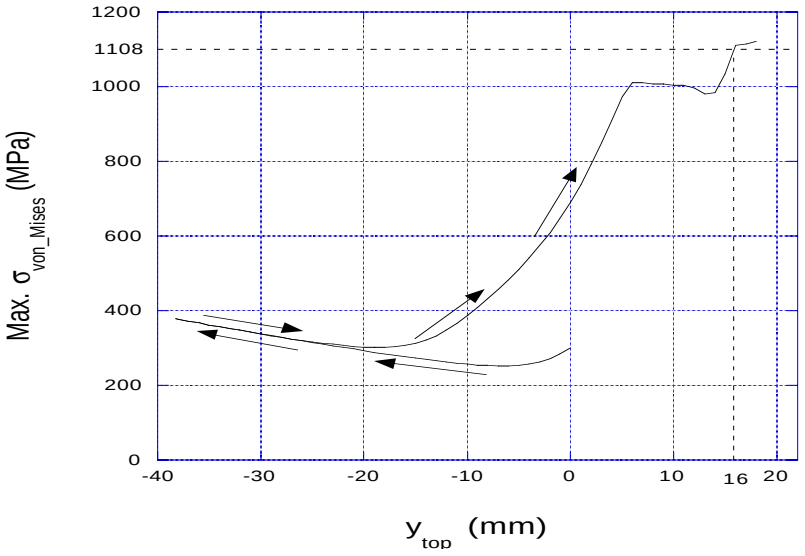

(d) t_{strip}=0.1016mm

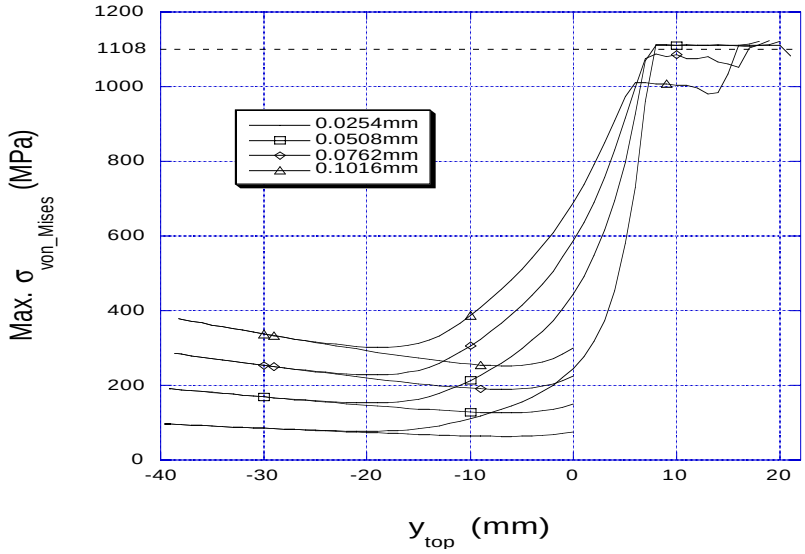

(e) Comparison of max. von Mises stress vs. y_{top}

Figure 5.11 Maximum von Mises stress through pushing and pulling phases

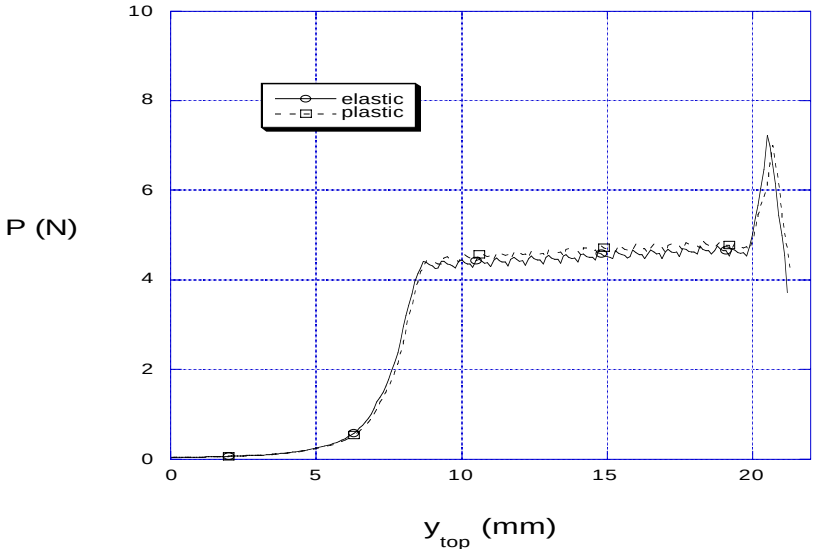

(a) t_{strip}=0.0254mm

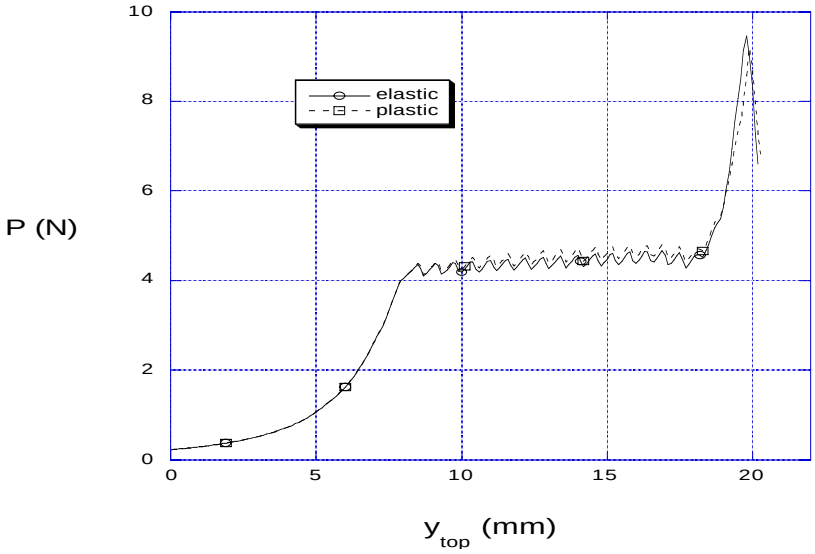

(b) t_{strip}=0.0508mm

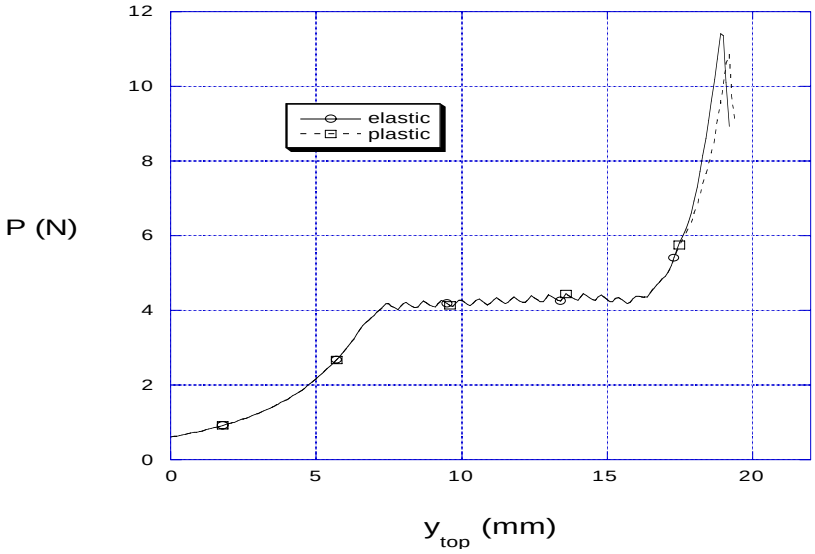

(c) t_{strip}=0.0762mm

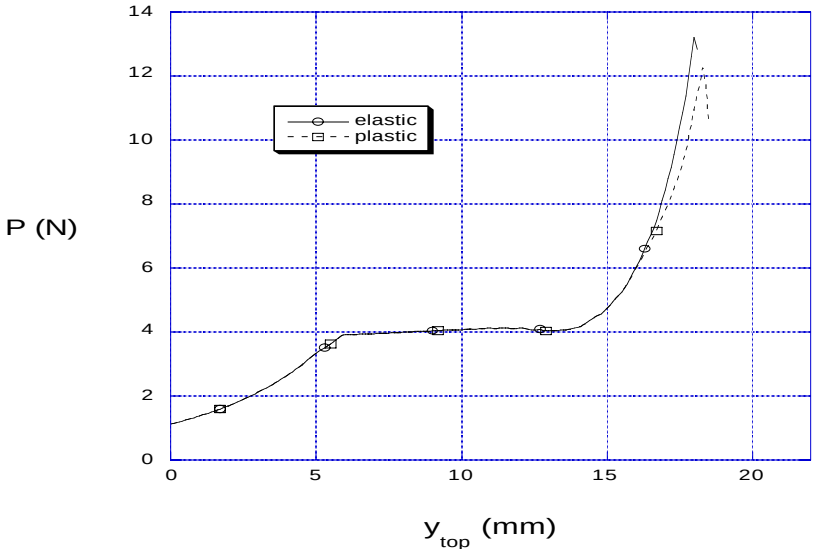

(d) t_{strip}=0.1016mm

Figure 5.12 Comparison of plasticity effect in pulling phase

5.3 Contact Pattern

Qi (2000) conducted a 3D finite element analysis using ABAQUS to calculate the effect of anticlastic bending of the elastica loop and simulate the contact process between the loop and a flat rigid surface with appropriate displacement increment and force increment. She presented contact patterns, normal contact stresses, strain distribution, and displacement profiles obtained during the 3D analysis, taking into account anticlastic curvature. According to her results, because of anticlastic bending behavior of the loop, contact is first initiated at the edge of the loop in the experiments and numerical analysis. However, since the ratio of thickness (0.165mm) and width (0.954mm) of the strip is large, the strip does not show distortion or flattening behavior in the transverse direction as in the present results.

The contact length ($L_{contact}$) versus the displacement at the top of the loop (y_{top}) relationship in the pushing procedure obtained from 2D finite element analysis using ABAQUS is illustrated in Figure 5.13. The contact length is the distance between the nodes of the contact front as shown in Figure 2.1b and in 2D analysis it is assumed that contact at the contact front in the transverse direction occurs simultaneously. All parameters are the same as in the previous section. The initial condition is a point contact and the contact length increases as the top of the loop is pushed down. Overall contact patterns are similar after second node contact, but the second node contact is different with respect to strip thickness. The contact pattern is not dependent on which spring function is chosen. It depends on the thickness and elasticity modulus of the strip. In the 3D numerical analysis, because of anticlastic bending behavior, the contact at the contact front in the transverse direction does not take place as in 2D analysis. Therefore, determination of the contact length in 3D analysis is ambiguous so that we should define which contact length will be measured (from center or edges in the transverse direction). Thoughout 3D analysis, for simplification and to save computational time, springs were activated at the same step in the transverse direction as in the 2D analysis and the parameters are the same as in section 5.1.2. Figure 5.14 shows the 3D y-coordinate contour in the pushing procedure. Especially, in Figures 5.14d-5.14f, because of anticlastic bending behavior, a parabolic shape contact boundary occurs in the transverse direction. This results are in good agreement with Qi's results. As pointed out, in anticlastic bending behavior section, edge parts contact first. The initial height of the teardrop shape loop after the forming procedure is 118.50mm. So if the absolute y-coordinate of a node in Figure 5.14 is larger than 118.50mm, contact occurs. Figure 5.15 illustrates the transition of total spring force versus contact length for t_{strip}= 0.0254mm in the pushing (rightward) and pulling (leftward) procedure. During the debonding procedure, as the contact length gets narrow, the corresponding total spring force is almost constant, but at the end of the pulling phase a peak occurs as explained in section chapter 5.1.1.

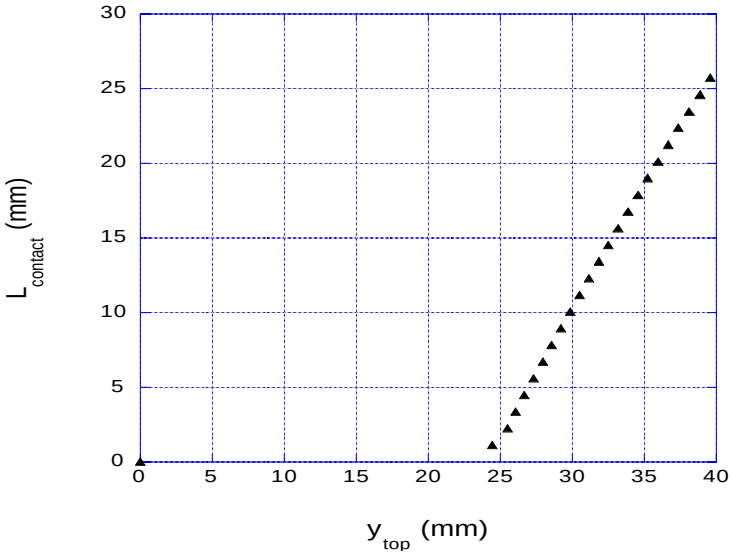

(a) t_{strip}=0.0254mm

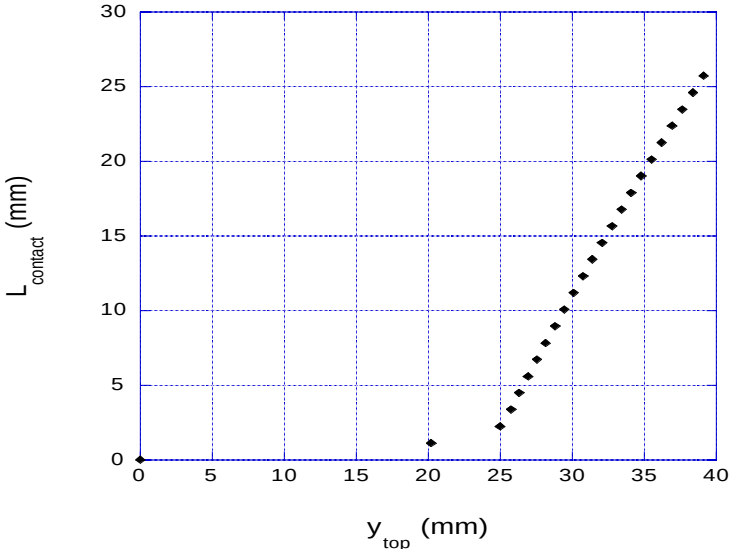

(b) t_{strip}=0.0508mm

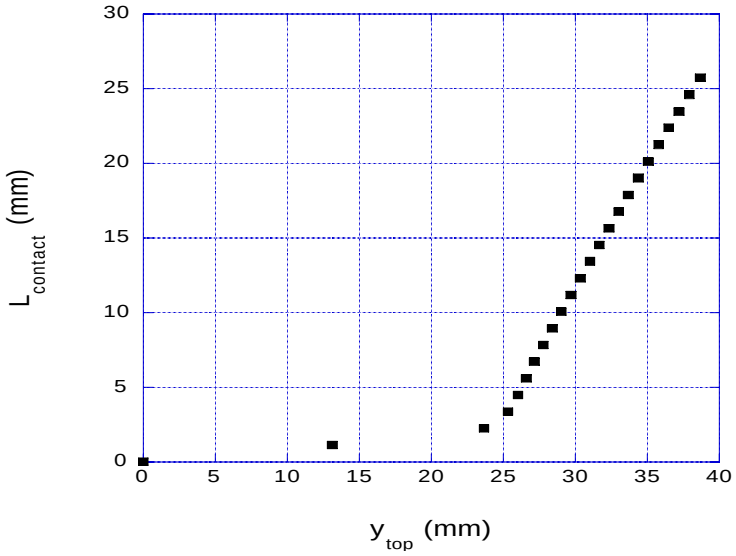

(c) t_{strip}=0.0762mm

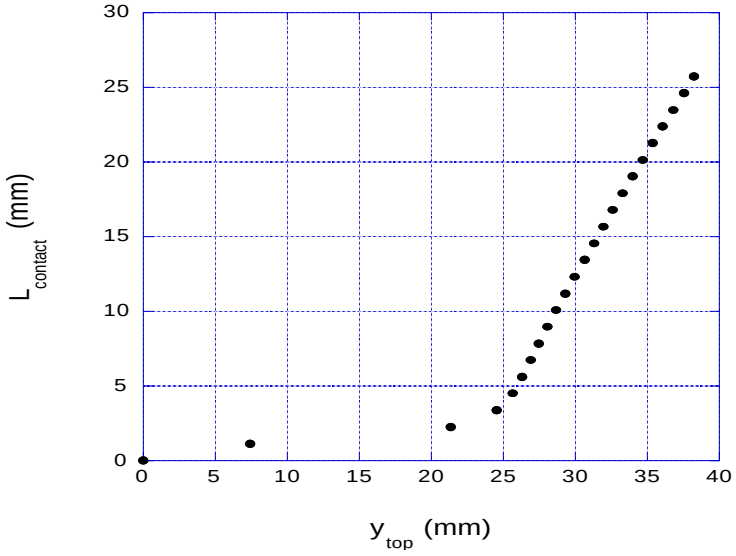

(d) t_{strip}=1.1016mm

Figure 5.13 Contact pattern in pushing phase

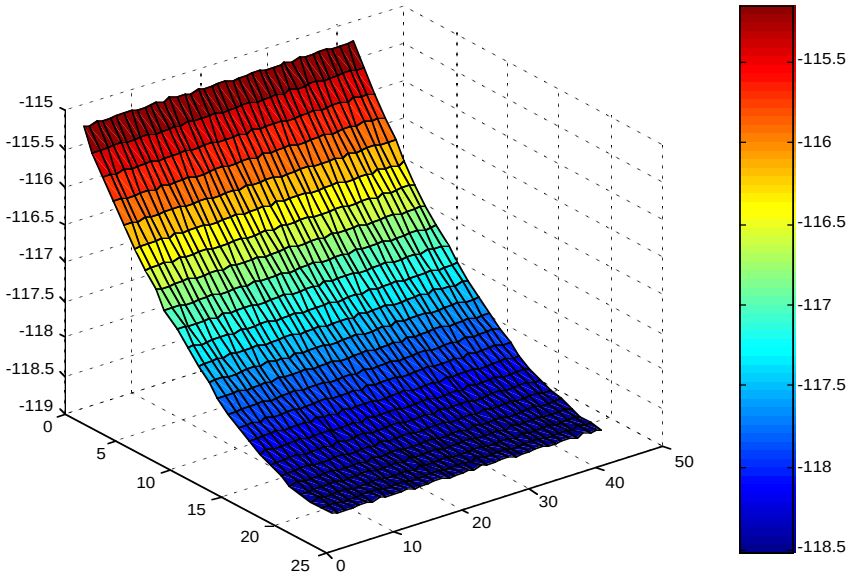

(a) y_{top}=0mm

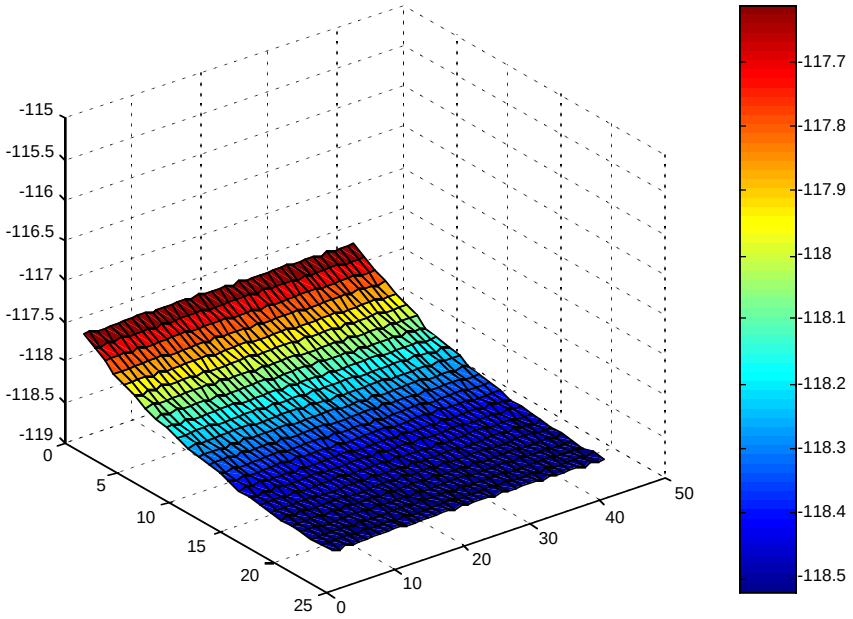

(b) y_{top}=20mm

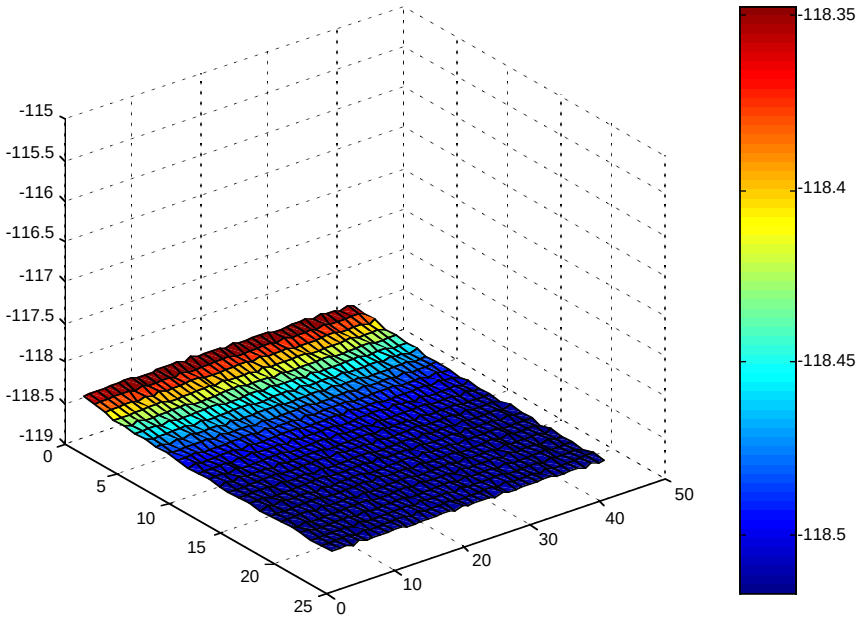

(c) y_{top}=30mm

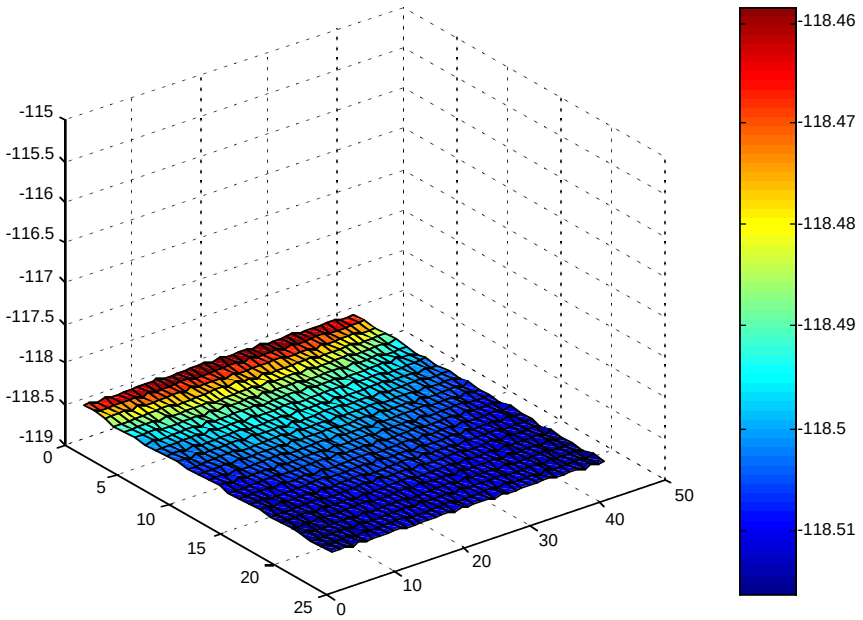

(d) y_{top}=35mm

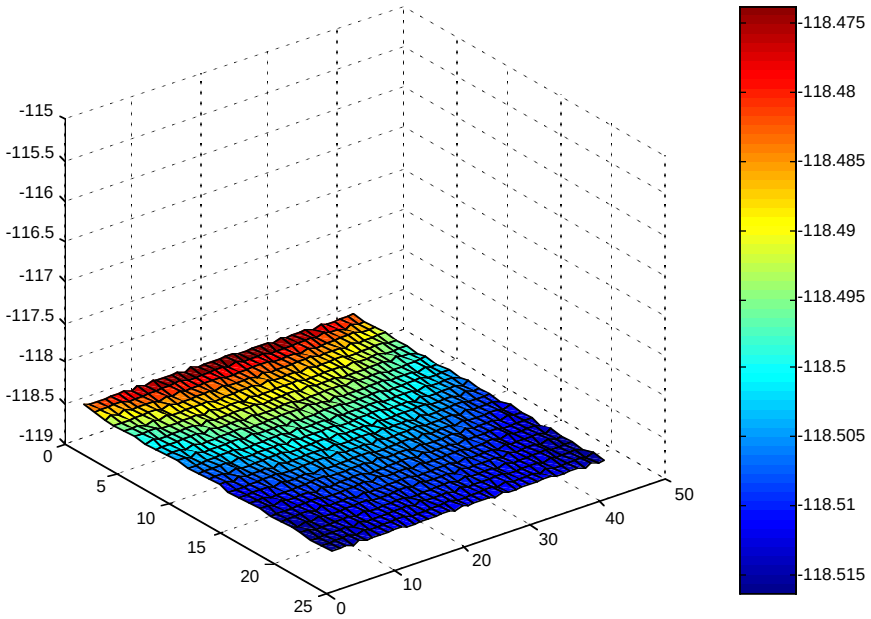

(e) y_{top}=37mm

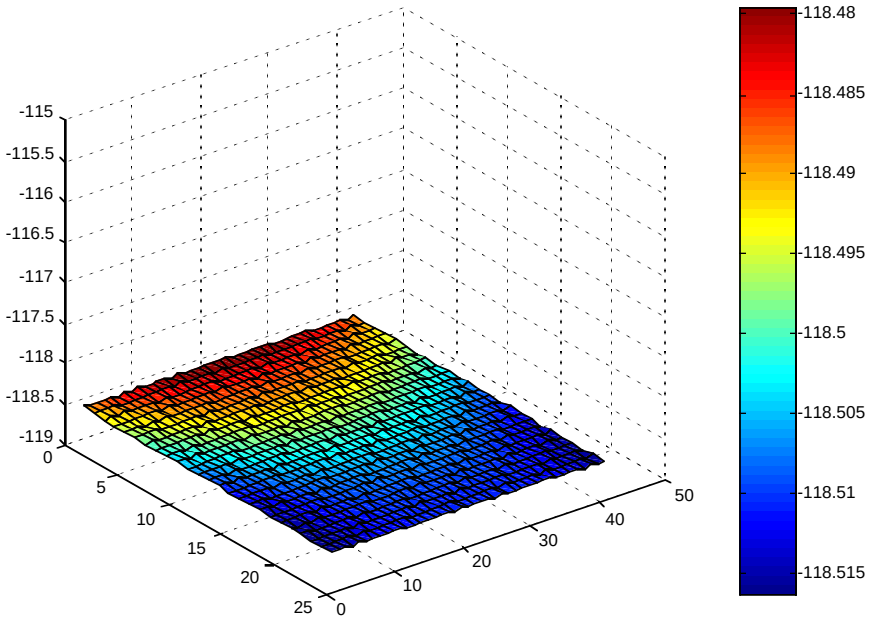

(f) y_{top}=39mm

Figure 5.14 3D contact contour in pushing phase

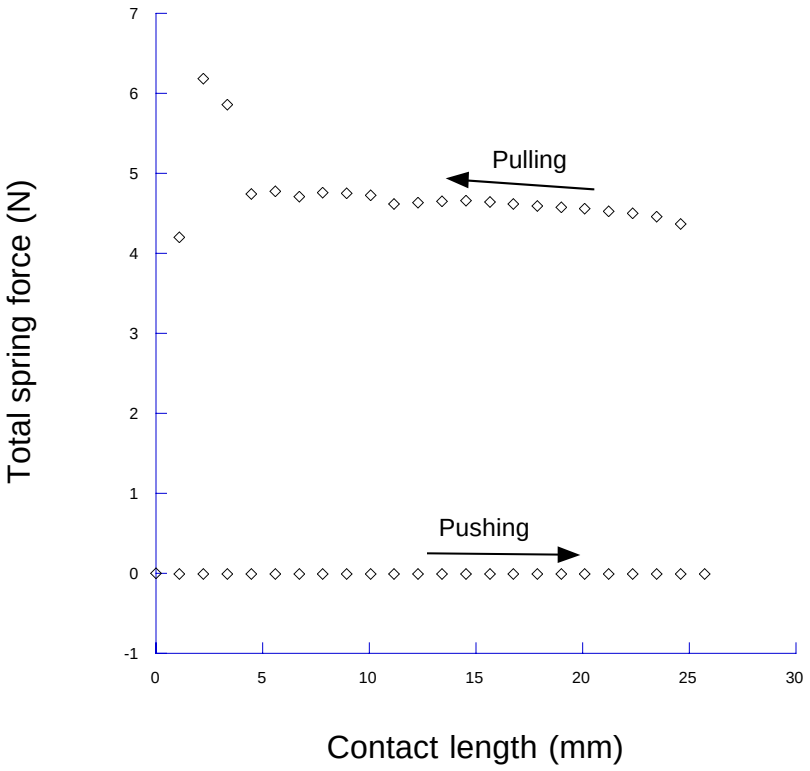

Figure 5.15 Total spring force vs. contact length (t_{strip}=0.0254mm)

5.4 Alternative Nonlinear Spring Function Results

An alternative triangular shape nonlinear spring function (Figure 5.16) is used in this section for research purposes. According to Zosel (1998), a sharp triangular shape for force versus time or stress versus strain curves is observed for polymers with low tack and the deformation is supposed to be homogeneous in the probe tack test. Figures 5.17 and 5.18 and Tables 5.1 and 5.2 present comparisons between results from numerical analysis and experiments for two different β_1 (=0.05 and 0.1) values with varying β_3 for thickness of strip = 0.1016mm. The contact length at the end of the pushing process is 25.4mm and the length of the loop (L_{loop}) is 279.4mm. As observed in the previous nonlinear spring parametric study, in the case of larger β_1, overall the pulling curve increases greatly with increasing β_3, and the same trend of the pulling force curve as for the trapezoid shape nonlinear spring function is observed. Increasing area of pulling zone, peak pulling force, and plateau stress are dependent upon β_1 as shown in section 4.1.1. If β_3 is smaller than 0.5, that is, using a sharper triangular shape, the process does not converge. As mentioned in chapter 3, the analysis was terminated before the maximum pulling force was achieved, due to ill-conditioning. However, according to the Arcan tensile test (Appendix C), the range of total elongation for VHB tape (at separation rate = 5mm/min.) may be from the adhesive thickness to twice the adhesive thickness, so that small total elongation (brittle failure) may not happen in real debonding.

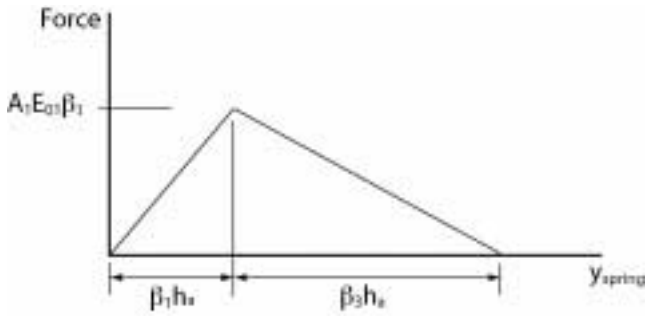

Figure 5.16 Triangular nonlinear spring function

Table 5.1 $\beta_1 = 0.05$, $t_{strip} = 0.1016$mm

β_3	P_{max}	Area	$P_{plateau}$
0.5	11.90	64.23	2.63
0.75	13.72	85.22	3.95
1	15.78	106.68	5.43
1.5	19.66	147.52	8.63
expt	20.95	95.32	5.91

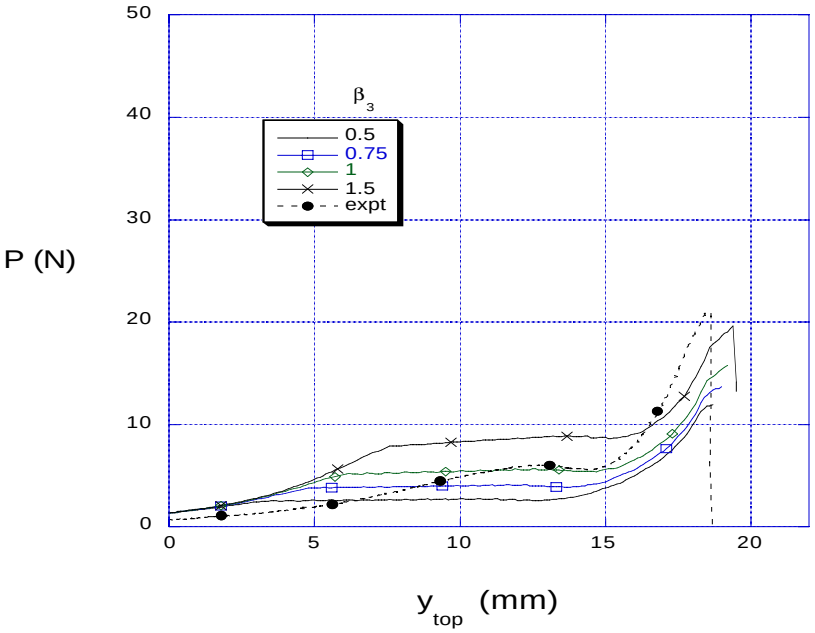

Figure 5.17 Pulling force curves

Table 5.2 $\beta_1 = 0.1$, $t_{strip} = 0.1016$mm

β_3	P_{max}	Area	$P_{plateau}$
0.5	18.74	131.75	6.81
0.75	23.12	174.36	10.31
1	27.15	222.00	13.40
1.5	34.42	300.29	19.98
expt	20.95	95.32	5.91

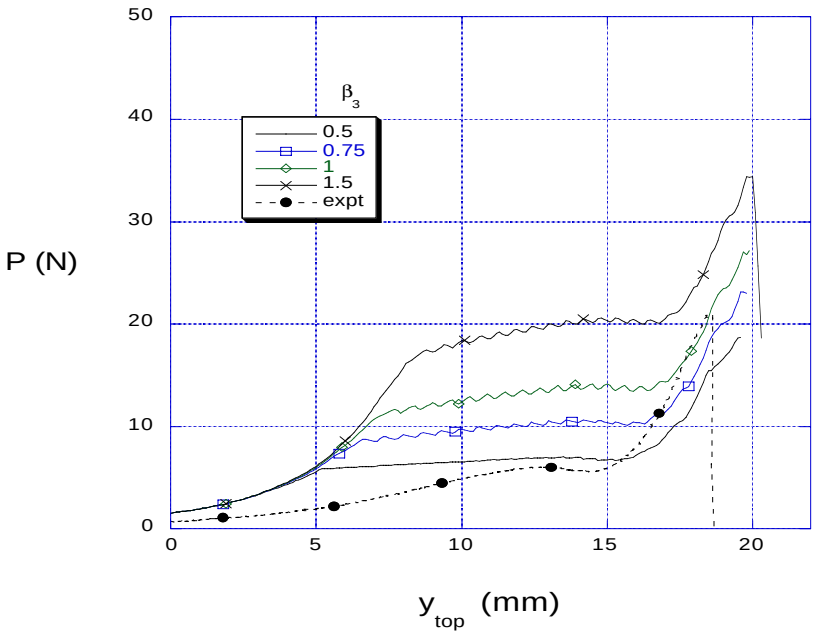

Figure 5.18 Pulling force curves

5.5 Pulling Force Curves

As mentioned previously, the pulling curve (tack curve) is dependent on the nonlinear spring function parameters. In this section, trying several different sets of physically unrealistic parameters (especially β_2), approximate pulling force curves are determined. The nonlinear elastic spring function parameters are $\beta_1 = 0.003$, $\beta_2 = 8$, and $\beta_3 = 0.5$ for t = 0.0254mm, $\beta_1 = 0.006$, $\beta_2 = 8$, and $\beta_3 = 0.5$ for t = 0.0508mm, $\beta_1 = 0.015$, $\beta_2 = 6.3$, and $\beta_3 = 0.5$ for t = 0.0254mm, and $\beta_1 = 0.008$, $\beta_2 = 3.3$, and $\beta_3 = 0.5$ for t = 0.0254mm, respectively. The contact length at the end of the pushing process is 25.4mm and the length of the loop (L_{loop}) is 279.4mm. Actually, these values are not realistic compared to the experimental results. Figure 5.19 shows the comparison between experimental and numerical result. Because of the long horizontal part of the nonlinear spring function, pulling off does not occur yet.

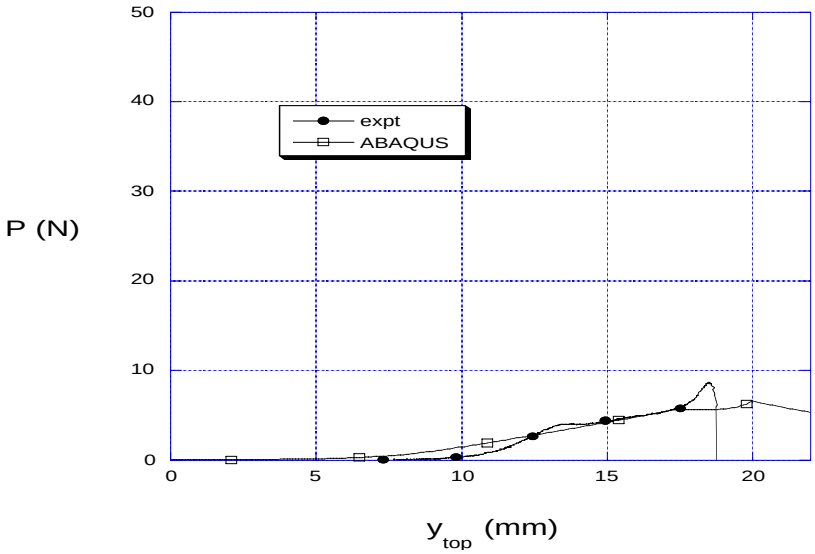

(a) t=0.0254mm

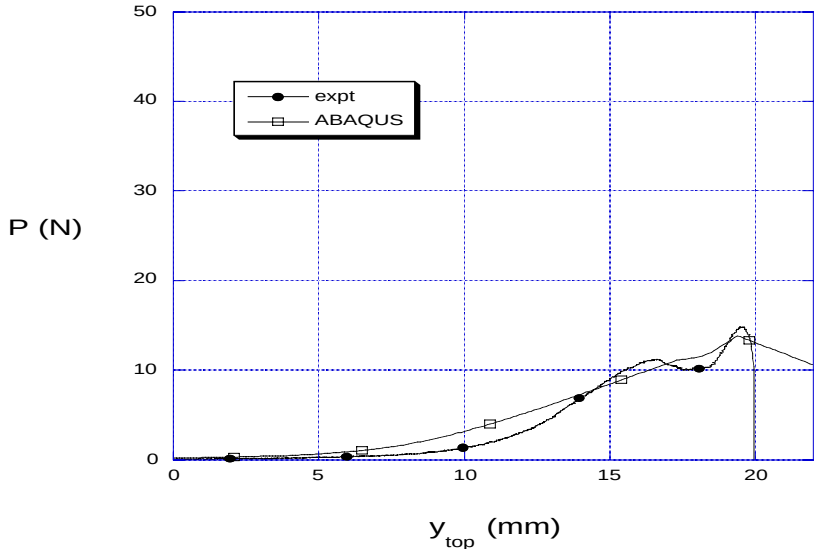

(b) t=0.0508mm

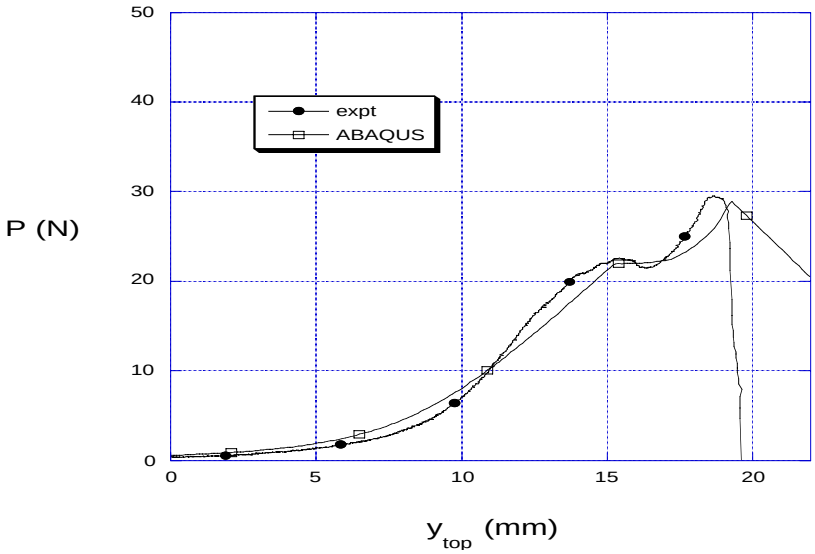

(c) t=0.0762mm

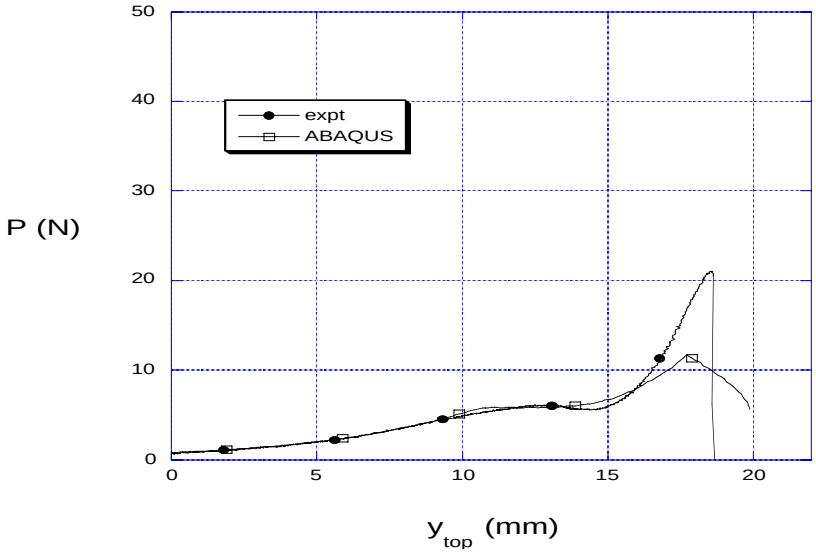

(d) t=0.1016mm

Figure 5.19 Pulling force curves

5.6 Effect of Initial Elasticity Modulus of Pressure Sensitive Adhesives

The effect of the elasticity modulus of a PSA is studied using some elasticity modulus values specified in Table 5.3. These values are determined from DMA test results with respect to different temperatures. The tensile storage modulus (E') from Figure 2.11a converts to tensile elasticity modulus (see Appendix D) with respect to different temperatures as shown in Figure 5.20. Zosel (1989) showed that Young's modulus of PSAs decreases as temperature increases. Figure 5.20's results are in good agreement with Zosel's result. However, since tack requires the adhesive to act as a liquid, if the adhesive becomes too stiff (too high a modulus), then the adhesive does not display tack. Like previous work in this chapter, the PSA is modeled by a Winkler-type elastic foundation where nonlinear elastic spring function parameters are $\beta_1 = 0.02$, $\beta_2 = 1$, and $\beta_3 = 0.2$. The thickness of the loop is 0.1016mm, the contact length at the end of the pushing process is 25.4mm, and the length of the loop (L_{loop}) is 279.4mm. During the bonding formation, it is assumed that the loop is perfectly bonded to the adhesive in the contact region throughout numerical analysis. In Figure 5.21, the overall pulling force curve dramatically increases as E increases. The oscillation of the pulling force curve is observed in Figure 5.21 as E increases. The increase of maximum pulling force and the area of the pulling zone are proportional to the elasticity modulus of the PSA, as shown in Figure 5.22.

Table 5.3 Effect of Initial Elasticity Modulus (E) of PSA

E, MPa	Temperature, $°C$	P_{max}, N	$P_{plateau}$, N	Area, mm^2
4	30	9.02	2.67	53.51
8	23	12.74	4.46	83.37
15	15	19.84	9.04	159.97
20	13	26.05	13.13	214.66
50	4	55.88	38.81	556.62
70	0	76.86	58.72	818.66
expt	23	20.95	5.91	95.32

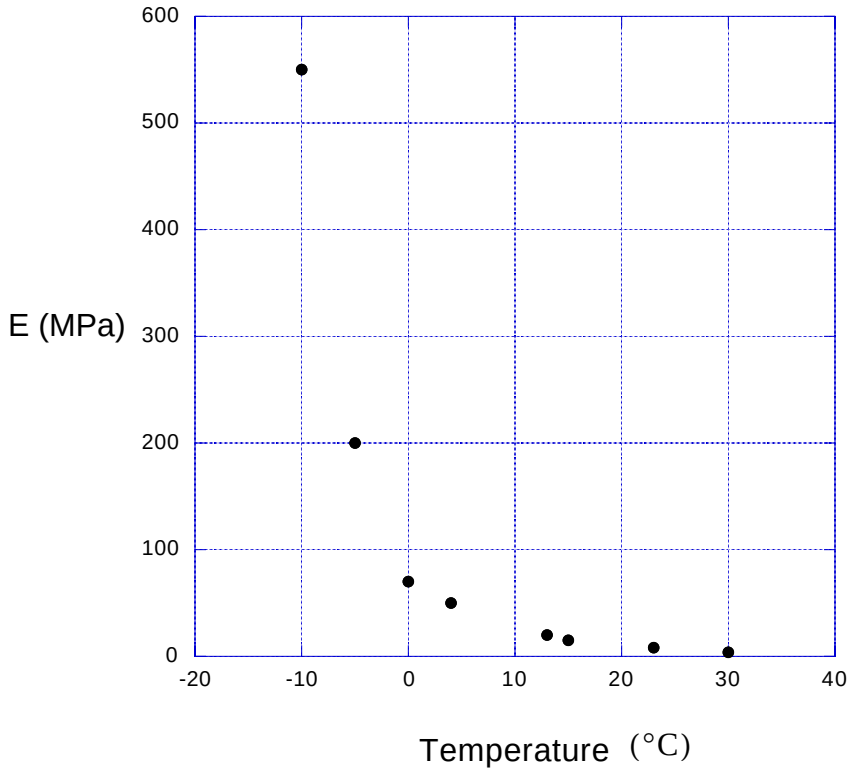

Figure 5.20 Elasticity modulus of PSA vs. temperature

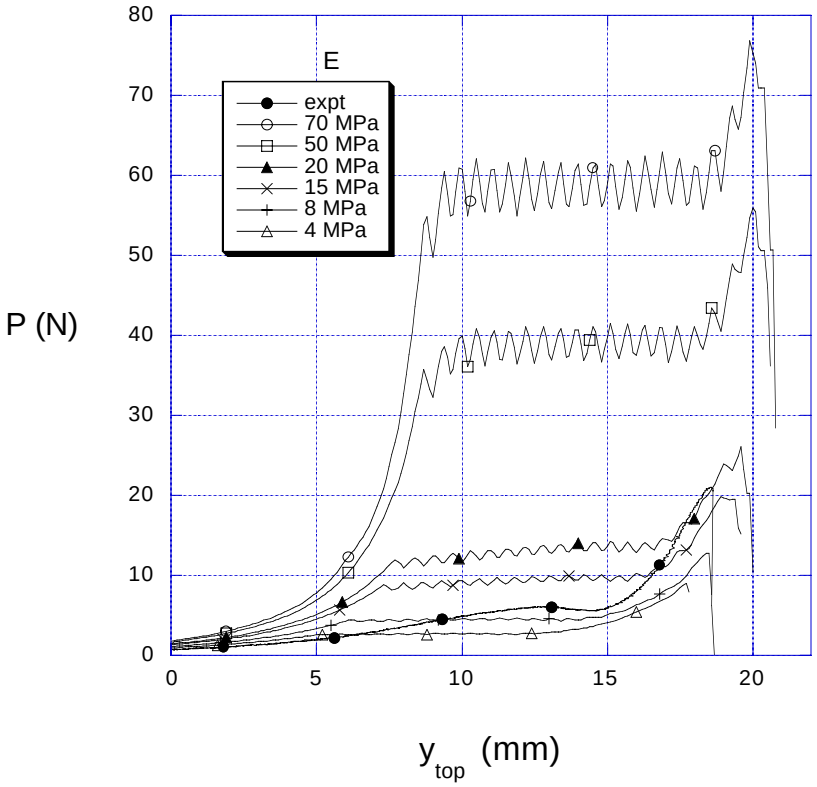

Figure 5.21 Pulling force curves for initial elasticity modulus of PSA

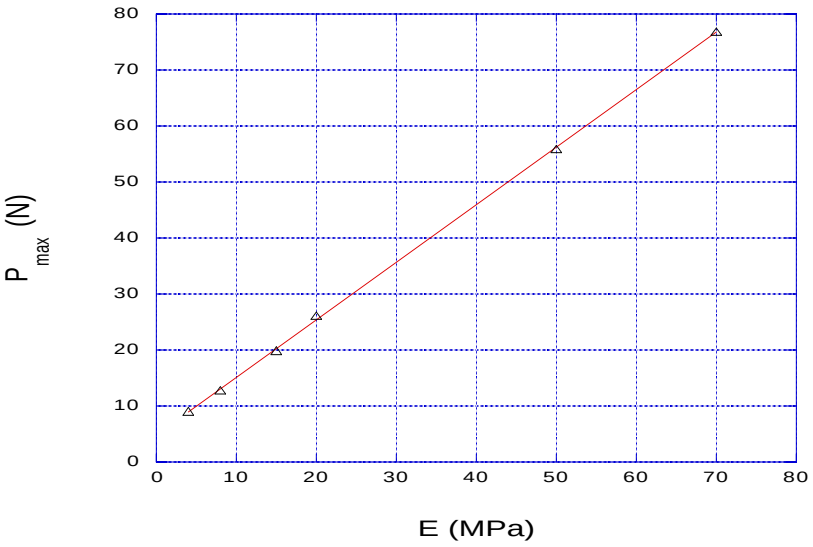

(a) P_{max} vs. E

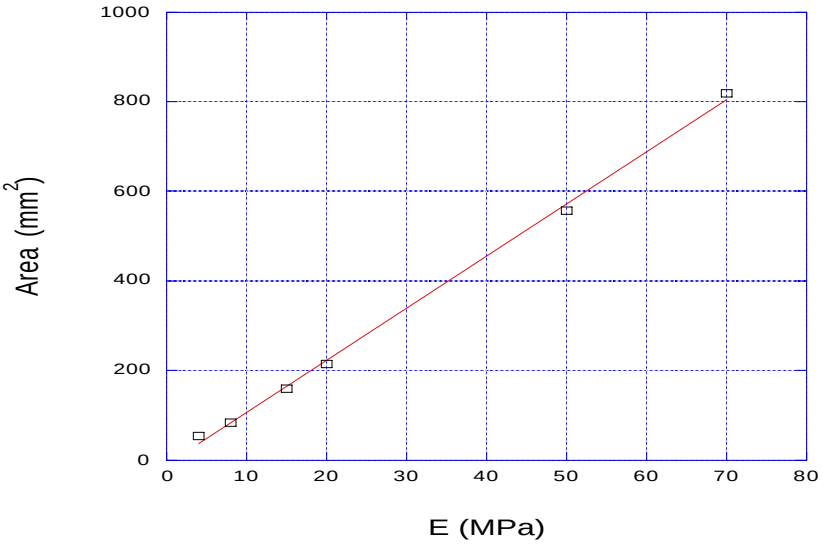

(b) Area vs. E

Figure 5.22 Effect of elasticity modulus of stainless steel strip

5.7 Effect of Displacement Rate and Temperature

Tack is a viscoelastic property of the adhesive. Therefore, temperature and displacement rate must be controlled variables in tack testing. Zosel (1985, 1989, 1992, 1998) has shown a correlation between modulus and tack and the dependence of the tack properties on temperature from the probe tack test. In his study, tack was defined as the adhesive fracture energy per unit of interface, determined under conditions of short time and low pressure. The adhesive fracture energy is obtained by integration of the force times velocity versus time curve over the separation phase and dividing by the probe area A: $w = (1/A)\int Fvdt$ where v is the velocity of separation. According to Zosel's experimental results, since with increasing temperature the material becomes more and more flexible and deformable and it develops contact on a molecular scale during the short contact time, tack increases initially. At higher temperatures, tack (fracture energy) is more related to the debonding process. The ability of a polymer to dissipate deformation energy has a maximum in the glass transition range and tack decreases with increasing temperature above that range. Figure 5.23 shows the influence of temperature on tack schematically. Creton and Leibler (1996) described the temperature dependence of the adhesion energy for two different times of contact, a very short one and a very long one. According to them, for short times of contact, the adhesion energy shows a pronounced maximum, approximately at $50°C$ above the glass transition temperature of the adhesive. This maximum is suppressed, however, when the time of contact is increased. There is debate about achieving perfect bonding during the bonding process in the loop tack test. Tack is the instantaneous wetting of a substrate under little or no applied pressure to rapidly develop a measurable strength, and almost perfect bonding can be achieved. Because of this, in the present numerical analysis it is assumed that the loop is perfectly bonded to the adhesive during the bonding formation. However, the procedure for measuring tack is a two-stage process of bond formation and bond separation, that is, the pulling procedure depends highly upon bond formation. In the present analysis, the two processes are independent of each other so that the results cannot be compared with Zosel's experimental results (Figure 5.23). Without including the bond process effect in the simulation, we do not accurately model the overall temperature effect.

As described above, since the pressure sensitive adhesive is a viscoelastic material, it is highly dependent upon displacement rate. At low debonding rates, the liquid component of the adhesive predominates, resulting in high extension but low values of tack energy. At high debonding rates,

the elastic response predominates, giving high values of tack energy. This is also demonstrated by an examination of adhesive fiber length that is formed at various rates of separation. A Winkler-type viscoelastic foundation is used to model the PSA here. For the foundation, a Kelvin-Voigt model (Figure 3.9) is employed. The nonlinear elastic spring function parameters in the Kelvin-Voigt model are $\beta_1 = 0.03$, $\beta_2 = 1.5$, and $\beta_3 = 0.2$. The thickness of the loop is 0.1016mm, the contact length at the end of the pushing process is 25.4mm, and the length of the loop (L_{loop}) is 279.4mm. The spring constant E and the viscosity η are 8MPa and $0.1590\text{MPa}\cdot\text{sec}$ at $23°\text{C}$ (laboratory temperature), respectively. The equivalent dashpot forces are applied and updated at every step (see section 3.3.2). To save computational time, a little large increment of y_{top} is used as follows:

• pushing procedure ($0mm \le y_{top} \le 38.249mm$): $dy_{top} = 1mm$
• pulling procedure ($38mm \le y_{top} \le 8mm$): $dy_{top} = 2mm$
• pulling procedure $8 < y_{top}$: $dy_{top} = 1mm$

Because of large dy_{top}, the wavelength of the pulling force curve is larger than for other results, as shown in Figure 5.24, but this does not affect results too much. The results for different displacement rates are given in Table 5.4. Just like the effect of elasticity modulus of PSAs, the overall pulling force curve increases as displacement rate increases (Figure 5.24 and Figure 5.25).

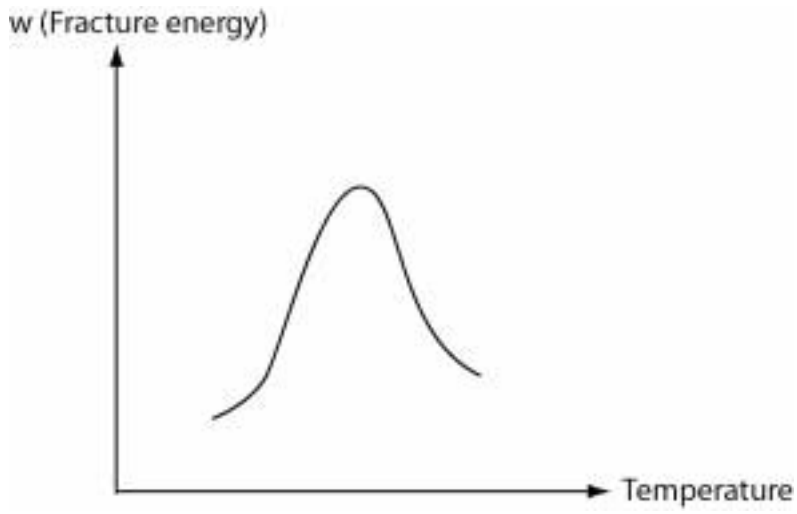

Figure 5.23 Schematic tack vs. temperature curve from Zosel (1992) experimental results

Table 5.4 Effect of displacement rate

Displacement rate, mm/min	P_{max}, N	$P_{plateau}$, N	Area, mm^2
no dashpot	21.68	10.69	165.44
12	21.54	11.32	185.42
50	23.32	13.46	211.15
100	28.94	15.94	263.15
200	38.97	21.54	350.92
300	52.167	28.95	438.02
expt	20.95	95.32	5.91

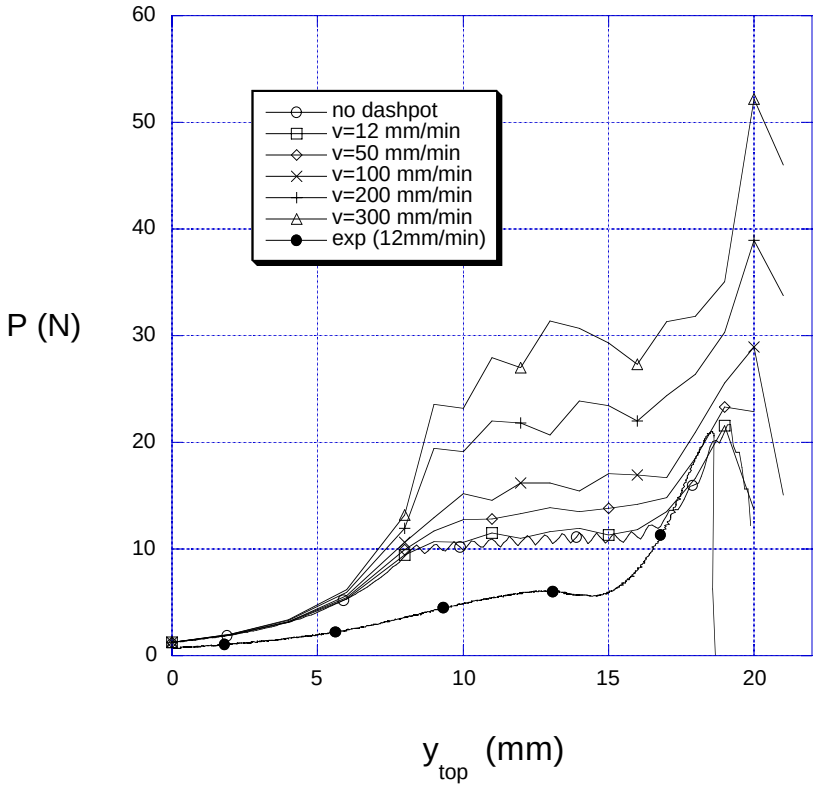

Figure 5.24 Pulling force curves for different displacement rate

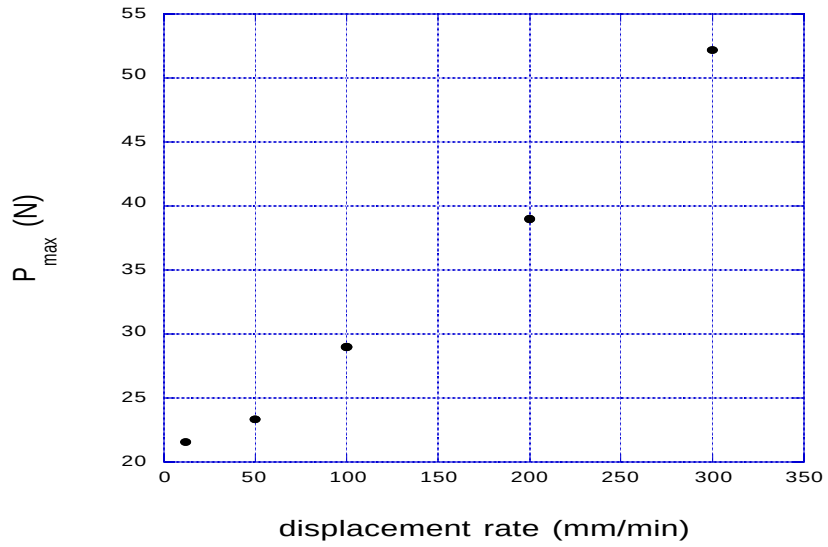

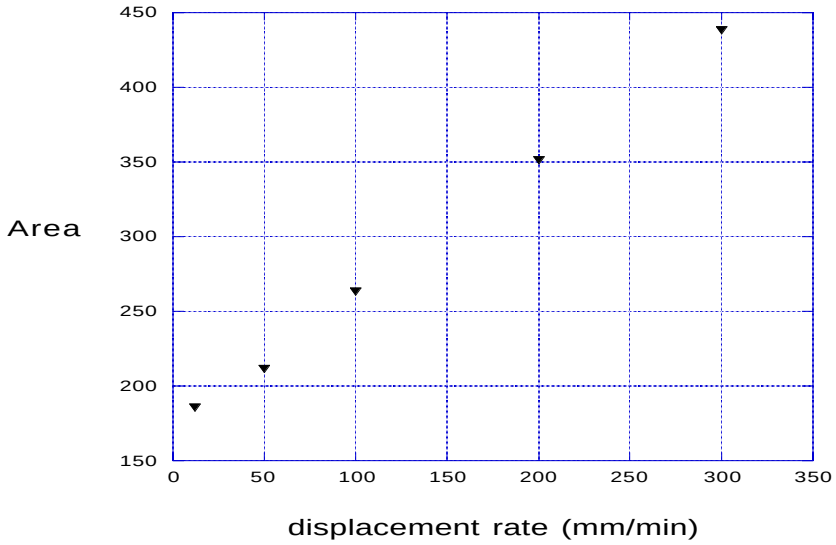

Figure 5.25 Effect of displacement rate

Chapter 6. SUMMARY AND CONCLUSIONS

Numerical inelastic analysis of the loop tack test for pressure sensitive adhesives (PSAs) has been carried out using the commercial finite element analysis program ABAQUS. Results were compared with experimental results. Shell elements (S4R) and hybrid beam elements were adopted to model the strip, considering the plasticity effect. Based on uniaxial tensile test results, the stress versus strain relationship for uniaxial stress was idealized as a bilinear elastic-plastic relationship. In the 3D analysis, anticlastic bending behavior was investigated. The pressure sensitive adhesive was assumed to be on the substrate rather than on the loop. It was modelled as a Winkler-type nonlinear elastic foundation or a viscoelastic foundation. The deformation of the PSA was approximated as uniaxial extension of independent adhesive strands.

The simulation of the loop tack test in ABAQUS consisted of four main processes: defining the mesh for the strip and the adhesive, teardrop shape loop formation, bonding phase, and debonding phase. They were generated by applying appropriate displacements. There is a compression zone for the bonding procedure and a tension zone for the debonding procedure in the nonlinear elastic spring function. The compression zone was defined based on the assumption that the adhesive layer may not deform more than 20% of its thickness. The tension zone was composed of a constant stiffness region, a zero stiffness region, and a negative constant stiffness region, taking into account the effect of fibrillation of the adhesive.

The failure criterion for debonding assumed that the adhesive will debond when the strands reaches a certain elongation, for both the nonlinear elastic spring model and the viscoelastic model. An alternative triangular shape nonlinear elastic function for homogeneous deformation of the adhesive (brittle polymeric materials) was also studied. The Kelvin-Voigt model was used to model the PSA in a Winkler-type viscoelastic foundation. Moduli of the nonlinear elastic spring and viscoelastic models were determined from available results of dynamic mechanical analysis (DMA) tests.

The loop tack test was investigated for four different thicknesses (0.0254mm-0.1016mm) of a stainless steel strip. Curves of pulling force versus displacement (y_{top}) were determined. The maximum pulling force in the pulling procedure is defined as the tack. A parametric study was conducted to understand the influence of several parameters (nonlinear spring function parameters,

contact area, length of loop, and strip thickness). The effects of the elasticity modulus of the PSA and the displacement rate were investigated and compared with previous researches' results. To better understand the formation of the loop, the finite difference method are also used to obtain the no-contact teardrop shape of the loop (see Appendix A).

Limitations of present study are that the shear stresses in the adhesive layer and the weight of the strip were ignored, the loop was perfectly bonded to the adhesive during contact, frictionless contact occurs between the loop and the adhesive, and the contact time was not included. In the 2D analysis, the anticlastic bending behavior was neglected. Since bond formation and debonding formation were based on a nonlinear elastic spring function, both processes are independent of each other. Therefore, it is hard to include wetting in this numerical analysis.

The following conclusions are drawn from the present study.

- From the numerical analysis results, we observed that the pulling force curve consists of three regions: the initial transition region, a plateau region, and the peak pulling force region. This was similar to the experimental results. However, there are still differences between the numerical and experimental results. Because of several uncertainties (the initial position of the loop, the contact area, length of the loop, and alignment of the loop with respect to the substrate plate), the repeatability of the available experimental results was not good.
- Variations of the nonlinear spring function parameters (β_1, β_2, and β_3) cause significant changes in the pulling force in the numerical analysis. The pulling force curve is very dependent upon the assumed total lengths ($(\beta_1 + \beta_2 + \beta_3)h_a$) of the springs at debonding.
- The numerical analysis results show that an increase of strip thickness causes an ascending trend of the peak pulling force, but the experimental results do not.
- Oscillation of the pulling force in the plateau region occurs due to debonding from discrete springs. The amount of oscillation depends on the spring parameter β_3, the mesh size of the contact part, the strip thickness, and the elasticity modulus of the PSA. Thus, oscillation of the pulling force in the numerical analysis is not only dependent upon one parameter.
- The deformed shapes of the thin strip and thick one are similar in the pushing procedure, but the behavior of these loops at the end of the pulling procedure (y_{top}<-10) is much different due

to stiffness and Poisson's ratio. The deformed loop shape of the thin one is nearly as triangular as in the experimental results.

- In the 3D analysis, because of geometrically nonlinear effects, the middle portion of the thin strip tends to flatten in the transverse direction rather than exhibit anticlastic bending behavior in the 3D analysis.
- The maximum von Mises stress becomes equal to the yield stress as the top displacement of the loop reaches 8mm for the 0.0254mm strip and the 0.0508mm strip, 18mm for the 0.0762mm strip, and 16mm for the 0.1016mm strip. For the same PSA, a thin strip yields earlier, but the total energy dissipated will be small because the thickness is small. Therefore, the contribution of plastic yielding to the pulling force is smaller for a thin strip than for a thicker strip.
- In the 2D analysis, the overall contact patterns are similar after the second node from the center makes contact with the PSA, but the displacement (y_{top}) at the second node contact is different for different strip thicknesses. The contact pattern depends upon the thickness and elasticity modulus of the strip. In the 3D analysis, due to anticlastic bending, a parabolic shape contact boundary occurs in the transverse direction.
- The pulling force curve increases overall as the elasticity modulus of the PSA increases. The pulling force increases as the displacement rate increases (and as the temperature decreases in the range above the transition temperature T_g).
- Since the transition of the pulling force curve from numerical results shows good agreement with experimental results, an interfacial deformation mode and a maximum elongation debonding failure criterion of PSA seem to be appropriate for the loop tack test cases studied here.

A simple Kelvin-Voigt model was used in the present study, but it does not describe the behavior of a PSA very accurately. Therefore, more complicated viscoelastic models should be implemeted in ABAQUS via a UMAT subroutine for solid elements or shell elements in further research. Also, further experiments should be carried out.

Appendix A. Finite Difference Method (No-Contact Case)

In this section the no-contact teardrop shape of the loop is simulated using the finite difference method and a 2D model. The strip is assumed to be elastic and inextensible, and the bending moment is assumed to be proportional to the curvature, i.e., the strip is an elastica. The weight of the strip is neglected. The length of the strip is 2*L* and the bending stiffness is *EI*. The highly-flexible strip is unstrained when flat. Its ends are brought together and clamped so that the strip forms a teardrop shape (Figure A.1a). Due to symmetry of the loop, only the right half of the loop is analyzed (Figure A.1b). From geometry, the moment-curvature relation, and equilibrium of an element, the governing equations are

$$\frac{dX}{dS} = \cos\theta,\ \frac{dY}{dS} = \sin\theta \tag{A.1a}$$

$$EI\frac{d\theta}{dS} = M,\ \frac{dM}{dS} = -P\sin\theta + Q\cos\theta \tag{A.1b}$$

where *S* is the arc length, θ is the angle of the tangent with the horizontal, *X* and *Y* are the horizontal and vertical coordinates, *P* is the horizontal force acting on half of the loop, *Q* is the vertical force acting on half of the loop, and *M* is the bending moment.

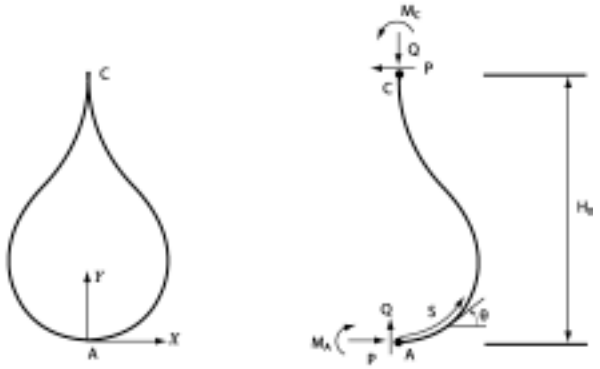

(a) (b)

Figure A.1 Equilibrium shape and free body diagram before contact

The following nondimensional quantities are introduced:

$$s = \frac{S}{L},\ x = \frac{X}{L},\ y = \frac{Y}{L},\ h_0 = \frac{H_0}{L} \tag{A.2a}$$

$$p = \frac{PL^2}{EI}, q = \frac{QL^2}{EI}, m = \frac{ML}{EI}, m_A = \frac{M_A L}{EI}, m_C = \frac{M_C L}{EI} \tag{A.2b}$$

where M_A is the moment at A (at the bottom of the loop), M_C is the moment at C (at the top of the loop), H_0 is the height of the elastica, and $H_0 = Y(L)$.

The equilibrium state of the no-contact case (*p*=constant, *q*=0) is considered. In the nondimensional form, the governing equations A.1 become

$$\frac{dx}{ds} = \cos\theta, \frac{dy}{ds} = \sin\theta, \frac{d\theta}{ds} = m, \frac{dm}{ds} = -p\sin\theta \tag{A.3}$$

with $x = y = \theta = 0$ at point A where *s*=0, and $x = 0, \theta = \frac{\pi}{2}$ at point C where *s*=1.

Equations A.3 are solved with a finite difference method. In a finite difference method, the derivatives are replaced by finite difference approximations and the differential equations are transformed into algebraic equations. In this case, using a forward difference approximation, we can write

$$f'(x) \cong \frac{f(x_{i+1}) - f(x_i)}{h} \tag{A.4}$$

where $h = x_{i+1} - x_i$. We apply equation A.4 to equations A.3, and then equations A.3 become

$$\frac{dx}{ds} = \frac{x_{i+1} - x_i}{h} = \cos\theta_i, \frac{dy}{ds} = \frac{y_{i+1} - y_i}{h} = \sin\theta_i \tag{A.5a}$$

$$\frac{d\theta}{ds} = \frac{\theta_{i+1} - \theta_i}{h} = m_i, \frac{dm}{ds} = \frac{m_{i+1} - m_i}{h} = -p\sin\theta_i \tag{A.5b}$$

where *n* is the number of segements, $h = 1/n$ is the distance between the nodal points, and θ_i, m_i, x_i, and y_i are the slope, moment, horizontal coordinate, and vertical coordinate, respectively, at node *i*.

We use a total of *n*+1 finite difference nodes on the strip (Figure A.2), with node *i*=0 at point A and node *i*=*n* at point C. The constraints are

$$x_0 = 0, x_n = 0, y_0 = 0, \theta_0 = 0, \theta_n = \frac{\pi}{2} \tag{A.6}$$

As a result, from equations A.5 we can get

Figure A.2 Finite difference nodes on the strip

$$x_1 = h,\ x_i = h + h\sum_{j=1}^{i-1}\cos\theta_j,\ y_1 = 0,\ y_i = h\sum_{j=1}^{i-1}\sin\theta_j \tag{A.7}$$

$$\theta_1 = hm_0,\ \theta_i = h\sum_{j=0}^{i-1} m_j,\ m_1 = m_0,\ m_i = m_0 - hp\sum_{j=1}^{i-1}\sin\theta_j \tag{A.8}$$

where p and $m_0, m_1, \ldots, m_{n-1}$ are unknown parameters and $i = 2, \ldots, n$. Using equations A.7 and A.8 in the constraints on x_n and θ_n gives

$$\sum_{j=1}^{n-1}\cos\theta_j = -1,\ h\sum_{j=0}^{n-1} m_j = \frac{\pi}{2} \tag{A.9}$$

The first equations in A.8 are used to eliminate the angles θ_i. Then the remaining equations in A.8, and equations A.9, comprise a system of nonlinear algebraic equations with unknown variables p and $m_0, m_1, \ldots, m_{n-1}$. Broyden's method is used to solve these equations. This method provides an updating formula which gives successive approximations to the Jacobian for each iteration. The initial approximations for $m_1, \ldots, m_{n-1}$ are chosen by linear interpolation based on m_0 and m_n. The algorithms are implemented in the software package MATLAB. After we obtain the solution for n+1 variables, we also calculate x_i and y_i using equations A.7. Then the configuration for the no-contact case can be illustrated (Figure A.3).

Table A.1 and Figure A.4 show convergence of the solution with respect to varying n. Except for m_n, the results in Table 1 converge monotonically toward the exact solution which is given in Plaut et al. (1999).

Table A.1 Convergence of p, y_n, m_n, and m_0

n	p	y_n	m_n	m_0
5	15.598	0.6605	-3.039	4.735
10	11.846	0.7708	-2.963	5.042
20	10.760	0.8130	-2.983	5.214
30	10.419	0.8255	-2.999	5.266
40	10.295	0.8316	-3.008	5.296
50	10.215	0.8351	-3.010	5.313
60	10.163	0.8374	-3.0143	5.327
solution	9.9127	0.8486	-3.0276	5.3844

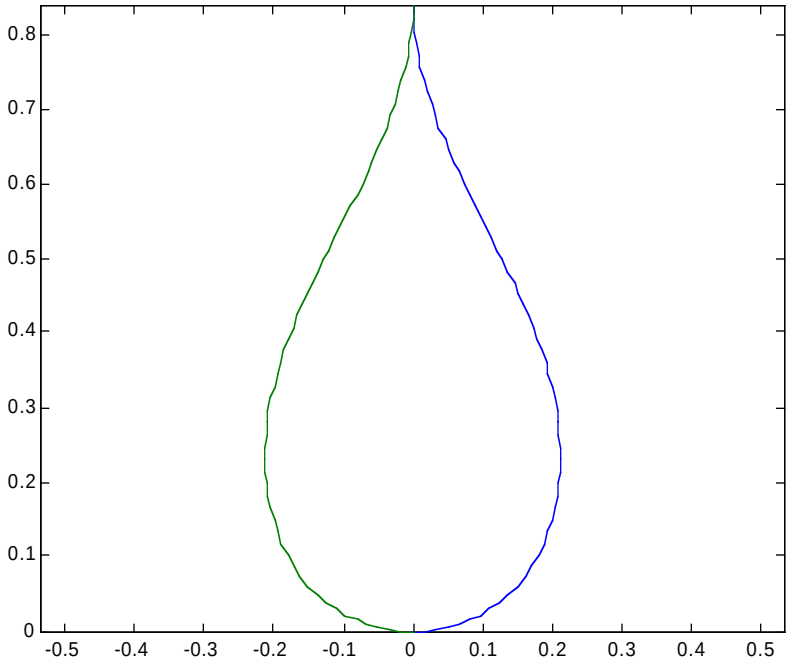

Figure A.3 Configuration for no-contact case

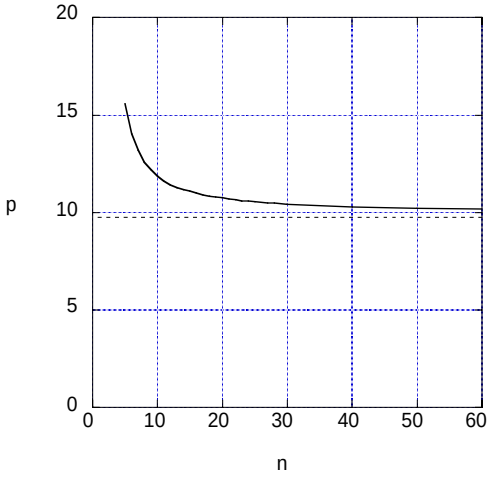

(a)

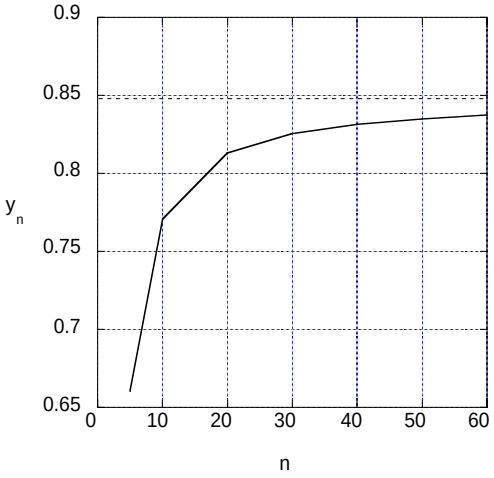

(b)

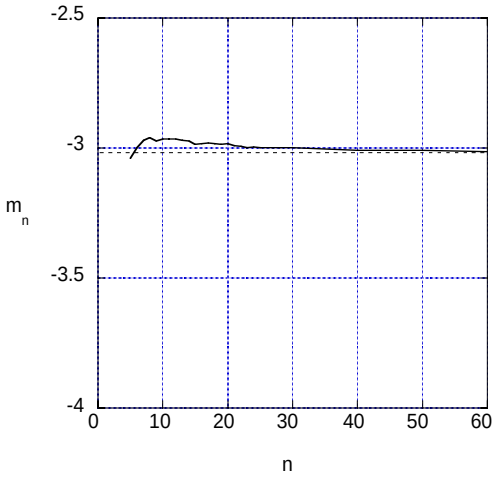

(c)

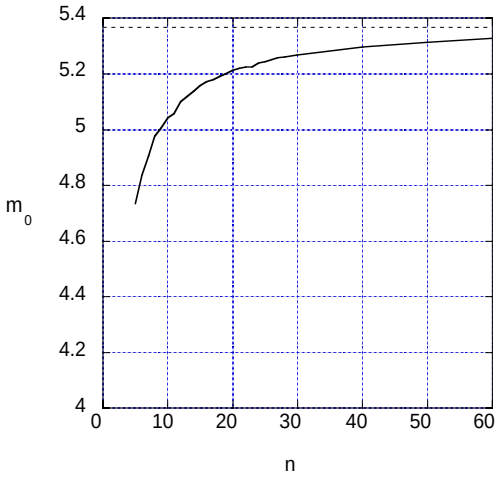

(d)

Figure A.4 Convergence of p, y_n, m_n, and m_0

Appendix B. Uniaxial Tensile Test

B.1 Mylar Strip

Several uniaxial tension tests were carried out using the same material to determine the yield stresses and strain-hardening characteristics of the strips. The results are shown in Figures B.1a to B.1g. The test detail specifications are listed in Table 1. Mylar with a thickness of 0.00508 cm, width of 3.81 cm, and length of 22.1 cm was used as the specimen. The top end of the straight, vertical strip was pulled upward at a constant rate, and then the direction was reversed and the top moved downward at the same rate. The behavior is inelastic and the material exhibits permanent deformation after unloading.

Table B.1 Uniaxial tensile test results

Test	Rate (mm/min)	Max. Disp. (mm)	Max. Load (N)
a	5	30.11	191.4
b	10	11.66	174.0
c	5	11.69	172.7
d	1	11.59	158.2
e	10	8.07	163.5
f	5	8.06	171.1
g*	5	8.55	164.8

*Test g: unload at 3.05 mm (extension) for one minute, then load, then unload at 5.12 mm (extension) for one minute, then load.

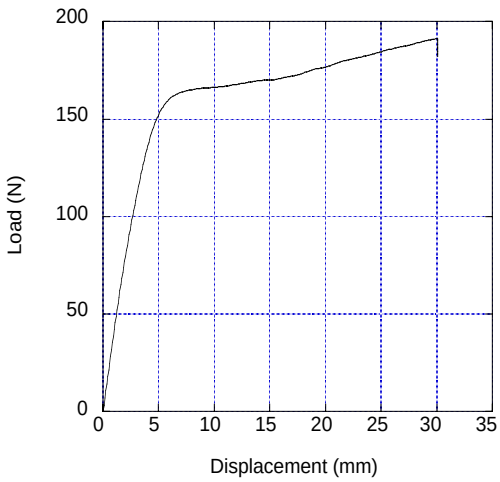
Load (N)
Displacement (mm)
0
50
100
150
200
0
5
10
15
20
25
30
35

(a)

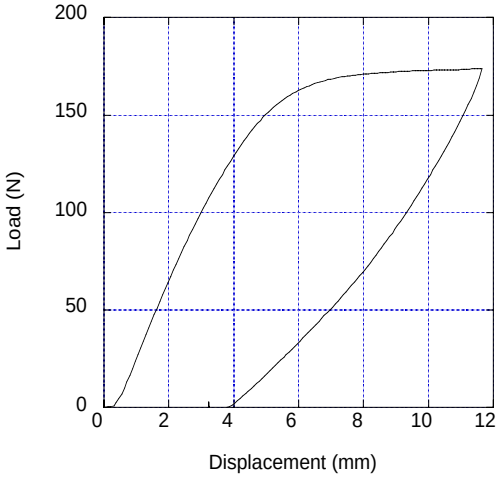
Load (N)
Displacement (mm)
0
50
100
150
200
0
2
4
6
8
10
12

(b)

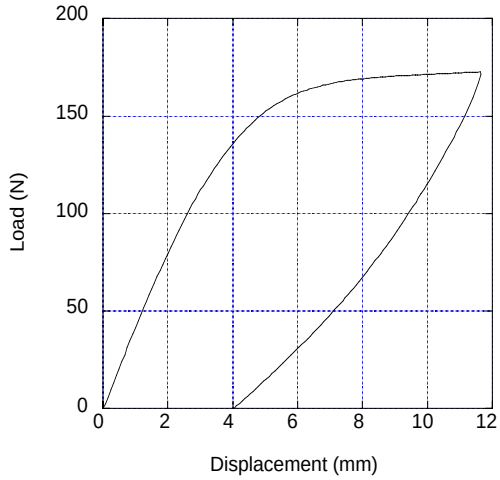
Load (N)
Displacement (mm)
0
50
100
150
200
0
2
4
6
8
10
12

(c)

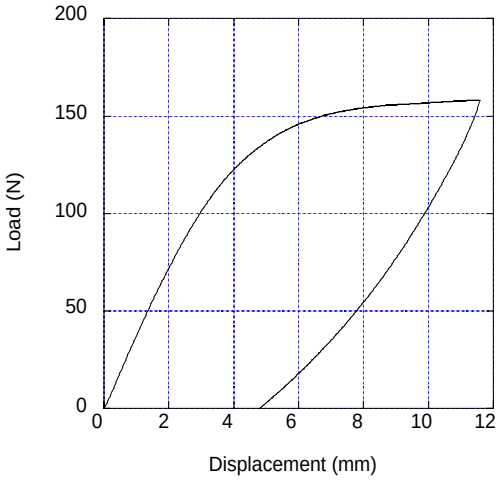
Load (N)
Displacement (mm)
0
50
100
150
200
0
2
4
6
8
10
12

(d)

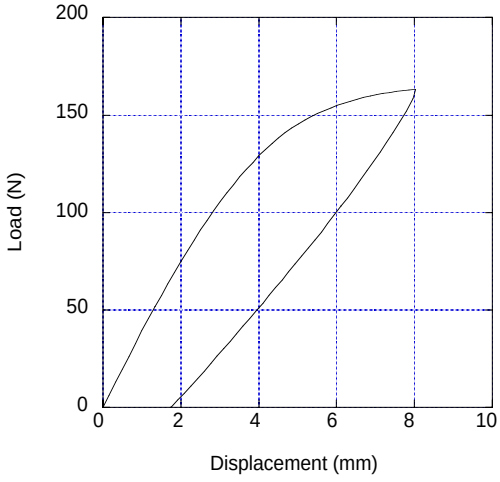
Load (N)
Displacement (mm)
0
50
100
150
200
0
2
4
6
8
10

(e)

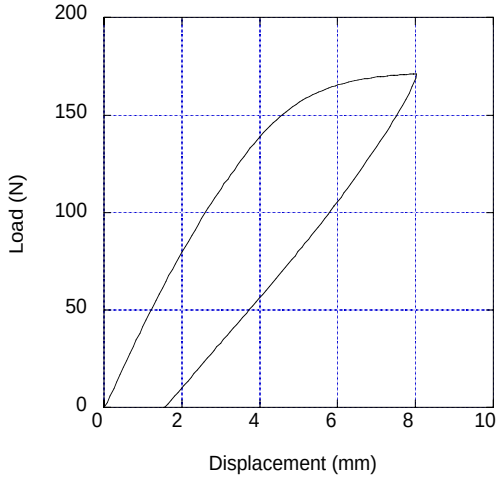
Load (N)
Displacement (mm)
0
50
100
150
200
0
2
4
6
8
10

(f)

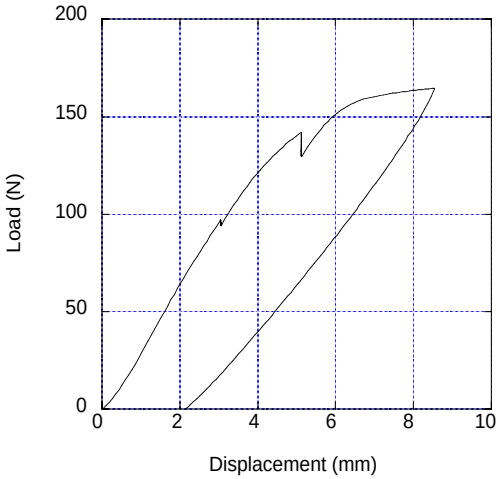

(g)

Figure B.1 Load-displacement diagrams for the Mylar strips

B.2 Stainless Steel Strip

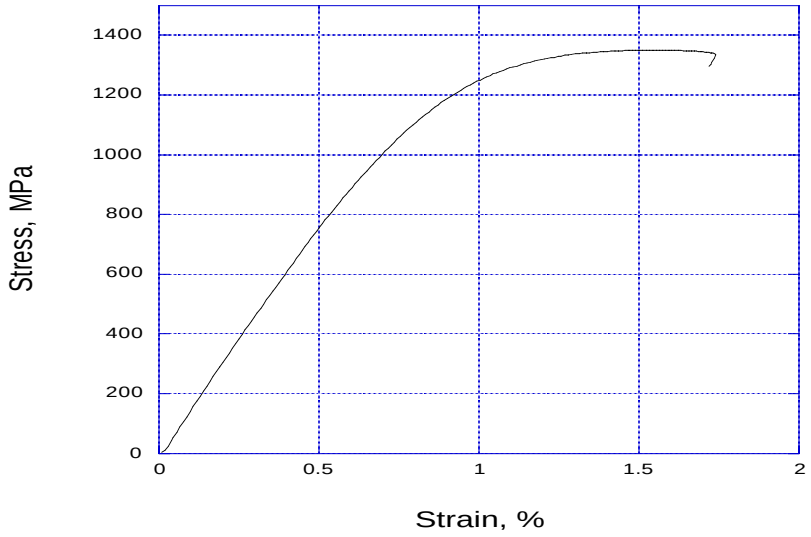

(a)

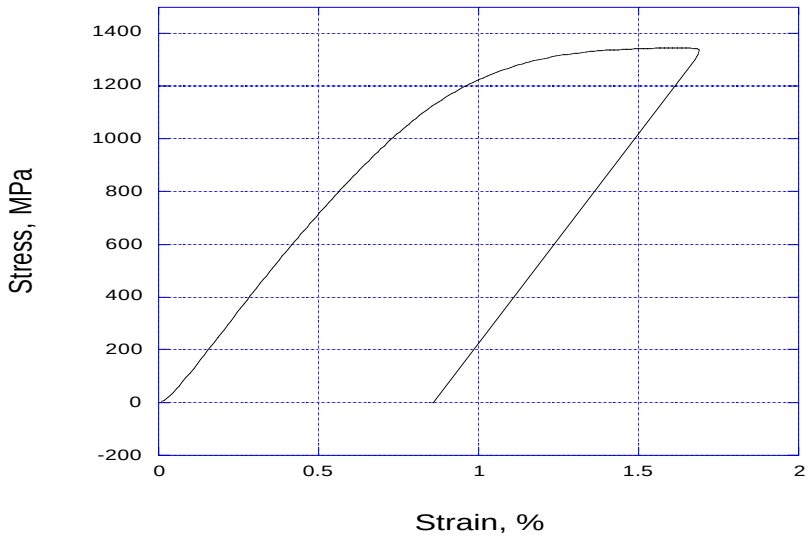

(b)

Figure B.2 Stress-strain diagrams for the stainless steel strips

Appendix C. Arcan Tensile Test for VHB Tape

The Arcan tensile test for VHB tape was conducted by John Hennage who is a graduate student in Mechanical Engineering. Originally this test was used for plane-stress testing of composite specimens by Arcan et al. (1978). The specimen and test fixture for the Arcan test are shown in Figure C.1 and C.2. The original Arcan test was modified for measuring properties of VHB tape. The dimensions of the VHB specimen were $1/2'' \times 2''$ and $0.045''$ thick. Tests were performed with respect to loading angle, rate, and temperature. A $0°$ loading condition was used for a tensile test (Figure C.1a) and a $90°$ loading condition was used for a shear test for VHB tape. Figure C.3 shows load versus displacement curves for a tensile test with different varying loading rates.

(a) $0°$ loading condition

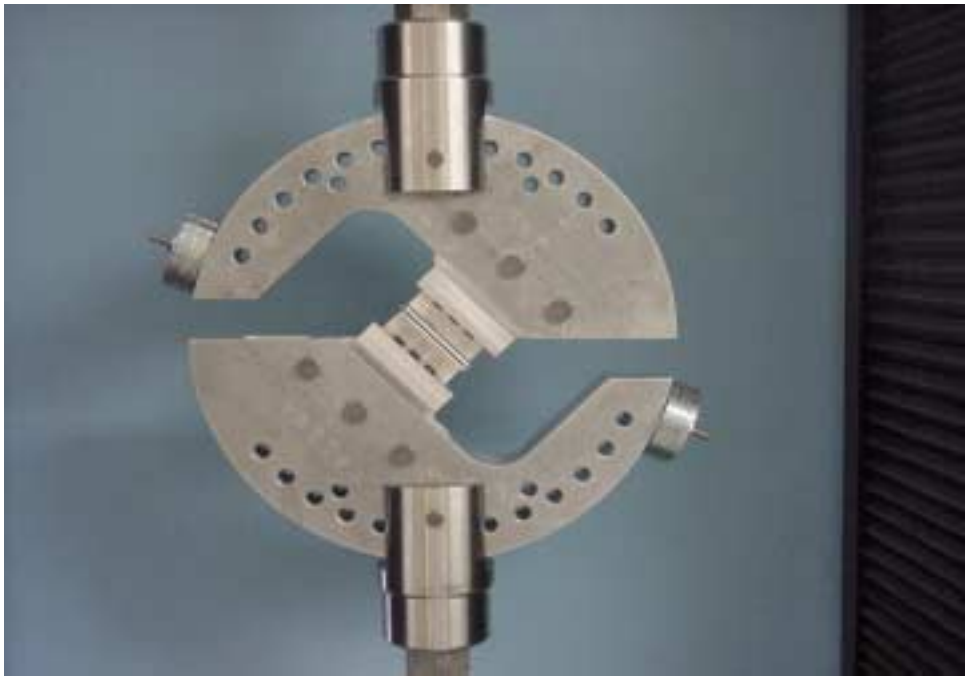

(b) 45° loading condition

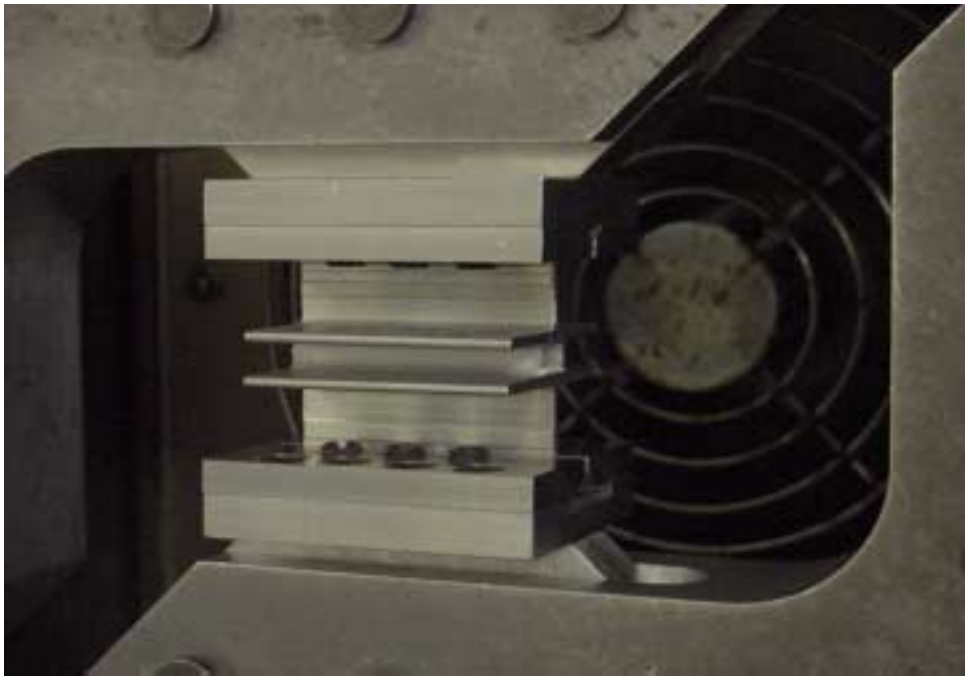

(c) Specimen for Arcan test

Figure C.1 Arcan test

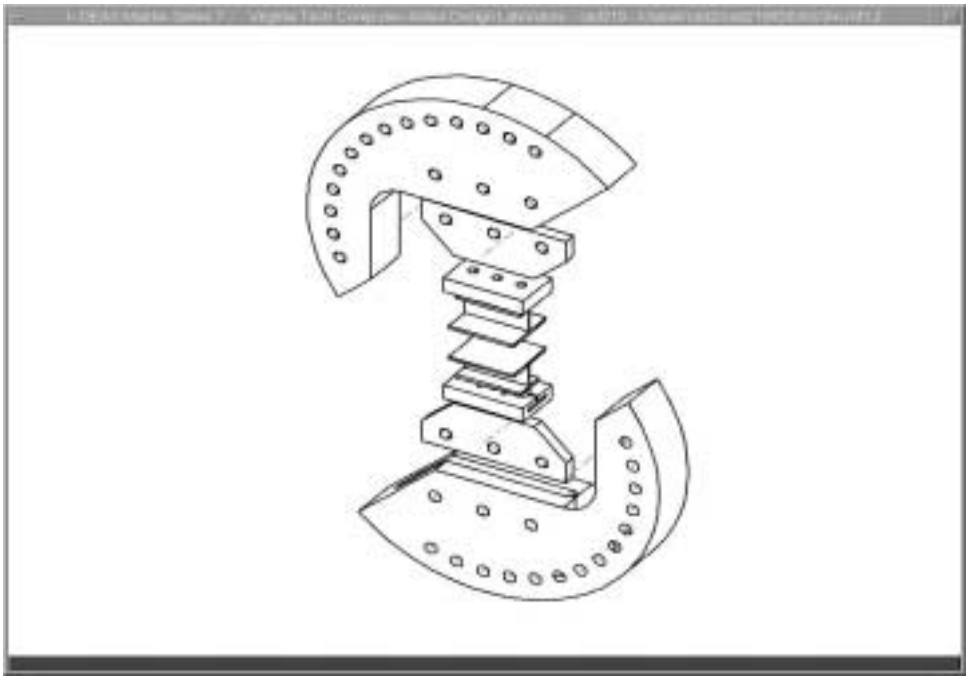

(a)

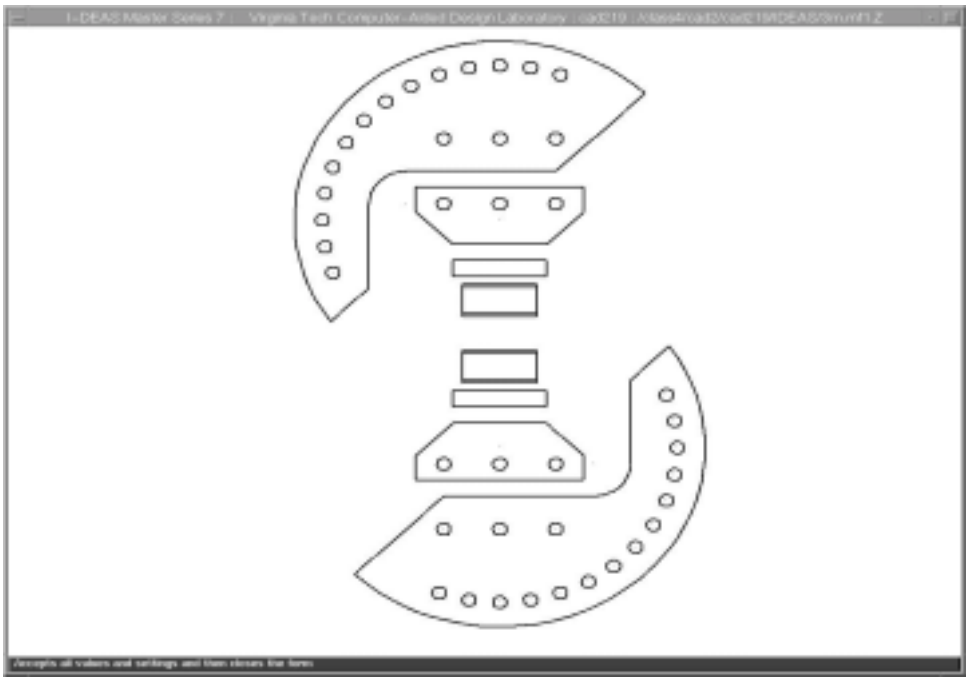

(b)

Figure C.2 A schematic of the Arcan test

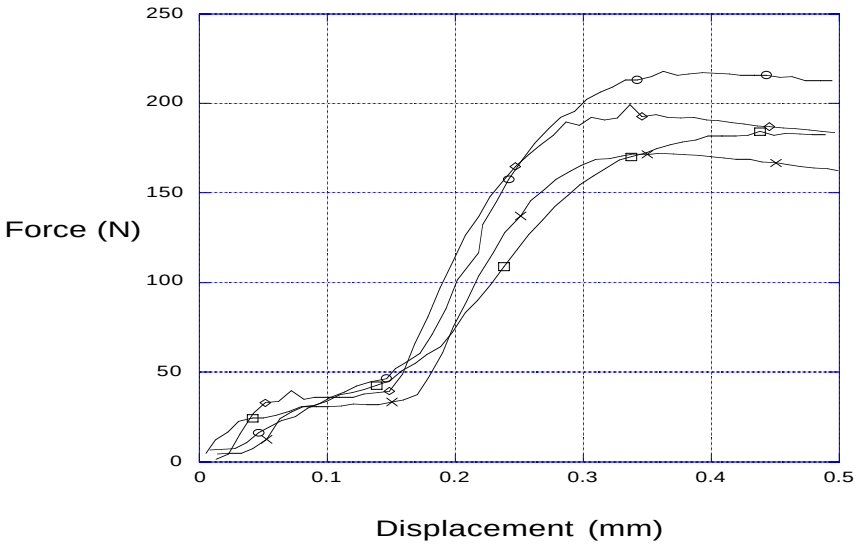

(a) Debonding rate = 0.05mm/min

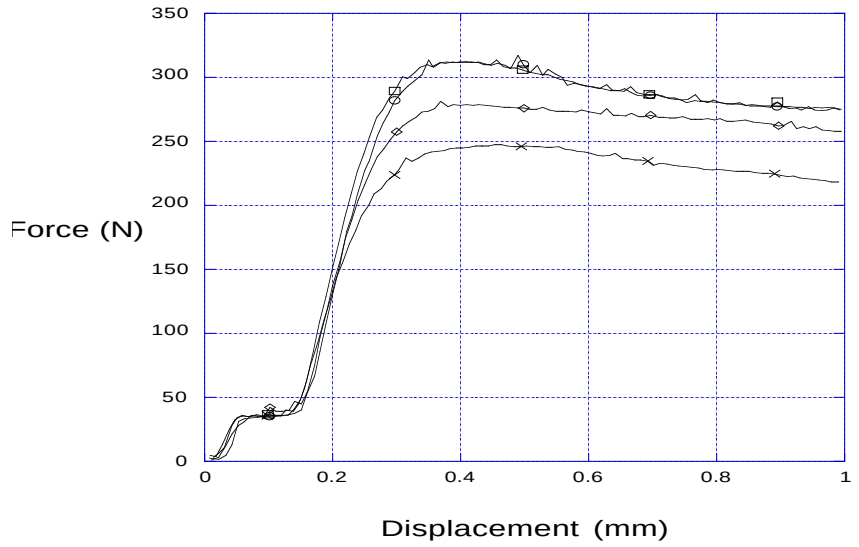

(b) Debonding rate = 0.5mm/min

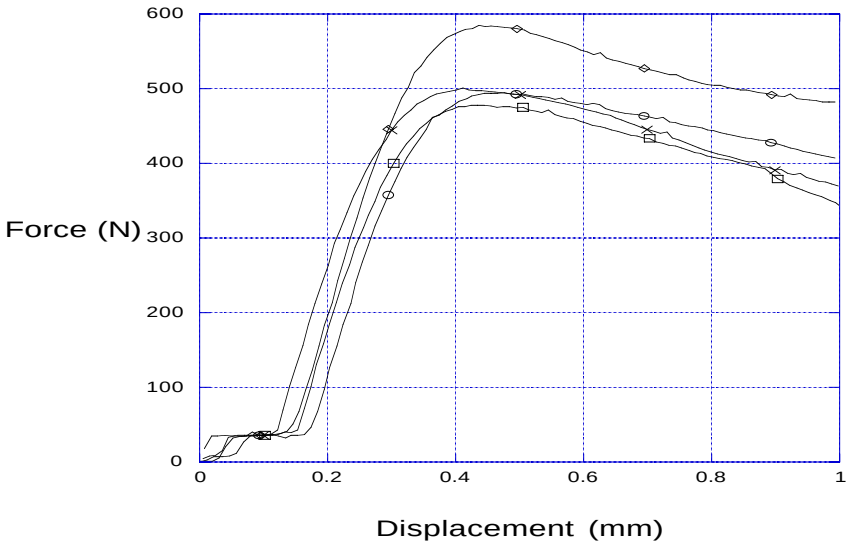

(c) Debonding rate = 5mm/min

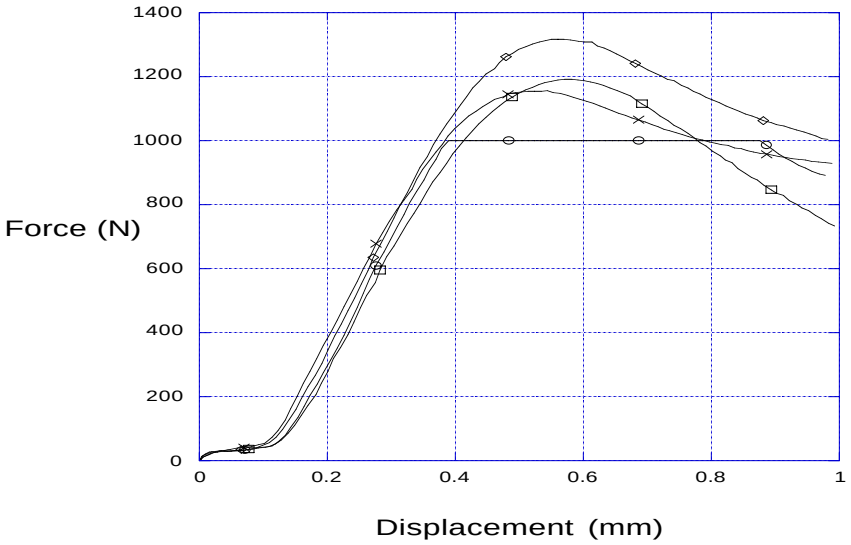

(d) Debonding rate = 50mm/min

Figure C.3 Load-displacement diagrams for the VHB tape in Arcan tensile test

Appendix D. Equations for DMA Data Conversions

Tensile stress $\sigma = \frac{P}{A} \quad (P = \sigma_{orig} \times t_l \times b_l;\ A = b \times l)$

Tensile strain $\varepsilon = \frac{d}{t} \quad (d = \varepsilon_{orig} \times l_l)$

Tensile Modulus $E = \frac{\sigma}{\varepsilon} = \frac{P/A}{d/t}$

Tensile Storage Modulus $E' = E\cos\delta$

Tensile Loss Modulus $E'' = E\sin\delta$

P: load
A: area of VHB tape
d: displacement
$\tan\delta$: loss factor, from experimental data
σ_{orig}: stress, from experimental data
ε_{orig}: strain, from experimental data
l_l: length of aluminum plate
t_l: thickness of aluminum plate
b_l: width of aluminum plate
b:width of VHB tape
l: length of VHB tape
t: thickness of VHB tape

REFERENCES

ABAQUS User's Manual Version 6.1 (2000), Hibbitt, Karlsson and Sorensen Inc., Pawtucket, RI, USA.

Aravas, N., K.-S. Kim and M. J. Loukis (1989), "On the Mechanics of Adhesion Testing of Flexible Films." Materials Science and Engineering, A, Vol. 107, pp. 159-168.

Argento, C., A. Jagota and W. C. Carter (1997), "Surface Formulation for Molecular Interactions of Macroscopic Bodies." Journal of the Mechanics and Physics of Solids, Vol. 45, pp. 1161-1183.

Ashwell, D. G. (1950), "The Anticlastic Curvature of Rectangular Beams and Plates." Journal of the Royal Aeronautics Society, Vol. 54, pp. 708-715.

Ashwell, D. G. (1952), "A Characteristic Type Instability in the Large Deflextions of Elastic Plates-I. Curved Rectangular Plates Bent About One Axis-II. Flat Square Plates Bent About All Edges. Proceeding of the Royal Society of London, A214, pp. 98-118.

Atkins, A. G. and Y. W. Mai (1986), "Residual Strain Energy in Elastoplastic Adhesive and Cohesive Fracture." International Journal of Fracture, Vol. 30, pp. 203-221.

Aubrey, D. W. (1992), "Pressure-Sensitive Adhesives." Handbook of Adhesion, D. E. Packham, ed., Longman, Essex, UK, pp. 335-341.

Barraclough, P. (1998), "Failure Criteria and Their Application to Visco-elastic/Visco-plastic Materials." Project PAJ1-Interim Report, National Physical Laboratory, Teddington, UK, August.

Bellow, D. G., G. Ford, and J. S. Kennedy (1965), "Anticlastic Behavior of Flat Plates." Experimental Mechanics, Vol. 5, pp. 227-233.

Cahn, R. W., P. Haosen and E. G. Kramer (1997), Material Science and Technology, Vol. 18: Processing of Polymers, Wiley-VCH, Weinheim, Germany.

Chang, E. P. (1997), "Viscoelastic Properties of Pressure-Sensitive Adhesives." Journal of Adhesion, Vol. 60, pp. 233-248.

Chang, F. S. C. (1960), "The Peeling Force of Adhesive Joints." Transactions of the Society of Rheology, Vol. 4, pp. 75-89.

Christensen, S. F. and S. C. Flint (2000), " A Practical Criterion for Rheological Modeling of the Peeling of Pressure Sensitive Adhesives." Journal of Adhesion, Vol. 72, pp. 177-207.

Chuang, H. K., C. Chiu and R. Paniagua (1997), "Avery Adhesive Test - A Novel Pressure-Sensitive Adhesive Test Method." Tech XX, 20th Pressure Sensitive Tape Council Proceedings, Boston, MA, pp. 39-60.

Conway, H. D. and W. E. Nickola (1965), “ Anticlastic Action of Flat Sheets in Bending.” Experimental Mechanics, Vol. 5, pp. 115-120.

Creton, C. and H. Lakrout (2000), “Micromechanics of Flat-Probe Adhesion Tests of Soft Viscoelastic Polymer Films.” Journal of Polymer Science: Part B: Polymer Physics, Vol. 38, pp. 965-979.

Creton, C. and L. Leibler (1996), “How Does Tack Depend on Time of Contact and Contact Pressure?” Journal of Polymer Science: Part B: Polymer Physics, Vol. 34, pp. 545-554.

Crocombe, A. D. and R. D. Adams (1981), “Peel Analysis Using the Finite Element Method.” Journal of Adhesion, Vol. 12, pp. 127-139.

Crocombe, A. D. and R. D. Adams (1982), “An Elasto-plastic Investigation of the Peel Test.” Journal of Adhesion, Vol. 13, pp. 241-267.

Crosby, A. J. and K. R. Shull (1999), “Adhesive Failure Analysis of Pressure-Sensitive Adhesives.” Journal of Polymer Science: Part B: Polymer Physics, Vol. 37, pp. 3455-3472.

Crosby, A. J., K. R. Shull, H. Lakrout and C. Creton (2000), “ Deformation and Failure Modes of Adhesively Bonded Elastic Layers.” Journal of Applied Physics, Vol. 88, pp. 2956-2966.

Dahlquist, C. A. (1969), ”Pressure Sensitive Adhesives:, in Treatise on Adhesion and Adhesives, R. L. Patrick (ed.), Marcel Dekker, New York, Vol. 2, pp. 219-270

Dahlquist, C. A. (1982), “ Creep.” in Advances in Pressure Sensitive Adhesive Technology, D. Satas, ed., Satas & Associates, Warwick, RI, pp. 78-83.

David, W. O., T. Nipithakul. M. Nardin, J. Schultz, and K. Suchiva (2000), “Influence of Nonrubber Constituents on Tack of Natural Rubber. I. At Very Short Times of Contact (Pendulum Test).” Journal of Applied Polymer Science, Vol. 78, pp. 1486-1494.

Drozdov A. D. and I. Gertsbakh (1993), “Detachment of an Elastic Beam from a Viscoelastic Support: A Variational Approach.” International Journal of Mechanical Sciences, Vol. 35, pp. 463-478.

Duke, A. J. (1974), “Plasticity in Peeling.” Journal of Applied Polymer Science, Vol. 18, pp. 3019-3055.

Duncan, B. C. (1999) “Failure Criteria and their Application to Visco-elastic/Visco-plastic Materials.” Project PAJ1: Final Report, National Physical Laboratory, Teddington, UK, October.

Duncan, B. C. and L. A. Lay (1999), “An Intercomparison of Tack Measurements.” Project PAJ1: Report No. 11, National Physical Laboratory, Teddington, UK, May.

Duncan, B. C. and K. Ogilvie-Robb (1999), “Assessment of the Correlation Between Tack and Visco-elasticity.” Project PAJ1: Report No. 16, National Physical Laboratory, Teddington, UK, June.

Duncan, B. C., L. A. Lay, A. Olusanya, R. A. Roberts and S. G. Abbott (1999), “The Measurement of Adhesive Tack.” Adhesion’99, Seventh International Conference on Adhesion and Adhesives, University of Cambridge, UK, pp. 313-318.

Duncan, B. C., S. Abbott and R. Roberts (1999), “Adhesive Tack.” Measurement Good Practice Guide, Report No. 26, National Physical Laboratory, Teddington, UK, July.

Eppink, D. L. and R. L. Frye (1999), “ Adhesives Benchmark Testing.” http://www.chemsultants.com.

Fung, Y. C. and W. H. Wittrick (1954), “The Anticlastic Curvature of a Strip with Lateral Thickness Variation.” Journal of Applied Mechanics, Vol. 21, pp. 351-358.

Fung, Y. C. and W. H. Wittrick (1955), “A Boundary Layer Phenomenon in the Large Deflection of Thin Plates.” Journal of Mechanics and Applied Mathematics, Vol. 8, Part 2, pp. 191-210.

Gay, C. and L. Leibler (1999), “Theory of Tackiness.” Physical Review Letters, Vol. 82, pp. 936-939.

Gent, A. N. and G. R. Hamed (1977), “Peel Mechanics for an Elastic-Plastic Adherend.” Journal of Applied Polymer Science, Vol. 21, pp. 2817-2831.

Gordon, G.V. and R. G. Schmidt (2000), “PSA Release Force Profiles from Silicone Liners: Probing Viscoelastic Contributions from Release System Components.” Journal of Adhesion, Vol. 72, pp. 133-156.

Goulding, T. M. (1994), “Pressure-Sensitive Adhesives.” Handbook of Adhesive Technology, A. Pizzi and K. L. Mittal, eds., Marcel Dekker, NY, pp. 549-564.

Hammond, F. H. Jr. (1982), “Tack.” Advances in Pressure Sensitive Adhesive Technology, D. Satas, ed., Satas & Associates, Warwick, RI, pp. 32-49.

Hata, T. (1972), “Mechanisms of Adhesive Failure.” Journal of Adhesion, Vol. 4, pp. 161-170.

Hu, F., A. Olusanya, L. A. Lay, J. Urquhart and L. Crocker (1998), A Finite Element Model For the Assessment of Loop Tack for Pressure Sensitive Adhesive Tapes and Labels., Project PAJ1: Report 8, National Physical Laboratory, Teddington, UK, August.

Hui, C. Y., Y. Y. Lin and J. M. Baney (2000a), “The Mechanics of Tack: Viscoelastic Contact on a Rough Surface.” Journal of Polymer Science: Part B: Polymer Physics, Vol. 38, pp. 1485-1495.

Hui, C. Y., Y. Y. Lin, J. M. Baney and A. Jagota (2000b), "The Accuracy of the Geometric Assumptions in the JKR (Johnson-Kendall-Roberts) Theory of Adhesion." Journal of Adhesion Science and Technology, Vol. 14, pp. 1297-1319.

Hyer, M. W. and P. C. Bhavani (1984), "Suppression of Anticlastic Curvature in Isotropic and Composite Plates." International Journal of Solids and Structures, Vol. 20, pp. 553-570.

Jagota, A., C. Argento and S. Mazur (1998), "Growth of Adhesive Contacts for Maxwell Viscoelastic Spheres." Journal of Applied Physics, Vol. 83, pp. 250-259.

Johnston, J. (1983), "Tack - Known by Many Names, It's Difficult to Define." Adhesives Age, Vol. 26, No.12, pp. 34-38.

Kafkalidis, M. S., M. D. Thouless, Q. D. Yang and S. M. Ward (2000), "Deformation and Fracture of Adhesive Layers Constrained by Plastically-deforming Adherends." Journal of Adhesion Science and Technology, Vol. 14, pp. 1593-1607.

Kamagata, K., T. Saito and M. Toyama (1970), "The Methods of Measuring Tackiness of Pressure Sensitive Adhesive Tapes." Journal of Adhesion, Vol. 2, pp. 279-291.

Keimel, F. A. (1994), "Theories and Mechanisms of Adhesion." Handbook of Adhesive Technology, A. Pizzi and K. L. Mittal, eds., Marcel Dekker, NY, pp. 3-15.

Kim, K. S. and N. Aravas, (1998), "Elastoplastic Analysis of the Peel Test." International Journal of Solids and Structures, Vol. 24, pp. 417-435.

Kim, K.-S. and J. Kim (1988), "Elasto-plastic Analysis of the Peel Test for Thin Film Adhesion." Journal of Engineering Materials and Technology, Vol. 110, pp. 266-273.

Kinloch, A. J., C. C. Lau and J. G. Williams (1994), "The Peeling of Flexible Laminates." International Journal of Fracture, Vol. 66, pp. 45-70.

Kuczma, M. S. (1992), "A Variational Formulation of Beams and Plates on Unilateral Viscoelastic Foundations." ZAMM, Vol. 72, pp. T178-T181.

Kuczma, M. S. and L. Demkowicz (1992), "An Adaptive Algorithm for Unilateral Viscoelastic Contact Problems for Beams and Plates." Computer Methods in Applied Mechanics and Engineering, Vol. 101, pp. 183-196.

Kuczma, M. S. and R. Switka (1990), "Bending of Elastic Beams on Winkler-type Viscoelastic Foundations with Unilateral Constraints." Computers & Structures, Vol. 34, pp. 125-136.

Lamb, H. (1891), "On the Flexure of a Flat Elastic Spring." Philosophical Magazine, Vol. 31, pp. 182-188.

Le, M. N., J. Qi, D. A. Dillard and J. G. Dillard (1999), “Analysis of the Loop Tack Test Method for Pressure Sensitive Adhesives.” Research Report, Virginia Tech, Blacksburg, VA.

Lin, Y. Y., C.-Y. Hui and H. D. Conway (2000), “A Detailed Elastic Analysis of the Flat Punch (Tack) Test for Pressure-Sensitive Adhesives.” Journal of Polymer Science: Part B: Polymer Physics, Vol. 38, pp. 2769-2784.

Mizumachi, H., (1985), “Theory of Tack of Pressure Sensitive Adhesive. I.” Journal of Applied Polymer Science, Vol. 30, pp. 2675-2686.

Mizumachi, H. and Y. Hatano (1989), “Theory of Tack of Pressure Sensitive Adhesive. II.” Journal of Applied Polymer Science, Vol. 37, pp. 3097-3104.

Moidu, A. K., A. N. Sinclair and J. K. Spelt (1995), “Analysis of the Peel Test: Prediction of Adherend Plastic Dissipation and Extraction of Fracture Energy in Metal-to-metal Adhesive Joints.” Journal of Testing and Evaluation, Vol. 23, pp. 241-253.

Moidu, A. K., Anthony N. Sinclair and J. K. Spelt (1998), “On the Determination of Fracture Energy Using the Peel Test.” Journal of Testing and Evaluation, Vol. 26, pp. 247-254.

Muny, R. P., “Getting the Right Results: A Review of PSA Testing Methods.” Adhesives Age, Vol. 39, No. 9, pp. 20-24.

Pao, Y. C. (1970), “Simple Bending Analysis of Laminated Plates by Large-deflection Theory.” Journal of Composite Materials, Vol. 4, pp. 380-389.

Pizzi, A. and K. L. Mittal (1994), Handbook of Adhesive Technology. Marcel Dekker, NY.

Plaut, R. H., S. Suherman, D. A. Dillard, B. E. Willliams and L. T. Watson (1999), “Deflections and Buckling of a Bent Elastica in Contact with a Flat Surface.” International Journal of Solids and Structures, Vol. 36, pp. 1209-1229.

Plaut, R. H., N. L. Williams and D. A. Dillard (2001), “Elastic Analysis of the Loop Tack Test for Pressure Sensitive Adhesives.” Journal of Adhesion, Vol. 76, pp. 37-53.

Pocius, A. V. (1997) Adhesion and Adhesives Technology: An Introduction. Hanser-Gardner Publishers, Munich, Germany.

Pomeroy, R. J. (1970), “The Effect of Anticlastic Bending on the Curvature of Beams.” International Journal of Solids and Structures, Vol. 6, pp. 277-285.

Qi, Jia (2000), “Measurement of Surface and Interfacial Energies between Solid Materials Using an Elastica Loop.” Master’s Thesis, Virginia Tech, Blacksburg, VA.

Roberts, R. A. (1997), “Review of Methods for the Measurement of Tack.” Project PAJ1: Report No. 5, National Physical Laboratory, Teddington, UK, September.

Roberts, R. A. (1999), “Loop Tack Round Robin.” Project PAJ1: Report No.10, National Physical Laboratory, Teddington, UK, February.

Russell, T. P. and H. C. Kim (1999), “Tack - a Sticky Subject.” Science, Vol. 285, pp. 1219-1220.

Satas, D., ed. (1989), Handbook of Pressure-Sensitive Adhesive Technology, 2nd Edition, van Nostrand Reinhold Co., NY.

Schultz, J. and M. Nardin (1994), “Theories and Mechanisms of Adhesion.” Handbook of Adhesive Technology, A. Pizzi and K. L. Mittal, eds., Marcel Dekker, NY, pp. 19-33.

Searle, G. F. C. (1908), “Experimental Elasticity: A Manual for the Laboratory.” University Press, Cambridge, pp. 38-58

Sun, S. M. and W. V. Chang (1995), “Nonlinear Elastic Analysis of the Adhesive Strength between Rubber-like Materials and Rigid Surfaces.” Rubber Chemistry and Technology, Vol. 68, pp. 1-12.

Timoshenko, S. P. and J. M. Gere (1963), Theory of Elastic Stability, 2nd ed. McGraw-Hill, New York.

Tobing, S. D. and A. Klein (2000), “Mechanistic Studies in Tackified Acrylic Emulsion Pressure Sensitive Adhesives.” Journal of Applied Polymer Science, Vol. 76, pp. 1965-1976.

Wei, Y. and J. W. Hutchinson (1998), “Interface Strength, Work of Adhesion and Plasticity in the Peel Test.” International Journal of Fracture, Vol. 93, pp. 315-333

Williams, J. G. (1993), “Root Rotation and Plastic Work Effects in the Peel Test.” Journal of Adhesion, Vol. 41, pp. 225-239.

Williams, N. L. (2000), “Elastic Analysis of the Loop Tack Test for Pressure Sensitive Adhesives.” Master’s Thesis, Virginia Tech, Blacksburg, VA.

Yang, Q. D., M. D. Thouless and S. M. Ward (2000), “Analysis of the Symmetrical 90°-peel Test with Extensive Plastic Deformation.” Journal of Adhesion, Vol. 72, pp. 115-132.

Yang, Q. D. and M. D. Thouless (2001), “Mixed-mode Fracture Analyses of Plastically-deforming Adhesive Joints.” International Journal of Fracture, Vol. 110, pp. 175-187.

Zosel, A. (1985), “Adhesion and Tack of Polymers: Influence of Mechanical Properties and Surface Tensions.” Colloid & Polymer Science, Vol. 263, pp. 541-553.

Zosel, A. (1989a), “Adhesive Failure and Deformation Behaviour of Polymers.” Journal of Adhesion, Vol. 30, pp. 135-149.

Zosel, A. (1989b), “Physical Properties and Adhesion Performance of PSAs.” Adhesives Age, Vol. 32, No.11, pp. 42-47.

Zosel, A. (1992), “Fracture Energy and Tack.” in Advances in Pressure Sensitive Adhesive Technology - 1, D. Satas, ed., Satas & Associates, Warwick, RI, pp. 92-127.

Zosel, A (1994), “Shear Strength of Pressure Sensitive Adhesives and its Correlation to Mechanical Properties.” Journal of Adhesion, Vol. 44, pp. 1-16.

Zosel, A (1997), ”The Effect of Bond Formation on the Tack of Polymers.” Journal of Adhesion Science and Technology, Vol. 11, pp. 1447-1457.

Zosel, A. (1998), “The Effect of Fibrilation on the Tack of Pressure Sensitive Adhesives.” International Journal of Adhesion and Adhesives, Vol. 18, pp. 265-271.

Zosel, A. (2000), “Built to Last.” Adhesives Age, Vol. 43, No. 8, pp. 34-40.

VITA

Youngjin Woo was born in Daegu, Korea. He received a Bachelor's degree in Civil Engineering from Kyunghee University at Seoul in 1993 and earned a Master's degree in Structural Engineering from the Department of Civil and Envirnomental Engineering at the University of Illinois at Urbana-Champaign in 1997. After completing his Master's degree, he worked at the National Center for Supercomputing Applications (NCSA) in Illinois as a research programmer for two years. He was involved with developing a finite element model for parametric study of structural damage of an aircraft wing frame due to internal explosion, using the ANSYS Parametric Design Language (APDL).

In 1999, he began a Ph. D. program in Civil and Environmental Engineering at Virginia Polytechnic Institute and State University. He focused his doctoral study in structural engineering, particularly in computational mechanics.